UNIVERSITAT DE BARCELONA

Functional surfaces obtained by thermal spray techniques

Marco Robotti

PhD Program H0D02 Enginyeria i tecnologies avançades

PhD thesis title: Functional surfaces obtained by thermal spray techniques

Marco Robotti

PhD thesis director: Dr. Sergi Dosta Parras,

Profesor Lector of University of Barcelona and Technical director of
Thermal Spray Centre (CPT), Carrer Martí i Franquès, 1, 08028, Barcelona.

Ai miei genitori

INDEX

5.3 Characterization techniques

6 Results and discussion

Paper 1: Powder production for photocatalysis

M. Robotti, S. Dosta, I. G. Cano, A. Concustell, N. Cinca, J. M. Guilemany, "Attrition and Cryogenic Milling powder production for Low Pressure Cold Gas Spray and composite coatings characterization", Advanced Powder Technology, accepted 19.04.2016, DOI10.2016/j.apt.2016.04.014.

Paper 2: Photocatalysis

M. Robotti, S. Dosta, C. Fernández-Rodríguez, M. J. Hernández-Rodríguez, I. G. Cano, E. Pulido Melían, J. M. Guilemany, "Photocatalytic abatement of NOx by C-TiO_2/polymer composite coatings obtained by low pressure cold gas spray", Applied Surface Science, accepted 22.11.2015, DOI10.2016/j.apsusc.2015.11.207.

Paper 3: Solar Photoelectrocatalysis

S. Dosta, M. Robotti, S. Garcia-Segura, J. M. Guilemany, "Influence of atmospheric plasma spraying on the solar photoelectro-catalytic properties of TiO_2 coatings", Applied Catalysis B: Environmental, accepted 22.02.2016, DOI10.1016/j.apcatb.2016.02.048.

Paper 4: Electrodes

M. Robotti, S. Dosta, M. Gardon, I. G. Cano, J. M. Guilemany, M. Kourasi, B. Mellor, R. Wills, "Enhancing the performance of common electrode materials by means of atmospheric plasma spray coatings", Journal of Energy Storage, accepted 06.12.2015, DOI10.1016/j.est.2015.12.001.

List of Tables

List of Figures

Nomenclature

AM Attrition milling

AO7 Acid orange 7

AOPs Advanced oxidation processes

APS Atmospheric Plasma Spray

BET Brunauer-Emmett-Teller

CGS Cold gas spray

CM Cryogenic milling

CTE Coefficient of thermal expansion

DC Dip coating

ECTFE Ethylene ChloroTriFluoroEthylene

EDS Energy dispersive spectroscopy

HEC High energetic conditions

LEBM Low energy ball milling

LEM low energetic conditions

LP-CGS Low pressure cold gas spray

LS Laser scattering

MOX metal oxide

NAM Negative active material

PAM Positive active material

PS Polystyrene

SCE Saturated calomel electrode

SEM Scanning electron microscopy

SOFCs Solid oxide fuel cells

SPEC Solar photoelectrocatalysis

Tg Glass-transition temperature

TGA Thermogravimetric analyser

Tm Melting temperature

TS Thermal spray

VOCs Volatile organic compounds

XRD X-ray diffraction

YSZ Yttria-stabilised zirconia

0 Motivation

The will to investigate and contribute to materials science and engineering represents the motivation of this PhD work. The importance of finding advance materials which can satisfy the requirements of society and enterprises is high and this itinerary passes through discussion of technical topics and scientific results. Certainly, there are always questions and doubts around the wide field of research: which materials to use? Which is the proper technology to apply them? Are the products able to work in their final application? In this PhD thesis, initial materials are mainly in powder form, the processes consist in producing, modifying, functionalizing and spraying these powder feedstocks and the final products are in form of coatings. The main objective consists in manufacturing multifunctional composite coatings by different spraying techniques. The final question, which is the base of the motivation, is the following: do the coatings have a functional role? The importance to solve problems of enterprises, society, environment and earth is fundamental. With this PhD research is demonstrated that nanostructured feedstock materials combined with Thermal Spray techniques are able to produce advanced functional coatings without changing the initial nanostructure of the feedstock. Furthermore, these manufactured products possess high performances in different application sectors: they are able to degrade hazardous contaminants in the air, reduce the quantity of pollutants in water, improve the earth and environment purification and consequently to enhance health and quality of life of people who live in it. The required characteristics are thus satisfied by this combination of advanced engineering materials and processes.

1 Summary

The main subject of this PhD Thesis is the manufacturing of titanium dioxide multifunctional coatings by means of two spraying technologies: Low Pressure Cold Gas Spray (LP-CGS) and Atmospheric Plasma Spray (APS). The characteristics of each spraying technique are a key factor to be able to understand the behaviour of the deposited material. Moreover, the process conditions strongly affect the functional response and activity of the metal oxide layers in different application sectors. The interaction of the feedstock material with stream of APS and with nitrogen or air jet (LP-CGS) was investigated. Substrate surface activation and pre-heating were fundamental steps to understand the bonding mechanisms of the initial powders onto different substrates (Fig. 1).

The starting scope of the PhD thesis consisted in developing nanostructured TiO_2 anatase coatings by LP-CGS technique. Using this method, no melting of material feedstock is needed for being deposited and this fact is fundamental because it is possible to preserve this metastable active anatase phase at room temperature. The large specific surface of this nanometric feedstock is useful for applying it in the field of heterogeneous photocatalysis and degradation of contaminants. In order to avoid clogging phenomena of the nanometric powder and not suitable deposition of only ceramic particles, mechanical blends were prepared with ductile materials which flow properly in the pipelines. The bonding of the composite feedstock onto different substrates is mainly mechanical, due to the kinetic energy transferred from the process and the plastic deformation of the ductile material. The presence of anatase phase on the top surface of the final coatings determines their photocatalytic behaviour. Samples successfully degraded NOx gases in less than half an hour (in collaboration with FEAM Grupo de Fotocatálisis y Espectroscopia Aplicada al Medioambiente, Universidad de Las Palmas de Gran Canaria).

A second research topic regarded different TiO_2 materials with the objective to test them in photoelectrocatalysis. Three commercial powders (TiO_2 rutile, TiO_2 anatase and TiO_{2-x}) onto Inconel alloy and carbon steel substrates were studied. The influence of APS thermally-activating technique is explained towards the non-stoichiometric secondary phases that are formed. The performance of the coatings as photoanodes in the solar photoelectrocatalysis (SPEC) treatment

of a model azo dye was explored (in collaboration with group LEMMA Laboratori d'Electroquímica de Materials i del Medi Ambient, Universitat de Barcelona). The functional role of these materials has an important added value in the environmental field because of the possibility to achieve cleaner waters in the smart cities of the future.

The third purpose of this research was to deposit metal oxides based on titanium dioxide by APS for being applied as electrodes in real batteries. Firstly, bibliographic deep investigation was carried out and conventional coatings were studied. It was noticed that hydrogen contained in the plasma jet of APS is able to reduce TiO_2 metal oxide feedstock, create oxygen vacancies and non stoichiometric compounds such as titanium sub-oxides (TiO_{2-x}) or Magnéli phases (Ti_nO_{2n-1}) during the in-flight interaction of the particles with the jet stream. This lack of oxygen in the crystal structure of TiO_2 powder leads to a donor level to the conduction band; therefore a corrosion-resistance ceramic material with an enhanced conductivity was obtained. Well-deposited coatings were manufactured onto various common standard electrode materials, such as stainless steel, aluminium films, carbon-polymer composite and nickel foam. Four TiO_{2-x} plates onto aluminium substrates were applied as electrodes in a laboratory scale battery. Cyclic voltammograms curves and charge/discharge cycle of the lead acid battery were carried out and gave excellent results (in collaboration with Faculty of Engineering and the Environment, University of Southampton).

The fourth objective of this doctorate consisted in developing new functional gas sensors by means of APS technology. With the aim of offering more innovation to conventional metal oxide sensors, it was determined to build-up the sensing layer on a thin ceramic substrate. This fact permits to increase the working temperature respect to polymeric or metallic substrates. Spraying conditions were accurately selected to reach good deposition and not to damage the brittle substrate. The APS process offered also the advantage to increase the quantity of oxygen vacancies in titanium dioxide powder in order to enhance its conductivity and sensing function. Satisfactory performances were obtained testing the response of the device in front of various target gases and sensing efficiency was deeply studied (in collaboration with group MIND Micro-nanotecnologías y nanoscopias para dispositivos electrónicos y fotónicos, Universitat de Barcelona).
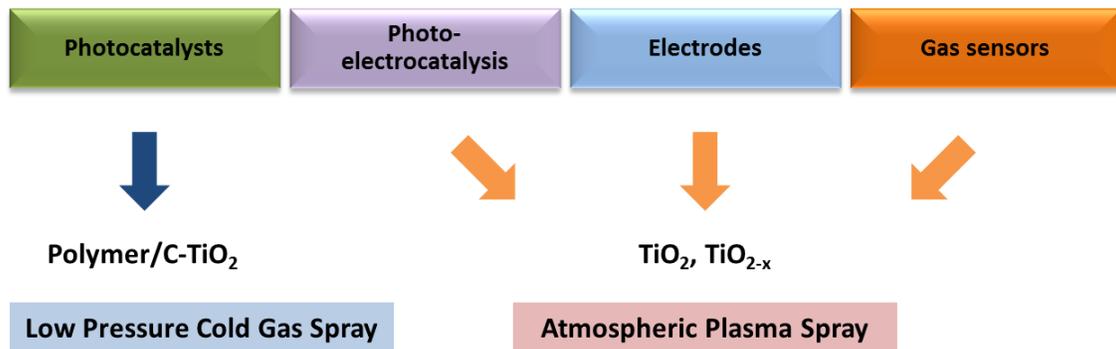
Fig. 1 PhD thesis scheme

1.1 Publications

[1P] M. Robotti, S. Dosta, I. G. Cano, A. Concustell, N. Cinca, J. M. Guilemany, "Attrition and Cryogenic Milling powder production for Low Pressure Cold Gas Spray and composite coatings characterization", Advanced Powder Technology, accepted 19.04.2016, DOI10.2016/j.apt.2016.04.014.

[2P] M. Robotti, S. Dosta, C. Fernández-Rodríguez, M. J. Hernández-Rodríguez, I. G. Cano, E. Pulido Melían, J. M. Guilemany, "Photocatalytic abatement of NOx by C-TiO$_2$/polymer composite coatings obtained by low pressure cold gas spray", Applied Surface Science, accepted 22.11.2015, DOI10.2016/j.apsusc.2015.11.207.

[3P] S. Dosta, M. Robotti, S. Garcia-Segura, J. M. Guilemany, "Influence of atmospheric plasma spraying on the solar photoelectro-catalytic properties of TiO$_2$ coatings", Applied Catalysis B: Environmental, accepted 22.02.2016, DOI10.1016/j.apcatb.2016.02.048.

[4P] M. Robotti, S. Dosta, M. Gardon, I. G. Cano, J. M. Guilemany, M. Kourasi, B. Mellor, R. Wills, "Enhancing the performance of common electrode materials by means of atmospheric plasma spray coatings", Journal of Energy Storage, accepted 06.12.2015, DOI10.1016/j.est.2015.12.001.

1.2 Congresses

[1C] M. Robotti, S. Dosta, M. Gardon, D. Rodriguez, C. Fernández-Rodríguez, J. M. Guilemany, "Photocatalytic cermet powders designed for being deposited using Cold Gas Spray", ITSC International Thermal Spray Conference 22.05.2014, Barcelona, Spain.

[2C] M. Robotti, M. Gardon, O. Monereo, G. Vescio, S. Dosta, A. Cirera, J. M. Guilemany, "Manufacture of active layer of radiation sensors coatings by Atmospheric Plasma Spray", CNMAT XII Congreso Nacional de Materiales 19.06.2014, Barcelona, Spain.

[3C] M. Robotti, S. Dosta, I. G. Cano, N. Cinca, A. Concustell, J. M. Guilemany, "LEBM and CRYO milling composite powder production for Cold Gas Spray technology", ITSC International Thermal Spray Conference 11-14.05.2015, Long Beach, California, USA.

[4C] M. Robotti, "Smart coatings for smart cities", Innovation Workshop on COLD GAS SPRAY 05.06.2015, Barcelona, Spain.

[5C] M. Robotti, S. Dosta, I. G. Cano, J. M. Guilemany, "Cold Gas Spray as a new deposition technology of nano TiO_2 anatase powders", keynote presentation ECERS 14th International Conference European Ceramic Society 25.06.2015, Toledo, Spain.

[6C] M. Robotti, S. Dosta, B. Mellor, R. Wills, I. G. Cano, J. M. Guilemany, "Improved high conductivity titanium sub-oxide coated electrodes", EUROMAT European Congress and Exhibition on Advanced Materials and Processes 20-24.09.2015, Warsaw, Poland.

[7C] M. Robotti, S. Dosta, I. G. Cano, A. Concustell, N. Cinca, J. M. Guilemany, "Composite powder production for Cold Gas Spray technology and multifunctional coatings characterization", RIPT Les Rencontres Internationales sur la Projection Thermique 7th edition 11.12.2015, Limoges, France.

[8C] M. Robotti, S. Dosta, I. G. Cano, J. M. Guilemany, "Atmospheric Plasma Spray manufacturing of TiO_{2-x} metal oxide gas sensors onto ceramic substrates for high temperature applications", ITSC International Thermal Spray Conference 10-12.05.2016, Shanghai, P. R. China.

[9C] M. Robotti, S. Dosta, I. G. Cano, J. M. Guilemany, "Photocatalytic abatement of NOx by C-TiO_2/polymer composite coatings obtained by low pressure cold gas spraying", SMT30 The 30th International Conference on Surface Modification Technologies, 29.06-01.07.2016, Milano, Italy.

1.3 Trade secrets

[1T] J. M. Guilemany, M. Gardon, M. Robotti, A. Concustell, S. Dosta, I.G.. Cano, "Self-cleaning, photocatalytic and superhydrophobic coatings obtained by Cold Gas Spray", Intellectual properties protection (iPP). Protegido por Secreto Industrial. Depósito Legal, 31/3/2014. Acta de protocolización número 431. pp 13. Barcelona. España.

2 Objectives

The achievement of multifunctional coatings with advanced properties in different application fields is the main purpose of this PhD thesis. A list of goals to be accomplished is presented below:

1. Developing new composite photocatalysts based on C-TiO_2 and ductile polymer by means of mechanical milling, understanding the mixing mechanisms involved in the different mixing processes and enhancing the presence of anatase phase in the coating, particularly on their top surface.

2. Study the flowability of the feedstock and build up C-TiO_2/polymeric coatings by LP-CGS technology. Test their photocatalytic activity towards NOx gases both in UV and visible light range and compare them to other coatings, such as commercial P25 TiO_2, SnO_2, commercial paints, dip coating. Moreover, test mechanical properties of the products.

3. Deposit three different TiO_2 feedstocks powders by APS technology and analyse the performance of these advanced photocatalytic coatings in the degradation of contaminants in liquid phase by means of visible and UV light or applied voltage (SPEC).

4. Understanding the photocatalytic processes on the top surface of the functional coatings and the role of the most important involved parameters, thus correlating the quantity of crystalline phases and amorphous ones with the SPEC degradation of azo dyes in liquid phase.

5. Manufacture novel electrode materials for acid lead batteries using lightweight and corrosion resistant substrate materials. Test their electrochemical properties inside an assembled a lead-acid battery at laboratory scale in order to perform a typical charge/discharge life cycle.

6. Selection of promising metal oxide materials as the active layer of gas sensors (TiO_2, TiO_{2-x}, ZnO among others). Deposit them by APS spraying process onto thin ceramic substrates and analyse coatings performances as gas sensor, in particular enhancing the activity of the semiconductor increasing the working temperature.

3 Relation of papers

Introduction, results and initial discussion chapters of this thesis are presented as a compilation of papers. Below are presented the main reasons that associate each of them:

The first paper regards the composite powder production. The difficulty to spray a ceramic material and particularly a nanometric or sub-micrometric metal oxide powder by LP-CGS led to the idea of modifying the feedstock material. Both size and composition of the initial powder were changed. A ductile polymeric and micrometric powder has been introduced in order to develop a new type of composite powder. Starting materials pass through milling mechanisms such as Attrition Milling (AM) and Cryogenic Milling (CM) and sieving processes, as explained in Fig. 2. This method does not only enhance the flowability of the advanced powder, but also leads to choose the optimal distribution target for the LP-CGS technique.
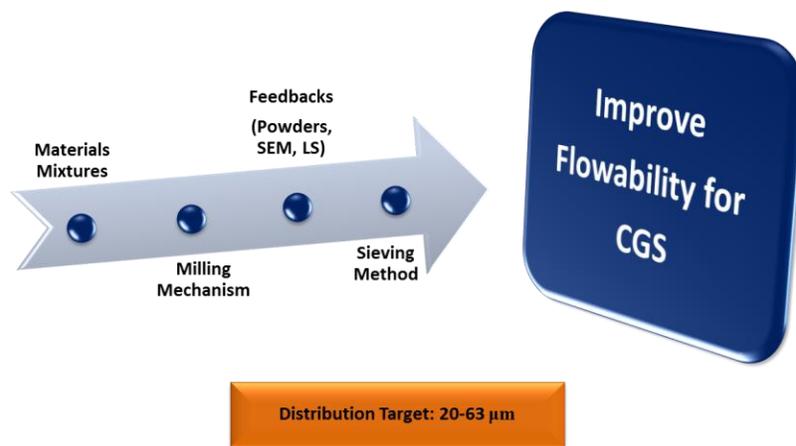
Fig. 2 Powder production through mechanical milling and sieving methods

This second paper explains the third milling method used in this PhD thesis, i. e. Low Energy Ball Milling (LEBM). Blends composed of polymer as ductile agent and nanometric C-TiO$_2$ anatase were prepared. The milling conditions were studied and compared with the ones of AM and CM blending processes. Through conventional thermal spray processes is not possible to achieve photocatalytic surfaces based on alloy or pure nanostructured TiO$_2$ anatase phase. In order to solve this problem, Low Pressure Cold Gas Spray was proposed as solution because it avoids undesired phase transformation and grain size growth. The manuscript includes results about coatings characterization. It was possible to confirm that LEBM maintains the 100% anatase phase in the final coatings as AM and CM anchoring processes. This crystalline phase is the most important for the photocatalytic product. Certainly, other aspects such as the type of catalyst, its doping, coating surface specific area resulted to be fundamental and play a key-role in the photocatalytic process. Performances of LP-CGS polymer/nanometric C-TiO$_2$ coatings (Fig. 3) were tested toward NOx and showed excellent degradation efficiency of these hazardous gases.
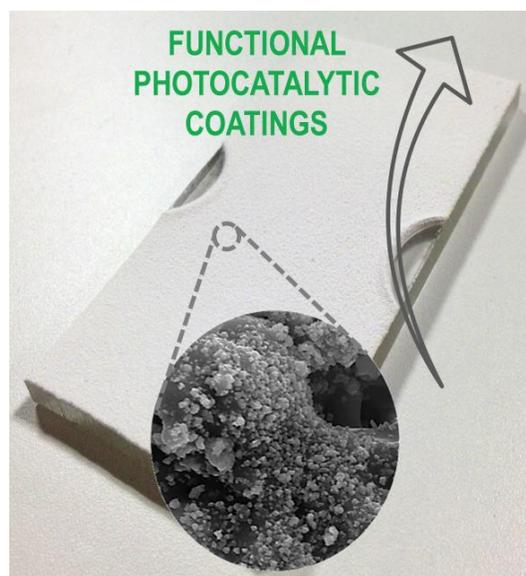
Fig. 3 LP-CGS composite photocatalytic plate

A comparison between three TiO$_2$ based feedstock materials, their changes in crystalline phase during the spraying process and their influence in the solar photoelectrocatalytic (SPEC) process are the foundations of this third paper. Initial nanostructured and agglomerated powders were characterised and consisted in 100% anatase phase, 100% rutile phase and sub-oxides powders. APS process was the medium which was used to manufacture nanostructured coatings onto Inconel alloy and carbon steel substrates. Different spraying conditions were used. In particular, both intensity and gas ratio Ar/H$_2$ were modified in order to achieve a change of composition between the starting materials in powder form and the resulting coatings. In the following Fig. 4 it is possible to observe, from a microscopic point of view, the effect of hydrogen reducing gas during the APS process. The initial powders present a white colour, but during the APS process H$_2$ gas reduces oxygen and TiO$_2$ in not anymore present in stoichiometric percentage. The presence of oxygen vacancies is the cause of the colour change of the coatings.
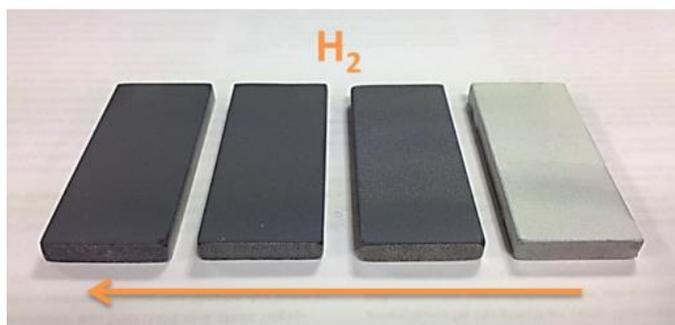
Fig. 4 Macroscopic effect of oxygen reduction by H$_2$ during APS process

The final products underwent many SPEC tests with proud results. Coatings were able to degrade a 0.43 mM AO7 solution in 0.05 M Na$_2$SO$_4$ at pH 7.0 and 35 °C in 180 minutes. It was found that coatings with higher proportion of crystalline phases of TiO$_2$ (anatase and rutile), greater 3D superficial roughness and appropriate thickness present better photoelectrocatalytic performances.

Non-stoichiometric phases of titanium dioxide are interesting not only for photoelectrocatalysis but also for applications as electrode materials inside lead acid batteries. This line of investigation consisted in developing new lightweight and corrosion resistance electrode materials using the APS technique and led to the four scientific paper of this PhD thesis. The know-how gained in previous internal studies, was transferred to the deposition of TiO_{2-x} powder onto four new substrates commonly used as electrodes in real batteries, such as 316 stainless steel sheet, aluminium alloy 2024, carbon-polymer composite and nickel foam. The spraying conditions were properly selected and controlled because they have important influence on the deposition onto the different substrates and on the electric resistivity of titanium sub-oxide coatings as well. Thickness, percentage of titanium sub-oxides and mechanical properties of the manufactured coatings were analysed. Electrochemical properties of coated pieces were compared with uncoated pieces. Collected data and successful performance obtained, encouraged the building-up of TiO_{2-x} coatings in simulated acid lead batteries. Coated aluminium sheets were selected and a real battery was mounted and tested in an electrochemical life cycle. This work gave the possibility to approach as much as possible the APS TiO_{2-x} advanced coatings to standard materials used in this application field.

4 Introduction

Titanium dioxide is a material widely available in nature, with low cost and highly stable from the chemical point of view. The most common crystalline structures of TiO_2 are: i) rutile, ii) brookite and iii) anatase. From the engineering point of view, the most interesting polymorphisms of titanium dioxide are rutile and anatase. Both structures present a coordination number among oxygen and titanium atoms of 6:3. In Fig. 5, anatase tetragonal crystalline structure is shown.
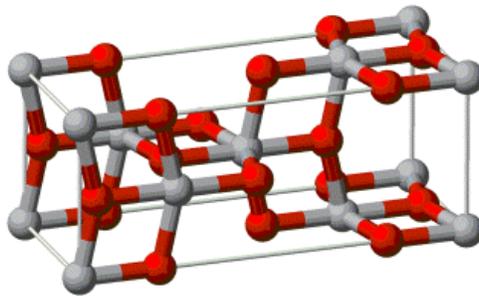
Fig. 5 Anatase tetragonal crystalline structure

In particular, anatase phase at environmental temperature is in a metastable form and this fact is reflected in a high reactivity which enhances the strength of TiO_2 as functional material. In fact, titanium dioxide is a semiconductor metal oxide with many advanced properties; among them, photocatalytic ones are very important, especially because the material is activated by UV light (λ < 400 nm) and visible light (λ > 400 nm). The photons of light possess energy comparable with the one of the band gap of the semiconductor. Another interesting characteristic is that the electrical resistivity of TiO_2 decreases with temperature. Even if the values of conductivity are not comparable with the ones of metals, some phenomena can already occur and begin. The intrinsic properties of this metal oxide semiconductor material and the possibility to increase its conductivity toward TS process enhance the interest and lead to utilise TiO_2 in many possible applications, such as AOPs, SPEC, electrodes for batteries and gas sensors.

4.1 Heterogeneous photocatalysis

[19 - 20, 36 - 54] Heterogeneous photocatalysis consists in an eco-friendly, sustainable technique very adapted to eliminate and degrade hazardous pollutants. This advanced process presents the advantage that requires very few energy because the catalytic materials can be activated by solar energy. A semiconductor material is excited with photons with energy equal or higher than the band gap energy of the material. Different MOXs can be used as catalysts in heterogeneous photocatalysis, for instance TiO_2, SnO_2, ZnO, CdS, WO_3, ZnS, Fe oxides, etc. In Fig. 6 band gap energies of different semiconductors are reported:
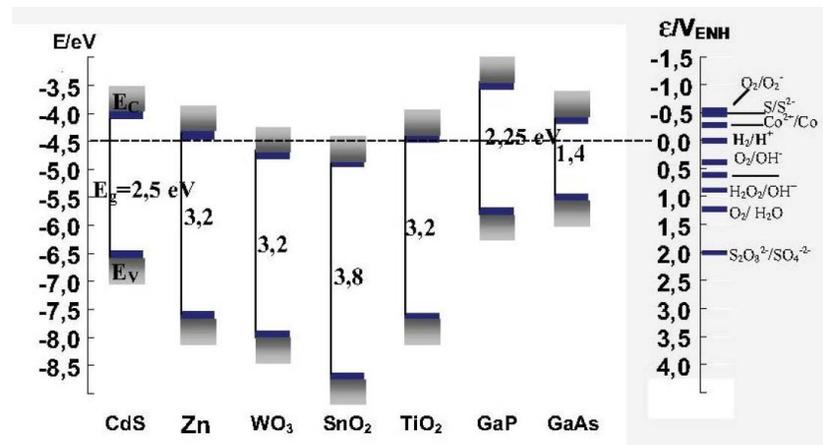
Fig. 6 Position of valence and conduction bands of different semiconductors

The majority of the presented semiconductor materials can be excited by energy coming from the photons of the light. These MOXs can be activated and absorb part of the radiation of the solar spectrum which arrives on the earth surface ($\lambda > 310$ µm) which correspond to the visible light (400 to 700 nm) and part of the UV light (UVA 315 – 400 nm). From these various materials, one of the most used and investigated is titanium dioxide. This MOX is often used as catalyst material to eliminate or decrease the concentration of toxic contaminants from water and air. The surface of semiconductor materials such as TiO_2, can be activated by UV or VIS light and photocatalytic reactions take place with both photo-reduction and photo-oxidation processes. Electrons are promoted from the valence band to the conductive one and they promote the photo-reduction reactions which create hydroxyl radicals (·OH). At the same time, on the valence band of the semiconductor holes are created, together with the activation of photo-oxidation reactions.

The principal steps which take place during the photocatalytic process are the following ones: i) adsorption of reactive substances, ii) superficial photocatalytic redox reactions and iii) desorption of products. In Fig. 7 it is possible to see a scheme of the photocatalytic process, which involves reduction and oxidation processes.
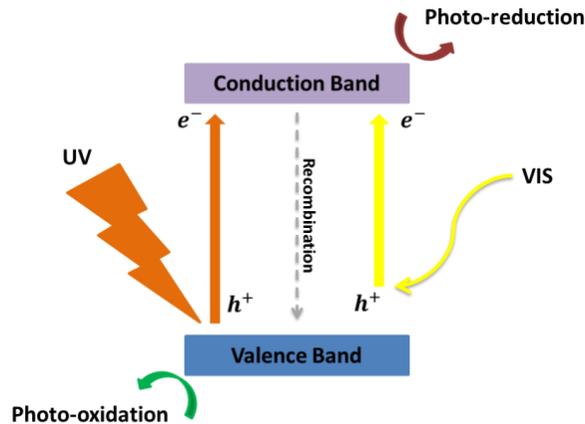
Fig. 7 Scheme of the photocatalytic mechanism

When the photocatalyst is irradiated with photons whose energy is higher than its band gap ($h \cdot v >$ Eg), the photons absorption favours an electron jump from the valence band to the conductive one, generating an electron-hole pair. Electrons and holes can recombine extremely fast, in the order of nanoseconds; this reaction time is similar to the kinetic of redox processes and it is also the main responsible of the low photonic yield of the photocatalytic reactions because of the loss of the given energy.

Titanium dioxide is a catalyst able to participate in many oxidative reactions and thus is able to degrade organic compounds and hazardous gases, such as NOx, SO_2, NH_3, toluene, VOCs, CH_4, CO, etc. This material is also capable to modify the surface and increase or decrease the relationship toward water molecules. Usually, TiO_2 offers hydrophilic surfaces, but in other cases is possible to obtain hydrophobic ones. From these properties, many applications come out (Fig. 8), such as:

- Air purification: through its photocatalytic action, TiO_2 helps to purify air, degrading hazardous compounds, such as nitrogen oxides, which have high environmental impact.

- Water purification: hydroxyl radicals ·OH which are formed during the redox reactions, remain adsorbed on the surface of the catalyst and are in charge of degrading the contaminants.

- Disinfection: the free radicals formed during the process are the responsible of eliminating and destroying cellular of microorganisms.

- VOCs elimination: TiO_2 induces the decomposition of organic molecules of VOCs destroying the molecular bondings.
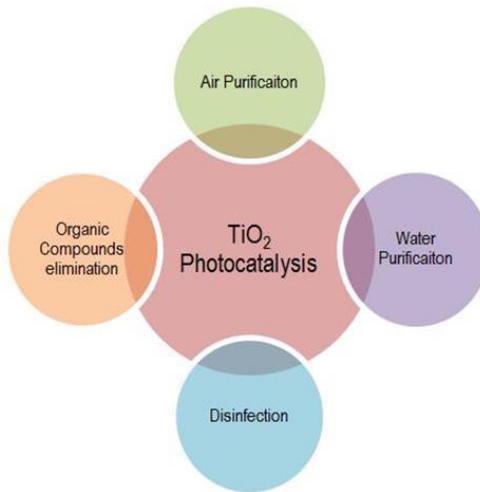
Fig.8 Summary scheme of possible applications of TiO₂ photocatalyst material

4.1.1 Catalyst doping: C-TiO$_2$

Another important parameter which involves TiO_2 and its activity as catalyst material is the possibility of doping its crystalline structure with other elements, mainly metallic atoms, but also not metallic ones, e. g. Carbon. The doping changes the characteristics of the initial material. The purpose is to increase the active working range of this MOX material. Introducing some specific elements inside the crystalline lattice of TiO_2 it is possible to decrease its band gap energy Eg. The lower is this energy difference among valence and conduction band, the lower is the quantity of energy required to activate this catalyst and the higher is the so called *cut off wavelength*.

$$E = \frac{hc}{\lambda}$$

If the working wavelength is higher it means that the material is able to react in a larger wavelength range. This factor is highly used in photocatalysis and new materials which able to react in this visible range (from 400 to 700 nm), i. e. with a smaller quantity of acquired energy represent the new requirements for the future of this research field. In this specific study, carbon modified TiO_2 was used for photocatalytic applications toward NOx gases.

4.2 Advanced Oxidation Processes

[60 - 91] AOPs consist in various techniques based on the production and use of highly oxidant species, namely hydroxyl radicals (·OH), which interact with every type of organic or inorganic compound. The advantages of AOPs processes are summarised in the following list:

- They induce a chemical and phase change of the contaminant;
- AOPs are very useful against pollutants in low concentration, i.e. ppb;
- The sub-products of reaction are formed in low concentration.

Among AOPs, photocatalytic process is one of the most used and studied. The possibility to use a clean energy source, the reuse of the photocatalytic material and the combination of this process with other oxidative methods represent the main advantages of the photocatalytic process. On the other hand, some inconvenient are present too: usually the radiation yield is low and another limit is represented by the efficiency of the photocatalysis. The efficiency of AOPs lays in the oxidative power of hydroxyl radical (·OH); this specie is able to react from 10^6 to 10^{12} times faster than other oxidative species. In Tab. 1 oxidation potentials of different species are reported:

Tab. 1 Oxidation potentials of the most reactive species

Species	E [V] at 25 °C
Fluorine	**3.03**
Hydroxyl radical	**2.80**
Atomic oxygen	**2.42**
Ozone	**2.07**

Hydroxyl radical ·OH is very strong reactive specie and occupies the second position of this classification, after only flourine and above atomic oxygen. Titanium dioxide, doped titanium dioxide and titanium sub-oxides represent the materials of the next future due to their photocatalytic properties. Taking advantage of such photocatalytic processes, these advanced materials can be employed in different functional fields, such as auto-cleanable surfaces, water decontamination devices, air purifying systems and inside photocatalytic areas in the smart cities of the future.

4.3 Influence of APS process: oxygen vacancies of TiO_{2-x}

[92 - 99] Titanium dioxides of reduced stoichiometry (TiO_{2-x}) are well known for their characteristics and properties. The electrical conductivity in combination with the chemical resistance of this material is of interest for many applications in electrochemistry. The opportunity to apply TiO_{2-x} or obtain them from TiO_2 reduction in form of coatings is highly interesting. APS technology can apply this active material in form of layers with their morphologically attractive form. Furthermore, APS is able to reduce TiO_2, increase the quantity of oxygen vacancies in the crystal lattice of this ceramic material and this way to reduce its resistivity. As results of this and other processes, titanium dioxide is not present anymore in its stoichiometric form, but in the desired non-stoichiometric phases, the so called titanium sub-oxides TiO_{2-x} and Magnéli phases Ti_nO_{2n-1}.
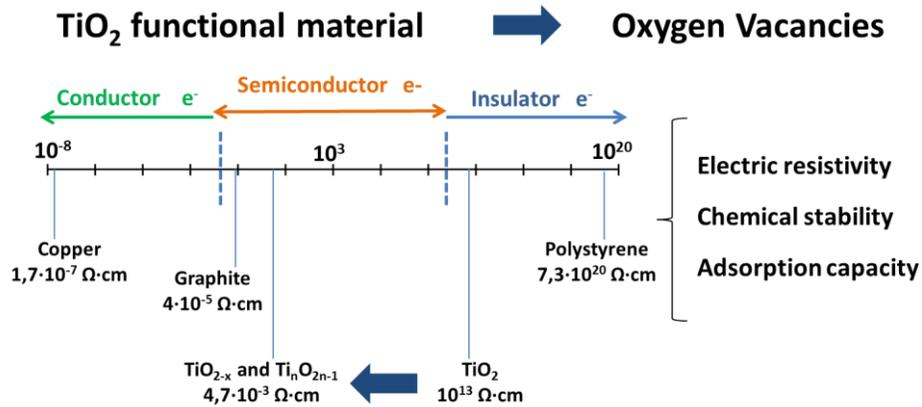
Fig. 9 TiO$_{2-x}$ and Ti$_n$O$_{2n-1}$ enhanced conductivity

This increase in conductivity of this MOX material (Fig. 9) permits to use it in specific applications such as AOPs, SPEC, gas sensing and electrochemical environments inside batteries.

4.4 Metal oxides for gas sensing

[100 - 101] MOXs are the most common group of materials used as gas sensors devices. They have a low fabrication cost and adaptability to many reducing or oxidizing gases. There is a wide variety of available MOXs, such as TiO$_2$, SnO$_2$, ZnO, WO$_3$ and Cr$_2$O$_3$ among others. Each metal oxide possesses a range of electronic, chemical and physical properties sensitive to changes of the gaseous components. The change in electrical conductivity represents the basement of the sensing mechanism for most MOXs sensors. This phenomenon is due to a charge transfer occurs between surface complexes (i.e. O-, O2-, H+ and OH-) and the molecules of the target gas. Chemisorption processes and catalytic reactions of these compounds are the main responsible for the gas sensitivity of the MOXs. The process requires a quantity of energy to activate to chemical reactions; usually temperatures between 200 °C and 500 °C are applied during the sensing experiment. MOXs results to be adequate materials for this application because they are thermally stable and capable to work in harsh environments. Fig. 10 shows the manufactured APS gas sensors.
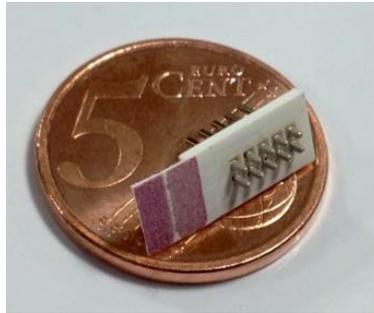
Fig. 10 MOX gas sensor manufactured by APS technology

4.4.1 Response and recovery times

The sensibility of the MOX material is measured through the change of resistance when the input of target gas is applied in the experiment. The response time (τ_{resp}) is defined as the duration between the initial time when the sensor is exposed to a constant gas concentration and the time when the signal has reached its 90% of maximum variation, keeping constant the gas concentration. On the other side, the recovery time (τ_{rec}) is defined as the duration between the time when the gas input is interrupted and the time at which the sensor signal has recovered the 90% of the baseline steady state value. Fig. 11 shows the time characteristics toward graphical details.
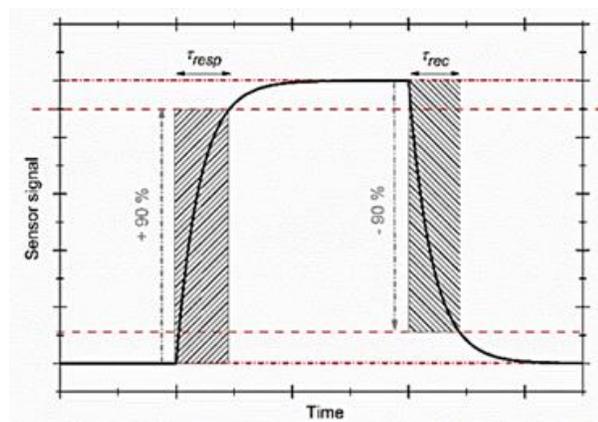
Fig. 11 Response and recovery time definitions in MOXs gas sensing process

5 Experimental procedures

5.1 Milling techniques

[1 − 18] Mechanical milling techniques are typically solid-state powder processes where cold welding and fracturing mechanisms take place. Typically, the main purpose is to utilise High Energetic Conditions (HEC) to produce crystalline, stable and metastable materials, amorphous alloys and intermetallic compounds. High impact energies lead to phenomena such as plastic deformation or fracturing of materials in powder form. Strong collisions among spheres, material and insides of vessels can significantly reduce the particle size distribution of the powder. Depending on the materials, ceramic, metallic or polymeric containers can be used.

In this PhD thesis, the idea was different compared to the classic scope of milling techniques. The objective was to study the mechanical anchoring of the materials maintaining constant some parameters (ball-to-material ratio, material of balls and containers) and only changing temperature and atmosphere inside the mixing volume. Typical high energetic conditions of crushing and reducing sizes were not applied. Low Energetic Conditions (LEC), practically low revolution rates (rpm) and low impact energies, represent the innovative trend to follow. Thanks to these soft process parameters it is possible to mechanical mix and blend in a proper way ceramics and polymers, achieving advanced composite materials. The scopes were: i) to reach proper milling conditions and optimise them, ii) to study the deformation of polymeric particles at different temperatures and finally iii) to investigate the incrustation of ceramic nanoparticles around the deformed surface of the bigger polymeric particles. The different hardness between ceramics and polymers was taken into account during the parameters selection. For this reason, a ductile soft micrometric polymer was selected as matrix onto which hard ceramic nanoparticles can be mechanically anchored thanks to the kinetic energy transferred from milling balls to the materials. Three different mechanical techniques were used in this study case: Attrition Milling (AM), Cryogenic Milling (CM) and Low Energy Ball Milling (LEBM). The mechanisms involved in these three processes permit to investigate the behaviour of the particles and their final characteristics, which are fundamental for the following LP-CGS spraying process.

5.1.1 Low Energy Ball Milling

Ball Milling is a dry milling process where the powder mixture undertakes high energetic impacts. The interaction between milling spheres, the insides of the vessels and the powder particles can be considered as a cold welding process (contact in solid state, without melting at the interface of the union of the two parts to be welded) or as a plastic deformation mechanism (due to a stress higher than the elastic limit of the material, which produces a permanent change on its shape) until a new powder is produced. These mechanical phenomena can lead to the transformation of crystalline structure due to solid state reactions. Unlike other powder methods, LEBM presents the fundamental characteristic to be carried out in solid state. This way, limitations related to the melting points and relative solubility are avoided and it is possible to synthetize alloys or composite materials with two components highly dispersed, very far from their thermal equilibrium state.

Materials classification: the characteristics of the initial powder determine the specific evolution of the process. Typically, materials in powder form are used, such as pre-alloys, carbides, oxides, intermetallic, etc. The predominance of welding or fracturing processes is determined by the response of the powder when it has to absorb the energy given by the milling balls. For this reason, mixtures can be classified according to the ductility of the raw material:

- Ductile-ductile: it is produced when two metallic materials are blended in order to obtain an alloy or an intermetallic compound. In this case, there is a predominance of the cold welding instead of fracturing.

- Ductile-fragile: in this case, a rapid dispersion process followed by mechanical anchoring is produced. Brittle particles undergo fracturing mechanism and afterwards are introduced into the ductile material. In the first moments of the milling process, ductile particles deform and flatten, while fragile ones sensibly decrease their size and remain trapped in the interlamellar spaces of the previous ones. Diffusion is favoured by the inherent heating of the technique. The homogenization of the product may be partial or total, depending on the dispersion of the fragile element in the matrix of the ductile one.

- Fragile-fragile: the fragile components are fragmented during the milling process and their particle size is continuously reduced. However, a milling limit is reached, from which the size id not further reduced. During the milling of such type of systems, it was observed how the weakest component fragments and is incrusted inside the less brittle one.

In the specific case of this thesis, the interaction corresponds to a fourth novel type so-called *nano-ductile*, which means that no fracturing of small ceramic particles occurs. For this reason, it is mainly the ductile material which undergoes the impact phenomena. Furthermore, if the second material is a polymeric one and the milling temperature is below its Tg, it is present in a fragile state, so the interaction is even different, i.e. *nano-fragile*. In this second case a fracturing process of fragile polymeric particle can take place and the anchoring mechanism can be affected.

Volume/balls ratio: that is one of the most important parameter of the Ball Milling system. The number of impacts per time unit increases with the number of balls. As much the number of impacts increases, as much cold welding and particle fracturing phenomena are favoured. This ratio depends on the energetic conditions of the Ball Milling, but also on the rotational velocity, the type of mill and the capacity to transfer energy to the material.

Milling intensity: it represents a critical parameter strictly related to the milling energy and consequently to the powder characteristics and its properties. When the intensity is increased, the energy transferred to the material is higher for each impact and the energy to be dissipated in form of deformation or heat is also higher.

Milling time: typically, this parameter is selected in order to have equilibrium between fracturing and cold welding phenomena. This time depends on the type of mill used, on the ball-to-volume ratio and on the working temperature. The higher is the milling time, better is the mechanical blending and homogenisation of the new powder. On the other side, if the milling time is exceeding, a negative effect is generated; the reducing size limit of the material is reached (Fig. 12), the contamination is higher and the formation of undesired phases can occur. In order to

avoid these problems, it is possible to select intermediate times and this can help to dissipate the temperature inside the vessels.
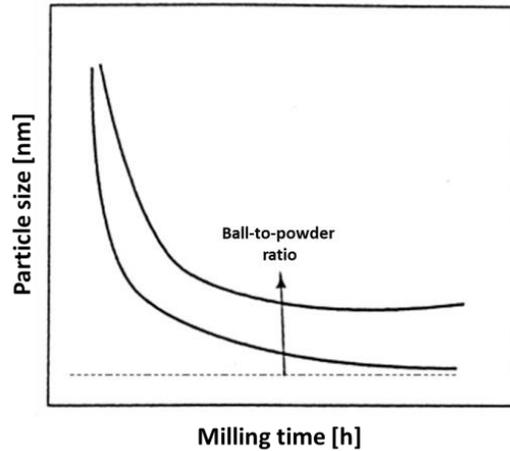
Fig.12 Particle size reduction with milling time [2]

This phenomenon occurs because, once reached the limit in the milling time, the particle size is lower than the dimensions of the voids between the milling spheres. The material remains trapped inside these voids and do not receive kinetic energy because the impacts are mainly between the spheres. For this reason, it is necessary to find the appropriate milling time in order to have the optimal conditions.

Milling balls size: the size of the milling balls plays a fundamental role in the mechanical process. The high is the diameter of the balls, the high is the inertia, the impact energy transferred to the material and subsequently the particle size reduction. Moreover, changing the dimensions of the spheres it is possible to have different voids among them and this fact is important when the milling time limit is reached, but the particle size is still not the desired one and the milling process should continue. In these types of cases, the solution consists in choosing a smaller ball diameter for the second step of milling or a combination of different balls dimensions. The chaotic effect will improve the milling efficiency, increase the energy transfer and thus continue to reduce the particle size of the material.

LEBM equipment (Fig. 13) is also called planetary mill due to the movement of its vessels. These containers rotate around their axis and at the same time around the axis of the equipment. Moreover, the rotational direction is opposite. Centrifugal force provokes that milling spheres move toward the opposite inside part of the vessels and impact against the material and that side of the container.
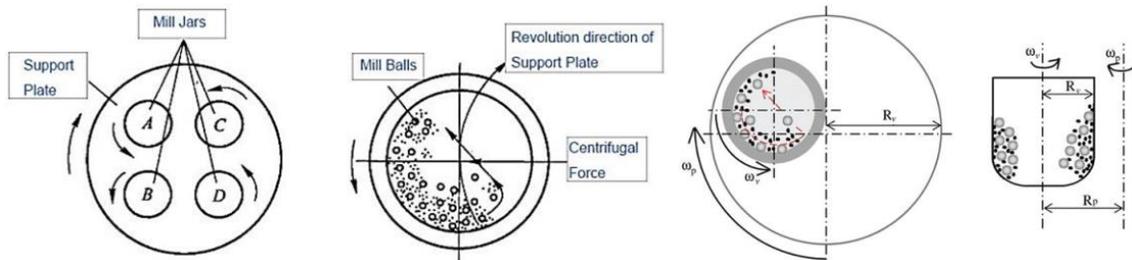
Fig.13 Scheme of LEBM equipment, mill jars and mill balls [2]

In this scientific work, powders were low energy ball-milled under different mixing conditions. Initially, only polymeric material was studied. Deformation and reduction in size of the polymeric material were observed. Afterwards, starting from the optimal mixing parameters, mixtures with different percentages of $C-TiO_2$ were carried out. Mixtures contained 10, 20, 30, 40 and up to 50% by volume of $C-TiO_2$. Different milling times were used: 0.5, 1, 4 and 8 hours, while the ratio of volume/balls was kept constant 1:1. Slow rates of revolution and $ZrO_2-Y_2O_3$ mixing balls with various diameters (from 5 to 10 mm) only blended the two raw materials. A large reduction in the volume of the polymer particles was avoided. In Tab. 2 LEBM optimal milling conditions taken into account for comparing this composite powder with other MOXs-polymeric mixtures, such as TiO_2 P25-polymer and SnO_2-polymer are reported:

Tab.2 Low Energy Ball Milling conditions

Vessel Material	Zirconia
Milling Atmosphere	Air
Milling Temperature	20 °C
Balls Material	Al_2O_3, YSZ (Yttria Stabilised Zirconia)
Milling intensity	50 - 150 rpm
Milling time	0.5 - 8 h

5.1.2 Attrition Milling

AM system consists in a vertical cylindrical container filled with balls and with inside a rotational impeller. A powerful motor rotates the impeller, which in turn moves the balls in the container. The centrifugal force of the impeller is acting on the balls, and the balls move toward the insides of the vessel and toward the material in powder form. The energy is transferred in terms of impacts and collisions to the material, which responds according to its own characteristics. The scheme of the equipment in presented in Fig. 14.
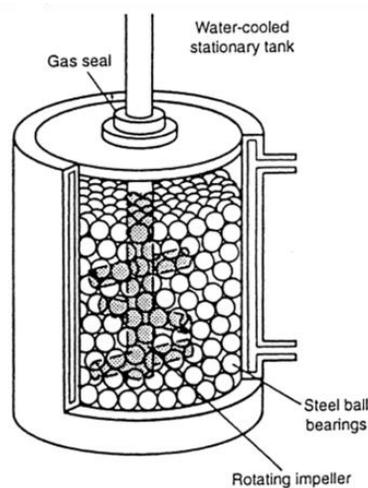
Fig. 14 Attrition Milling system [2]

The higher are the revolutions per minute (rpm), the higher are the impact energies between the materials. This way the impact energy can be dissipated in form of material deformation or heat, i. e. the temperature inside the working container can increase. For this reason, water cool system is coupled to the AM machinery. Phenomena like fractures and micro-welding mechanisms can occur; both mechanisms are produced by the impacts among spheres, container wall and agitator impeller. Tab. 3 shows the parameters which were utilised in the development of this work:

Tab.3 Attrition Milling parameters

Impeller Material	Steel
Vessel Material	Steel
Milling Atmosphere	Air
Milling Temperature	20°C
Balls Material	Al_2O_3
Milling Intensity	50 - 150 rpm
Milling Time	0.5, 1, 4 h

5.1.3 Cryogenic Milling

The configuration of CM is similar to the one of AM reported in Fig. 14; the biggest difference is related to the atmosphere present inside the milling environment. Instead of air, CM works with liquid nitrogen medium, which is capable to reduce significantly the milling conditions and other type of phenomena can take place depending on the materials. For instance, if polymeric materials are used, CM allows to work below their ductile-brittle transition temperature. In other words, N_2 atmosphere permits to work in a specific range of temperatures in which the material is in a fragile state. This fact can enhance the embrittlement mechanism of the material, which leads to a higher fracturing process and consequently to higher particle size reduction. N_2 atmosphere has the remarkable advantage to be inert gas, i.e. this environment avoids any possible chemical reaction that could occur with the presence of oxygen. Inside the vessel, the milling environment consists of milling balls, powders and flowing liquid nitrogen. Usually, CM is used to strengthen materials through grain size refinement and the dispersion of fine, nanometric scale particles; in this scientific work, the polymeric material was at a temperature much lower than its Tg and for this reason its behaviour is similar to the one of a rigid solid. It is thus interesting to observe the embrittlement effect of the polymeric particles and their reduction in their dimensions. Another significant difference factor is that the liquid nitrogen present in CM allows much shorter milling time to reach finer particle sizes and smaller recrystallized grains when compared to mechanical alloying performed in air (AM). In the following Tab. 4, CM milling parameters which were used in this research are shown.

Tab.4 Cryogenic Milling parameters

Impeller Material	**Steel**
Vessel Material	**Steel**
Milling Atmosphere	N_2
Milling Temperature	**< -76°C**
Balls Material	Al_2O_3
Milling Intensity	**50 - 150 rpm**
Milling time	**0.5, 1, 4 h**

5.2 Conventional Thermal Spray deposition techniques

[55 – 59] Conventional Thermal Spray (TS) processes are coating techniques which use high thermal energy generated by chemical (combustion) or electrical (plasma, arc) methods to melt, soften, accelerate fine dispersion metallic or non-metallic droplets or particles to speeds in the range of 50 to 1000 m/s. TS processes have the great advantage that a wide variety of materials can be sprayed and deposited onto different substrates; starting from raw materials in powder form and though these processes, coatings made by mono or multiple layers are produced. Both thermal and kinetic energy is transferred to the particles and result in a high deformation when they impact on the surface of the substrates. Thus the so-called splats adhere to the substrate surface. During the spraying, a continuous stream of molten and semi-molten particles impact onto the substrate surface. At the impact, particles cool down at very high rates to form the deposit; solidification, heat transfer and mass transfer are the principal phenomena involved during the process. A bond starts forming between the surface, the particles and even with those particles coming next; this process is usually called *Thickness Build-up*. This mechanism is based on the adhesion of splats on the substrate and their particle by particle coating formation. In reality, coating is not formed only by the overlapping of the lamellae, but also by porosity, un-melted spheres and oxides inclusions, as it is possible to notice in Fig. 15.
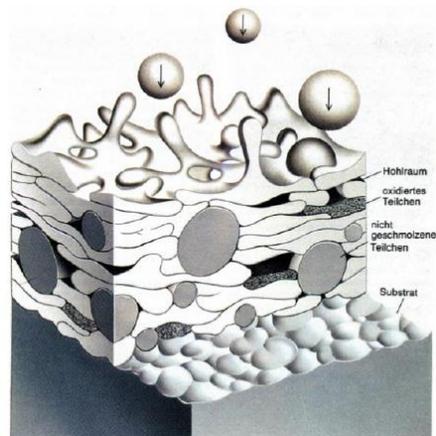
Fig. 15 Typical coating formation process [58]

Different spraying techniques are shown in Fig. 16. Each category has its own characteristics, i. e. gas or flame temperature, particle velocity and enthalpy. These peculiar properties of each spraying system are reflected in the final products: the coatings. Their properties, such as bond strength, quantity of porosity, thickness, hardness, wear resistance, impurities and quantity of oxides among others, strongly depend on the used spraying technique.
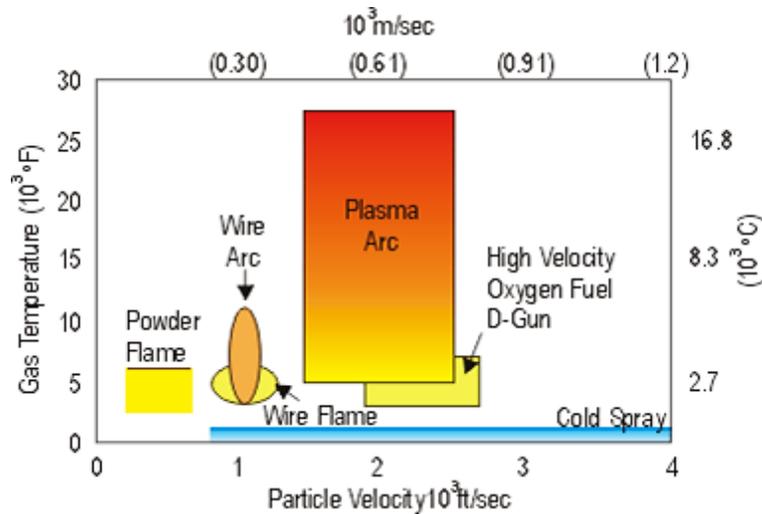
Fig. 16 Temperature vs velocity of thermal spray processes [58]

TS processes involve rapid solidification leading to new phases or amorphous structures and might be accompanied by a change in chemical composition and thirdly the spraying atmosphere may lead to oxidation or reduction.

5.2.1 Atmospheric Plasma Spray

The spraying torch is formed by a Cu cathode and a convergent W anode. The process gases such as Ar, H_2, He, N_2 or mixtures of them, are injected into the annular space between the two cylindrical electrodes of the gun. The high voltage existing between cathode and anode causes the gas ionization; this process regards atoms which release their electrons because they are excited up to high energy levels. The ionization provokes the formation of a direct current arc among cathode and anode and this arc continues the ionization process and the dissociation of the feeding gases. The generated plasma gas is a conductive gas that contains charged particles, both ions and electrons. The high-temperature conductive plasma expands and escapes through the

open end of the gun to form a very hot, high-velocity plasma jet. Depending on the gases, the content of energy transferred to the plasma changes. H_2 and N_2 are diatomic gases which produce plasma with high energy due to the dissociation reaction:

$$N_2 > Energy > 2N$$
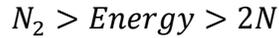
And due to the subsequent ionization reaction:

$$2N > Energy > 2N^+ + 2e^-$$
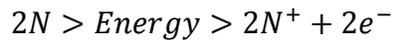
Ar and He viscosity give plasma with higher temperatures. For the plasma generation, Ar gas is preferred and it is the typical primary gas utilised. H_2 gas is a typical secondary gas and has the peculiarity to be a reducing and high thermal conductivity gas. The high dissociation and ionization energies confer to the plasma jet a lot of energy; this way, plasma torch can produce temperatures in the range between 7000 and 20000 °C. The exit Plasma temperature range goes from 5000 to 6000 °C; these high values are capable to melt every existing material. This is the reason why APS technology is able to spray materials with very high melting point, such as refractory metals or ceramics and can produce dense and resistance coatings. After its production, plasma stream exits from the anode and different mixture processes can start. The position of the powder injector can vary; it can be placed inside the spraying gun or at its end outside the plasma jet. In the experiments carried out in this PhD thesis, an external injector system had been chosen and utilised. Ar and H_2 have been used as plasma gases and Ar also as carrier gas of the powder. As described, APS technique starts from raw materials which are heated until their melting point and accelerated by the gas stream toward the substrate. These high temperatures and velocities are responsible of the particle deformation and adhesion onto the substrate. In Fig. 17 path and reactions of particles inside and with the plasma jet are reported.
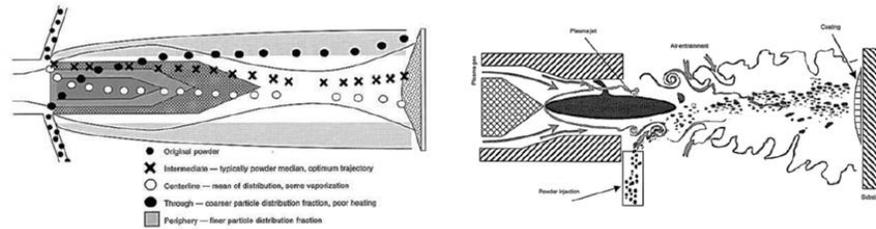
Fig. 17 Particle trajectory (left) and physical interactions among particles feedstock and thermal spray heat source (right) inside the APS system [58]

The small particles acquire high velocity and follow the plasma stream; when they arrive on the surface of the specimen both kinetic and thermal energies acquired by the particles are transformed in deformation phenomena at the impact, such as change in the particle shape and lamellae formation. A bond starts forming between the surface, the particles and also with those particles coming next (thickness build-up process). This mechanism is based on the adhesion of splats on the substrate and their particle by particle coating formation. The coating is not only formed by the overlapping of the lamellae, but porosity, un-melted spheres and oxides inclusions can also be present. The binding mechanism between coating and substrate is hardly studied. When particles arrive onto the substrate, they become solid thanks to the high cooling rate. The collision between particles and substrate or other particles already deposited gives fusion and thus a chemical bonding with the surfaces takes place. It is possible to achieve various coating microstructures and properties; these features are strongly dependent from the different spraying parameters which influence the bond:

- Spraying technique (type of torch, gun configuration, process gases, pressure);
- Type, density and viscosity of the material;
- Chemistry, morphology, particle size distribution of the feedstock;
- Temperature and thermal energy;
- Process time;
- Kinetic energy (particle impact speed);
- Injector position, injection angle, impact angle;
- Coating spraying parameters (flow rates, voltage, amperage, carrier gases, flows, number of cycles);

- Processing variables (number of passes, spraying distance, spraying trajectory, cooling system);
- Substrate surface activation and cleaning;
- Surface area;
- Chemical-physical properties (solidification speed) of both material and substrate.

In this PhD thesis, a TS equipment based on APS A-3000S with an F4 plasma torch (Sulzer Metco, Germany) was used (Fig. 18). The plasma jet was formed by a mixture of Ar and H_2 gases.
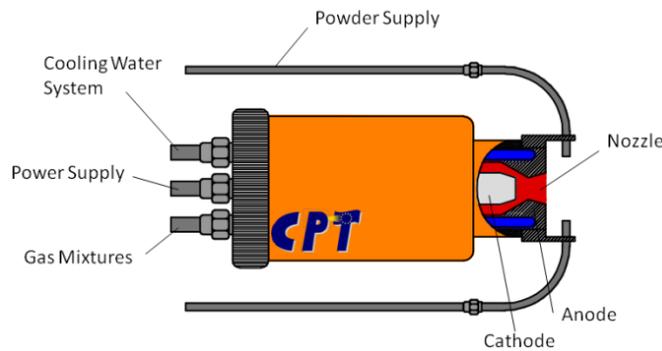
Fig. 18 APS A3000S system equipped with F4 Plasma torch

In the Tab. 5 presented below, the APS design of experiment is shown. The chosen APS parameters for spraying MOXs materials are the following: Intensity of Plasma, Argon flow rate, quantity of Hydrogen flow and stand-off distance. The intensity of plasma is responsible of stronger or lower energetic conditions. The quantities of used gases affect the heat transferred to the particles and can increase or decrease particles temperature and velocity; this way, a molten or semi-molten state of these micro-materials inside the plasma jet are determined. In particular, the higher is H_2 flow, the higher is the heat transferred to the particles because this gas possesses a higher thermal conduction coefficient. It is also fundamental to change the stand-off distance in order not to damage or overheat the substrate.

Tab. 5 APS experimental parameters

Intensity [A]	400 – 650
Ar [l/min]	32 – 47.5

H₂ [l/min]	1 – 15
Stand-off distance [mm]	60 – 160
Spraying angle [º]	90
Rotation feeder [rpm]	15
Ar career gas [l/min]	3.5

APS technique is a cost-effective technique capable to rapidly coat large areas with high deposition efficiency. Typically, the presence of formed porosity represents a disadvantage of this technology because it affects the mechanical properties of the layers. In this specific research case, however, porosities represent another advantage because they increase the specific superficial area which is in contact with the liquid (SPEC), electrochemical solution (electrode) or with the hazardous gas (sensors). Porosity values depend on the material and spraying conditions, in particular, lower velocities can boost the porosity present in the final coatings. Microstructural and compositional changes of powder feedstocks and coatings were studied. It was observed that H_2 gas contained in the plasma mixture was capable to reduce TiO_2 feedstock powder into non stoichiometric compounds, namely TiO_{2-x} and Ti_nO_{2n-1}, during the in-flight trajectory of the particles. The great accumulation of oxygen vacancies in the crystal lattice of titanium dioxide led to a donor level in to the conduction band. Therefore, the conductivity of the semiconductor was increased and thanks to this factor, titanium suboxides were used as SPEC photo-anodes, electrodes in lead acid batteries and finally as gas sensors.

5.2.2 Cold Gas Spray

[21 – 30] Cold Gas Spray is a solid-state technique that is capable to form coatings or solid components through the impacts of pure metals, metallic alloys and composite particles onto a target substrate at very high speeds. From wind tunnel modelling of gas and particles inside a supersonic flow, it was verified that it would be possible to deposit a wide range of materials onto different substrates without the use of temperature to melt or semi-melt the spraying raw material like in conventional TS process. CGS process only uses kinetic energy in order to have splats deposition and following layers build-up. The particles have a typical

distribution in the range from 5 to 60 microns and are accelerated in a stream of preheated (300 - 1100 °C) nitrogen or helium gas through a converging-diverging De Laval nozzle (Fig. 19).
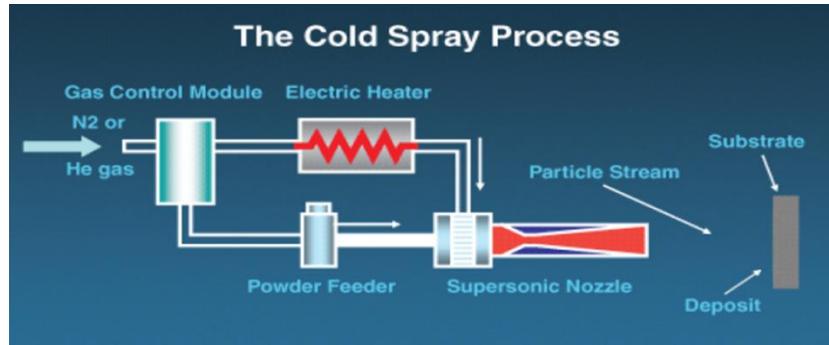
Fig. 19 Scheme of the Cols Gas Spray process [21]

The gas is compressed and after the minimum section of the nozzle expands to supersonic velocity, typically in the range 500 to 1500 m/s, while pressure and temperature begin to decrease. The high pressure causes particle deformation and this fact confirms the solid-state nature of the CGS process. Each particle, depending on the characteristics and properties of the material (composition, morphology, particle size distribution) and of the process (pressure and temperature of the gas and nozzle geometry among others), should receive enough kinetic energy to overpass its critical velocity. Once the particles possess a velocity higher than the critical one, the so-called *adiabatic shear instability* phenomenon takes place. When the spherical particles impact onto the substrate, a strong pressure field propagates spherically into the particle and substrate from the point of contact. As result, a shear load is generated which accelerates the material laterally and causes localised shear straining. The shear loading under critical conditions leads to adiabatic shear instability where thermal softening is locally dominant over work strain and strain rate hardening. This adiabatic shear instability phenomenon results in viscous flow of material at an outward flowing direction with temperatures close to melting temperatures of the material. Thus, the heated and highly strained interfaces are pressed together and the bonded. The coating build-up is not a simple one-particle impact, but rather a series of multiple collisions that transfer the kinetic energy to the substrate initially and then to the coating. In comparison with thermal spraying processes where the metal particles are melted before striking the substrate, CGS avoids oxidation of the sprayed material, grain growth, tensile stresses, high porosity, and phase changes during the process. The only changes in the coating material are due to

deformation and cold working. These coatings properties are not achievable with conventional TS technologies and make CGS coatings unique ones.

CGS advantages:
- Low porosity and low oxide content in the coatings
- Feedstock composition and grain structure is preserved
- High density and hard materials
- High homogeneity of the coatings
- Possibility to spray micro and nano sized particles
- Low energy consumption
- High deposition efficiencies
- Possibility to collect and reuse 100% the particles
- No combustion or toxic wastes
- Compressive residual stresses
- Minimum substrate preparation

Starting material: raw material, substrate and in particular their ability to plastically deform is fundamental for having the particle bonding. Metallic deformable particles give the highest deposition efficiency in CGS process. On the other side, rigid or brittle materials do not show plastic deformation phenomena and give erosion of the substrate. These types of materials are therefore sprayed together with other ductile materials which act as matrix. In some cases, it is possible to spray these stiff particles onto ductile substrates and the result is a monolayer of incrusted particles. The hard particles can penetrate inside the deformable substrate, but no coating build-up mechanism is possible, so the following layers cannot grow.

Powder morphology: non-spherical particles with irregular and roughened surfaces play a key-role inside CGS process because they have a different in-flight and impact behaviour than spherical ones. The drug force, contact area and stress concentration at the impact with the substrate are higher in the case of irregular and roughened particles.

Particle size distribution and particle velocity at the impact: these two parameters are fundamental to understand the phenomena that can occur during the CGS deposition process. In the following Fig. 20, critical velocity and particle impact velocity curves are shown. When the impact velocity exceeds the critical velocity the particles are in the good deposition sector. It is possible to select an optimum particle size range to be sprayed by means of CGS: -45+10 µm.
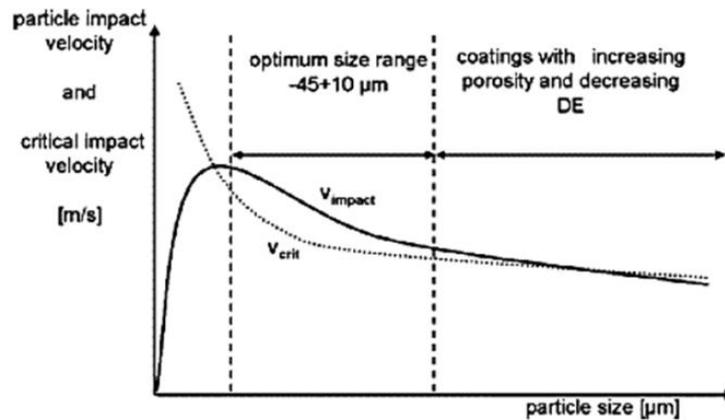
Fig. 20 Optimum particle size distribution for CGS equipment [22]

If to use higher particle dimensions, coatings with higher porosity and less deposition efficiency are obtained. Once selected the optimum particle size distribution, curves of critical and erosion velocities can be reported. Behaviours such as optimal deposition area, no deposition area and erosion sector can be summarised (Fig. 21):
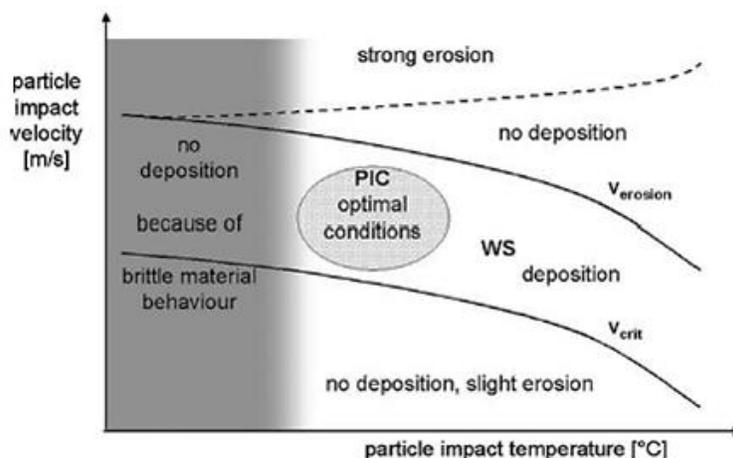
Fig. 21 Influence of impact particle temperature and velocity in CGS process

Typically, the smaller is the particle size distribution, the higher is the particle velocity. These fine particles with such high achieved velocity are responsible of the erosion of the substrate material. It is remarkable that a difference of one order of magnitude in the particle size dimension can significantly change the behaviour and the phenomena that occur during the impact of such materials.

Temperature: it is a key parameter in CGS process. The higher is the gas temperature, the higher is the gas velocity; consequently particle impact velocity is also increased. Secondly, materials elastic and plastic properties are temperature dependent. Elasticity and plasticity of the material increase with this variable; thus, softening and appearance of adiabatic shear instabilities phenomena are enhanced and promote the bonding mechanism.

Surface activation: the substrate roughness is a parameter that can have a direct influence on the particle adhesion. As the bonding is related to the mechanical anchoring of particles, if the substrate possesses a larger specific area the particle-substrate bond formation is higher. For this reason, substrate must be prepared and surfaces must be activated. A common technique to increase the surface roughness is the shot peening procedure. With this method, ceramic particles (commonly Al_2O_3) as propelled toward the substrate with a pressure between 3 and 6 bars in order to plastically deform the surface and boost its superficial specific area. At the end of this procedure, samples are cleaned and situated in the spraying spot.

Spraying angle: the inclination of the substrate is strictly related to the deposition efficiency, as can be observed in the Fig. 22 below. The highest bonding takes place with a spraying angle of 90°, while below a certain angle, no material deposition occurs. Three main regions can be identified: i) no deposition region, ii) transient region and iii) maximum deposition region.
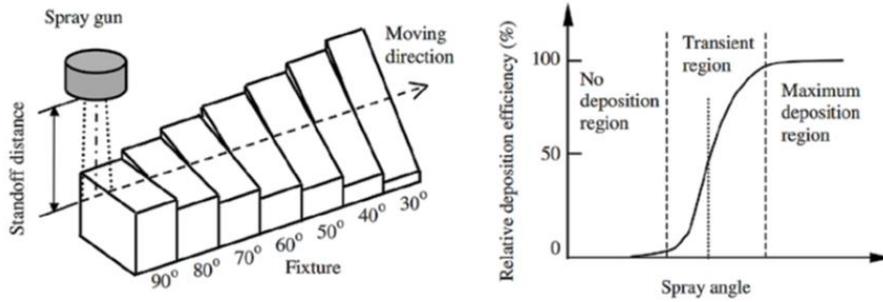
Fig. 22 CGS deposition efficiency vs spraying angle parameter [22]

Very little research has been reported into the possibility of depositing ductile polymers by CGS, despite considerable interest in the formation of polymer coatings by thermal spraying and in the use of thermoplastic powders for rapid prototyping by other methods of deposition and agglomeration. This work is focused on the deposition of polymeric and composite particles by means of LP-CGS.

5.2.3 Low Pressure Cold Gas Spray

[31 − 35] Low Pressure Cold Gas Spray technology is a competitive, cost-effective and fast process. Technically, LP-CGS possesses a lower particle velocity in comparison to HP-CGS and does not utilise high temperatures, so any high temperature phase transformation of the materials is avoided. Moreover, this new type of technology uses compressed air or nitrogen as propellant gas, so LP-CGS is also environmentally friendly because no dangerous gases and no chemically aggressive wastes are released during the deposition procedure. LP-CGS possesses another great advantage: it is a compact and portable equipment. This fact represents an important practical characteristic for industrial enterprises because in situ sprayings can be carried out. The Low Pressure Cold Gas Spray system used in this research is the low pressure kinetic gas spray system (DYMET 423). This LP-CGS equipment works with an electrical power supply of 3.5 kW and presents a gas consumption of 400 L/min. In Fig. 23 the scheme of this technology and some characteristics of the nozzle can be observed.
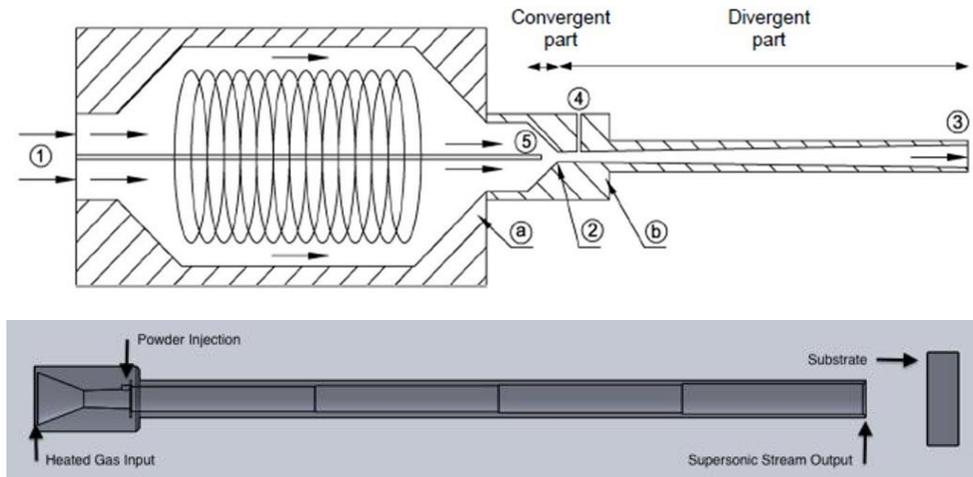
Fig.23 Low Pressure Cold Gas Spray scheme (top) and SK-20 nozzle geometry (down)

This equipment can be used with compressed air and nitrogen, among others, as propellant gas (1). The nozzle SK-20 is a stainless steel converging-diverging De Laval type (2), with a round exit and an expansion ratio of about 1.56 (3). The convergent-divergent design of the nozzle is able to accelerate powder particles to supersonic velocities. The diverging part measures 10 mm in length, the barrel part measures 120 mm in length and the exit size is of 2.5 mm in radius. The powder is injected into the gas jet from radial direction at the diverging part (4) of the nozzle. The gas can be heated up to 632 °C with a resistance (5) inside the spraying gun before the powder injector. During LP-CGS spraying process, many parameters can be modified, such as gas heating temperature, pressure, powder feeding rate, number of cycles and distance between cycles among others. Pressure, gas temperature and critical particle velocity represent the most important features of this technology. The operation pressure can be modified from 5 to 10 bars; this pressure range is adequate for both jet acceleration and powder to nozzle transportation. In this specific study, the inlet gas pressure was fixed at 6 bars. In the Tab.7 below, it is possible to observe the experimental spraying conditions used during this PhD thesis.

Tab.6 LP-CGS experimental parameters

Temperature [°C]	50 – 450
Gun velocity [mm/s]	100 – 500
Distance [mm]	10 – 60
Pressure [bar]	6
Spraying angle [º]	90

The pressure represents a key parameter because it provides high kinetic energy to the in-flight particles at the outlet in order to reach a proper bonding onto the substrate. The powder supply rate can be modified, but cannot overpass 30 g/min to avoid jet overload. Temperature has also been changed in this research; this parameter, together with pressure, is fundamental to investigate the plastic deformation and anchoring of particles onto the substrate. Moreover, the higher is the temperature, the higher is the gas acceleration to supersonic regime. Usually, low temperatures help to improve coatings quality, while high temperatures can enhance the deposition efficiency. Even the substrate temperature plays an important role; it can enhance coating deposition, reduce internal stresses and minimise the oxidation processes. The LP-CGS spraying distance is in the range between 5 and 15 mm; lower distances lead to particle rebound, the so-called *Bow Shock effect*, while higher distances decrease particle deformation. Spraying angle and deposition efficiency are linked; 90° represent the optimal angle in order to have the highest deposition of material onto a substrate. Many different materials can be deposited onto various substrates; thickness from 5 μm up to 10 mm can be achieved, depending on the final application of the coating. Typical porosity values of obtained coatings are in the range 1 – 5 %. Unfortunately, with this technology it is not possible to directly spray nano powders mainly because of flowability problems or because static agglomeration of the extremely fine particles. These factors have led to the innovative idea to develop a new kind of composite material during this scientific research. A second ductile material can be employed (polymeric in this PhD thesis, but also metals) and mixed with hard material (MOXs in this case, such as $C-TiO_2$, TiO_2 and SnO_2). The objectives of the deformable material are i) to be the softer matrix part of the composite mixture, ii) to accommodate the nanoceramic particles around its surface, iii) to improve feedstock flowability avoiding clogging problems, iv) to plastically deform during the spraying process and finally v) to promote the coating formation. Through this way, the

deposition of brittle materials like ceramics, which do not show plastic deformation, can be overcome.

5.3 Characterization techniques

- Initial powders and coated samples were mounted in a conductive phenolic resin (Konductomet, Buehler) and in an epoxy resin (EpoFix, Struers). Metallographic preparation was done following the standard ASTM E3-95.

- Laser Scattering (LS): particle size distribution was carried out using a Laser Diffraction Particle Size Analyser (Beckman Coulter LS 13 320, Universal Liquid Module)

- Scanning electron microscopy (JSM-5310, Jeol and ProX, Phenom) and optical microscopy (DMI 5000M, Leica) were used for the observation of feedstock powders, substrates and coated pieces.

- Energy Dispersive Spectroscopy (EDS): common point and scanning analysis (Xflash detector X5010, Bruker) were carried out in powders and coatings.

- X-Ray Diffraction (XRD): crystalline composition of different powders, substrates and coatings was analysed by means of a diffractometer (X'Pert PRO MPD, PANalytical).

- Specific surface area of the starting feedstocks was obtained by BET (Brunauer-Emmett-Teller) analysis using N_2 adsorption.

- The composite powders were milled with three different equipments: planetary mill (PM400 RETSCH), attritor mill (Model O1HD, Union Process Inc.) and cryogenic mill, (Model O1HD modified by CPT, Union Process Inc.).

- Grit-blasting: Al_2O_3 particles grade 24 were propelled to substrates using a stream of compressed air (MAB-4, Mab Industrial, S.A.).

- Substrates were cleaned using ultrasonic equipment (Ultrasons-HD, J.P. Selecta) and acetone (Panreac) before the spraying process.

- Composite powders were deposited by means of LP-CGS Spray equipment (423, Dymet), while APS A-3000 system with an F4 plasma torch was used for spraying TiO_{2-x}. Both facilities are coupled with a three-dimensional 3D robot (ABB).

- Roughness of the substrate was conducted in this research using a SJ-210 profilometer (Mitutoyo).

- Micro-Raman spectroscopy: surface composition of metal oxides and some polymers is accurately analysed by Raman spectroscopy (Labram HR800, Horiba).

- Durability of coatings was measured by Taber$^{®}$ Rotary Platform Abrasion Tester (Model 5135/5155, TABER INDUSTRIES).

- Hydrophobicity property was determined by contact angles measurements (Image J).

- The surface of the coatings and 2D and 3D roughness parameters were measured by confocal optical microscope (DCM3D, Leica). Moreover, two specific softwares (SensoSCAN and LeicaScan Mountain) were used for analysing data.

6 Results and discussion

This first paper focuses on powder production for Low Pressure Cold Gas Spray system by two milling techniques: Attrition and Cryogenic Milling. ECTFE polymer and C-TiO$_2$ were selected as raw materials. Firstly, only polymeric particles behaviour inside the two milling environments was studied. Secondly, polymeric-ceramic composite mixtures started to be produced. The influence of cryogenic temperature on the polymer material was studied. The effect of adding ceramic nanoparticles was also described. The flowability of manufactured powder resulted improved compared to the initial nanometric C-TiO$_2$ and most important, adequate for the LP-CGS process. First composite coatings were manufactured and characterised.

Original Research Paper

Attrition and Cryogenic milling powder production for Low Pressure Cold Gas Spray and composite coatings characterization

M. Robotti, S. Dosta *, I.G. Cano, A. Concustell, N. Cinca, J.M. Guilemany

CPT Thermal Spray Centre, Departament d'Enginyeria Química I Metal·lúrgica, Universitat de Barcelona, Martí i Franquès 1, E-08028 Barcelona, Spain

ABSTRACT

Inside the wide field of thermal spray, the possibility to spray ceramic nano-particles by Low Pressure Cold Gas Spray (LP-CGS) represents an interesting and innovative trend. In this work, titanium dioxide TiO_2 nanoparticles were mixed with a polymer in order to obtain a tailor-made nanocomposite powder and afterwards cold-sprayed coatings were produced, which might be attractive for their photocatalytic activity. Firstly, two different routes were used to incorporate the ceramic nanoparticles within the polymeric matrix: Attrition Milling (AM) and Cryogenic Milling (CM). Samples composition was not varied, while milling time was changed. The main objective was to investigate the mechanical physical union of TiO_2 nanoparticles around polymeric microparticles. The effect of ceramic particles on the structure and morphology of the polymer, as well as the influence of the temperature of the different combining processes were studied. The fundamental properties of the nanocomposite mixture were investigated by Scanning Electron Microscopy (SEM), Laser Scattering (LS Beckman Coulter) and X-ray Diffraction (XRD). Secondly, the best mechanically combined mixture was selected in order to be sprayed by LP-CGS technology. Adequate spraying parameters were chosen in order to develop different composite coatings. Thickness, roughness and porosity of manufactured products were measured.

© 2016 The Society of Powder Technology Japan. Published by Elsevier B.V. and The Society of Powder Technology Japan. All rights reserved.

1. Introduction

Nanocomposites materials are nowadays in the spotlight of both industry and research groups. The increasing interest in this type of composites arises from the possibility of preparing tailor-made materials that combine the advantages of ceramic nanoparticles, for instance electrical conductivity and photocatalysis [1,2], with the ones of polymers, e.g. ductility, deformability and plasticity. Nanostructured ceramics are conventionally defined as inorganic materials composed of structural units with a size scale of less than 100 nm in any dimension. Nanoceramics are classified as zero-dimensional nanocrystals, one-dimensional nanowires and nanotubes, two-dimensional nanofilms and nanowalls, and three-dimensional bulk materials with at least one nanocrystalline phase. These materials permit to obtain superior and unique properties in conventional ceramics with coarser structured units. As a large fraction of interfacial areas is created between a nanofiller and a polymeric matrix due to the high surface to volume ratio of nanoparticles, it is expected that the interphase formed in nanocomposites will have more importance for the final properties

than that in conventional polymer composites. However, this only should occur with uniform dispersion of nanoparticles [3,4], which most of the times is a really difficult challenge. For this reason, characterization of interphases in nanocomposites with uniform dispersion is a key factor to understand their final properties and performance. Up to this moment, several strategies [5,6] have been followed to achieve uniform nanoparticle dispersions within polymer matrices; however, most of them required the use of solvents, chemical modification of the matrix and/or the filler, long processing times, and even sometimes high processing temperatures. Nevertheless, they do not seem to ensure uniform dispersion in terms of isolated nanoparticles when sizes of particles are less than 50 nm and filler loads are greater than 5% by weight (wt). Recently, with solid-state methods, such as Attrition milling (AM) [7,8], mechanical mixture of nanoparticles that remain well-bonded around the polymer has been achieved. Usually, AM provides good results with small chemical modifications, if any, of the polymer or the nanoparticles, avoiding, at the same time, the use of solvents and high processing temperatures [9]. A second mixing method, Cryoattrition Milling CM, commonly used for amorphous alloys and intermetallic materials, is also taken into account as new potential alternative for composite powder blending at low energy conditions. The main theory of the dispersing mechanism of

* Corresponding author. Tel.: +34 934034449.
  E-mail address: sdosta@cptub.eu (S. Dosta).

particles on polymer proposed in this paper is the so-called mechanical anchoring [3,10]. This phenomenon takes into account the deformation of the polymer, especially on the surface, and the consequently mechanical adhesion of ceramic particles onto it. This approach has been studied in recent years and considerable effort has been devoted to the development of methods for the preparation of composite particles consisting of polymer cores covered with shells of different chemical composition. Several of these composites have been used as catalysts, coatings, raw materials recovery, drug delivery and anticorrosion protection [1,11,12]. In this case, ceramic–polymeric nanocomposites will be manufactured and developed for coating production through the Low Pressure Cold Gas Spray technology [22,23,26]. Polymeric particles with shells of nanoceramics do not lose their flowability and this is a significant aim inside the spraying process [24]. Therefore, the present work is twofold: (i) polymer nanocomposite obtainment by Attrition milling and Cryogenic milling of a polymer with oxide nanoparticles and (ii) coating build up by LP-CGS with the optimized powders.

2. Experimental materials and methods

In this work, titanium dioxide TiO_2 nanoparticles were room temperature and cryogenically milled with a copolymer as ductile matrix. The polymeric material is a commercial one: Halar® 6014 from Solvay. Laser Scattering (LS 13 320, Universal Liquid Module) was carried out in order to determine the particle size distribution of the raw materials. Two different mixing systems were used to produce composite powder materials: Attrition Mill (Model 01HD, Union Process Inc.) and Cryogenic Mill (Attritor 01HD, Union Process Inc.). Top surface of starting powders and milled composite mixtures as well as cross sections of final coatings were observed by SEM scanning electron microscope (Pro-X, Phenom). Diffraction data were studied by X'Pert PRO MPD diffractometer (PANalytical). Composite coatings were obtained by means of Low Pressure Cold Gas Spray system (Dymet 423). Produced coatings were mounted in an epoxy resin (EpoFix, Struers) and subsequently metallographic preparation was carried out.

2.1. Polymer

The polymeric matrix is a semi-crystalline, melt processable resin copolymer. The polymeric chain consists in a sequence of ethylene and chlorotrifluoroethylene monomers. Good chemical resistance, excellent thermal properties, optimal permeation resistance, anti-corrosion behaviour and outstanding flame resistance are just part of its interesting characteristics. Since the aim of this manuscript was to study the behaviour of polymeric and ceramic nanoparticles inside both AM and CM systems, it was necessary to study a narrow range of particle size distribution in order to comprehend well the mixing mechanisms. For this reason, the polymer was sieved in two different ranges: 20–40 μm (PR101-S1 in Fig. 2a) and 60–80 μm (PR101-S2 Fig. 2b). Though this way, it is possible to work with more homogeneous starting materials, so that it is easier to understand what happens to finest particles and to biggest ones during the mixing processes: also, the particle size of the final composite powder will be important regarding cold spray application. Not only the deformation of polymeric particles is important, but also the crystallinity of the material; in Fig. 3 the XRD pattern is shown and it is possible to notice a crystalline diffraction peak at 17.4° and a second broader peak at around 40° which represents the amorphous part of the polymeric matrix.

2.2. Titanium dioxide

LS curves showed in Fig. 4a confirm the fact that the titania powder possesses a medium particle size distribution of 1.88 μm. Two peaks can be observed: a first peak consists in sub-micrometric particles from 0.05 μm to 0.3 μm, while the second peak represents the majority of material volume. In this second case d_{90} corresponds to 4.4 μm. In the SEM top surface micrograph on Fig. 4b it is possible to notice both small particles and groups of agglomerated ones. This phenomenon is mainly due to electro-static agglomeration because of the small dimensions of titania. Nevertheless, powders with these grain sizes could not be easily sprayed by Low Pressure Cold Gas Spray technique [28] due to their bad flowability. Diffraction peaks of TiO_2 shown in Fig. 5 correspond to the anatase phase and possess a wide width due to the nanometric size of the powder. This broadening is an intrinsic characteristic of the material, i.e. the large width is due to the nano sized crystals of the material. Titania nano dimensions were specifically selected in order to achieve the best mechanical union with micrometric polymeric particles. The new composite material has a polymeric matrix surrounded by TiO_2 nanoparticles and this way it is possible to have a correct flowability inside the LP-CGS nozzle and also be able to spray ceramic nanomaterials [18,21,25].
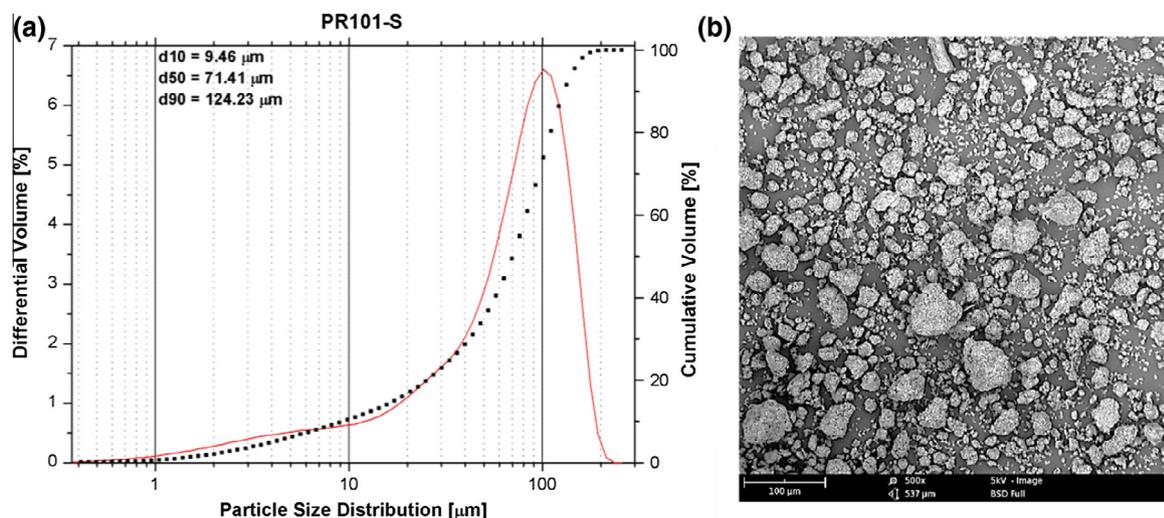
Fig. 1. Wide particle size distribution (a) and SEM (secondary electrons) top surface (b) of polymer.
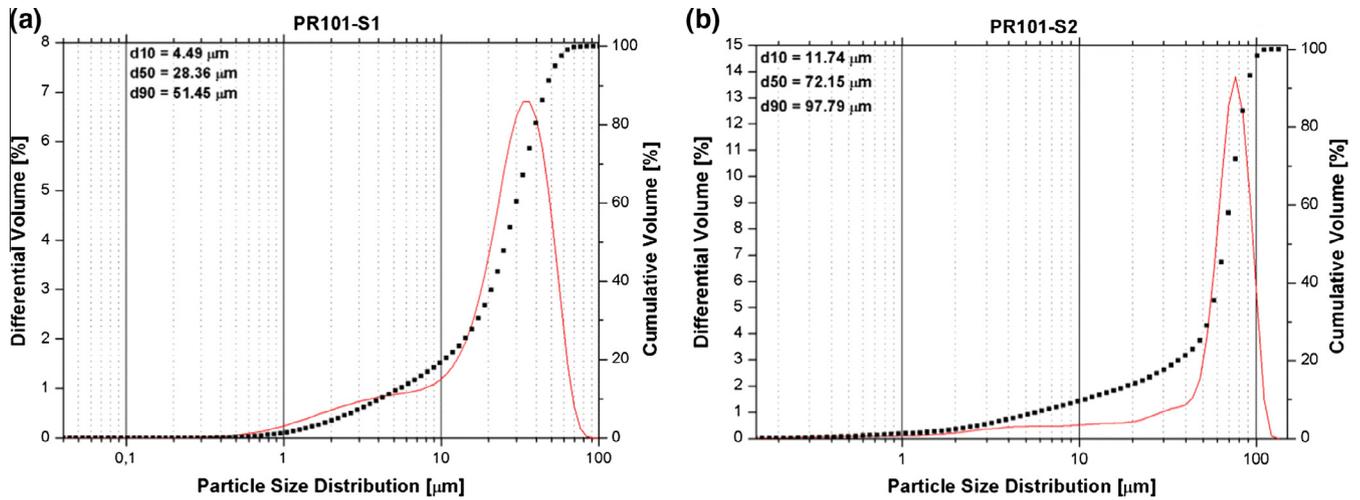
Fig. 2. LS of sieved polymeric particles: PR101-S1 (a) and PR101-S2 (b).
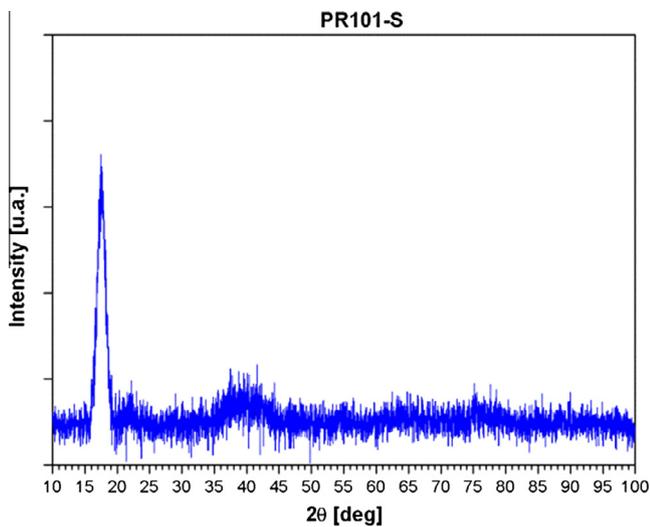
Fig. 3. XRD analysis of the polymeric material.
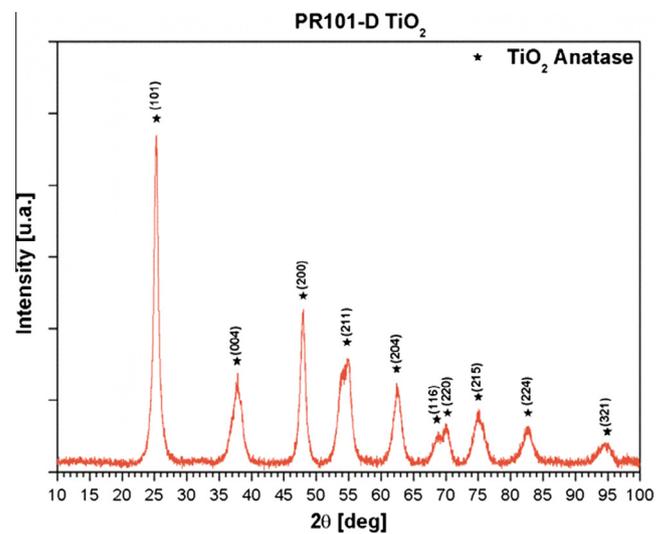
Fig. 5. XRD anatase pattern of titanium dioxide.
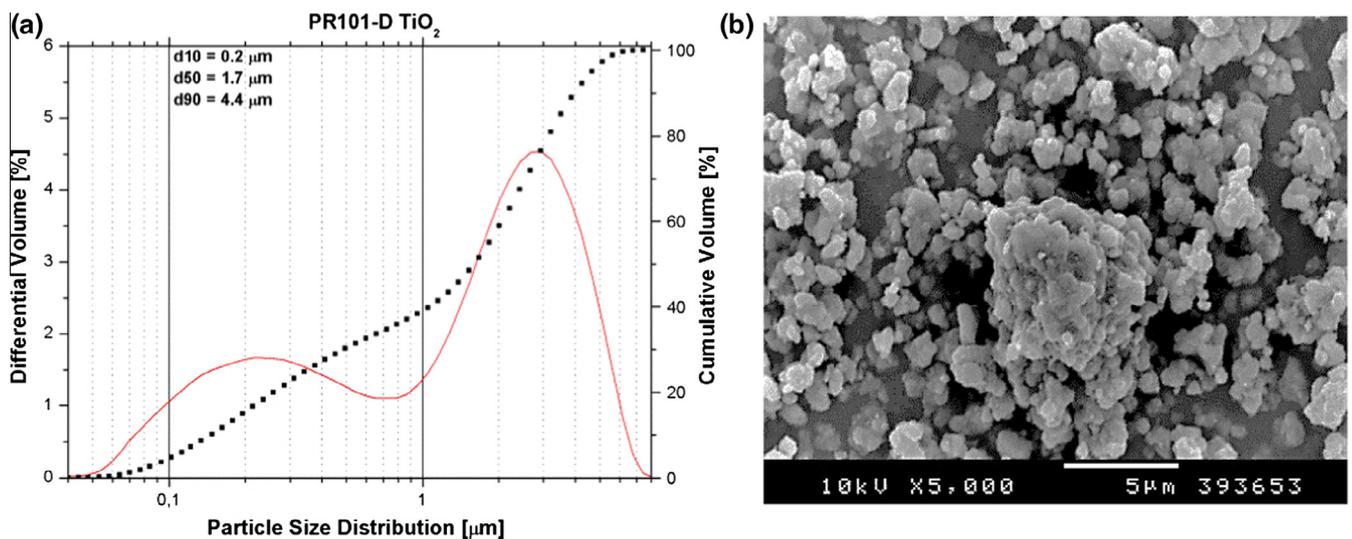
Fig. 4. LS analysis (a) and SEM (secondary electrons) top surface of TiO_2 powder (b).

2.3. Mechanical milling techniques

Mechanical milling techniques are typically solid-state powder processes where cold welding and fracturing processes take commonly place [30]. They are typically used for production of crystalline, stable and metastable materials, amorphous alloys, intermetallic compounds and, in general, to develop homogeneous materials in form of High Energetic Conditions (HEC) are often used in order to achieve high impact energies that can plastically deform or fracture the material in powder form [15–17]. Strong impacts among balls, powder, and walls of containers can significantly reduce particle size distribution. Vessels and impellers of ceramic, metallic or polymeric materials can be used in function of their hardness and in function of the materials of the powders. In this work, typical high energetic conditions of crushing and reducing particles sizes are not applied. Low Energetic Conditions (LEC) are applied in order to mix properly ceramic–polymeric nanocomposite materials and study the incrustation of ceramic nanoparticles around the bigger polymeric ones. The hardness of these two different materials was taken into account during the selection because a ductile soft polymeric was selected as matrix in which hard ceramic nanoparticles can be incrusted and mechanically adhered thanks to the kinetic energy transferred from ceramic balls to the material. Two mechanical techniques are used in this study case: Attrition and Cryogenic Milling. These different mechanisms allow study the behaviour of the particles and their final characteristics which have to be the best ones for the following LP-CGS spraying process [24].

2.3.1. Attrition Milling (AM)

AM consists in a vertical container filled with balls and with inside an impeller. A powerful motor rotates the impeller, which in turn rotates the balls in the container. The higher the revolutions per minute (rpm) are, the higher the impact energies between the materials. This way the temperature can increase and fractures and micro-welding mechanisms can happen. For this reason, water cool system is coupled.

2.3.2. Cryogenic Milling (CM)

CM possesses the same configuration of AM, but with a different atmosphere; instead of air this equipment works with liquid nitrogen medium. For this reason the system works below the ductile–brittle transition temperature of the polymer [3,5]. The use of N_2 is useful to avoid chemical reactions and to work in a specific range of temperatures in which the material is a fragile state [31]. Inside the vessel, the milling environment consists of milling balls, powders and flowing liquid nitrogen. Usually, CM is used to strengthen materials through grain size refinement and the dispersion of fine, nano-meter scale particles; in this scientific work it is interesting to observe the embrittlement effect of the polymeric particles and their reduction in dimensions. Another common difference among AM and CM is that the liquid nitrogen present in CM allows much shorter milling times to reach the finest particle sizes and smaller recrystallized grains when compared to mechanical alloying performed in air [14]. In the following Table 1, milling parameters which were used in this research are shown.

Table 1
Mixing parameters.

	Cryogenic milling	Attrition milling
Milling time (h)	0.5; 1; 4	0.5; 1; 4
Impeller material	Steel	Steel
Vessel material	Steel	Steel
Grinding medium	N_2	Air
Milling Temperature	$<-76\ °C$	$20\ °C$
Balls material	Al_2O_3	Al_2O_3

Composition of the starting powders, mixing time, ball-to-material ratio, material balls and containers are kept constant. The objective is to study the mechanical anchoring of the two different materials only changing temperature and atmosphere inside the mixing volumes. The grinding medium influences directly the milling efficiency. AM works at environment temperature (25 °C), controlled by water cooling system, while CM works at cryogenic temperatures, i.e. temperatures below $-76\ °C$, which represents the brittle–ductile temperature of the polymer.

3. Results and discussion

Firstly, characterization of initial materials was done. Polymeric and ceramic powders were studied by different experimental techniques. Secondly, a deeper characterization of final coatings is shown. The most interesting properties of these composite products are exposed and interesting future applications are proposed as well.

3.1. Characterization of raw materials

In this first section, polymer particles characterization is presented. Fig. 1b shows SEM micrograph of such powder. It can be observed that particles are between 1 μm and 110 μm, with an average size of 48 μm. Moreover, the particles possess an irregular and rough morphology. The micrograph of Fig. 1b confirms the results of particle size range distribution by LS of Fig. 1a. This polymeric material was chosen in order to have a good polymeric matrix which can plastically deform during the spraying tests by LP-CGS. Moreover, the particle shape of this specific polymer is very helpful for the final coatings roughness and subsequently for final applications, such as gas or liquid contact, self-cleaning or photocatalysis. In this second part, the most important utilised material was characterized; titanium dioxide TiO_2 powder was chosen as nanoceramic material for this experimental investigation. As well-know, this n-type semiconductor material has three different crystalline structures: anatase, rutile and brookite. From the engineering point of view, the most interesting TiO_2 structures are anatase and rutile. In this work, anatase TiO_2 was selected mainly because of its interesting photocatalytic properties that can break down many organic compounds under UV or VIS light [2,20]. Photocatalytic properties of anatase titanium dioxide were discovered by Akira Fujishima in 1967 and published in 1972 [29]. Among many photocatalysts materials, TiO_2 was the most widely studied and used in many applications because of its strong oxidizing abilities for the decomposition of organic pollutants, chemical stability, long durability, nontoxicity, low cost and transparency to visible light. These photocatalytic characteristics come from the formation of photogenerated charge carriers, i.e. holes and electrons, which occur upon the absorption of ultraviolet (UV) light corresponding to the band gap [2,27]. In Fig. 4a it is possible to observe the sub-micrometric particle size distribution of this starting powder and in Fig. 4b it is shown a SEM micrograph as well. X-ray diffraction was also chosen as characterization technique to confirm the 100% anatase crystalline phase of this raw material (Fig. 5).

3.2. Milling results and coatings

Results of AM and CM at different milling times, 30 min, 1 h and 4 h and with the two different sieved portions are presented. Table 2 with all sample references is presented below:

In Fig. 6 polymeric particles are shown. From the left to the right it is possible to observe particles that were sieved and afterwards the different particles which underwent Attrition Milling process.

Table 2
References of milled powders.

Reference	Powder type	Reference	Powder type
PR101-S1	Sieved 20–40 µm	PR101-S11	Sieved 20–40 µm + CM 4 h
PR101-S2	Sieved 60–80 µm	PR101-S12	Sieved 60–80 µm + CM 30'
PR101-S3	Sieved 20–40 µm + AM 30'	PR101-S13	Sieved 60–80 µm + CM 1 h
PR101-S4	Sieved 20–40 µm + AM 1 h	PR101-S14	Sieved 60–80 µm + CM 4 h
PR101-S5	Sieved 20–40 µm + AM 4 h	PR101-T1	Sieved 60–80 µm + TiO_2 AM 30'
PR101-S6	Sieved 60–80 µm + AM 30'	PR101-T2	Sieved 60–80 µm + TiO_2 AM 1 h
PR101-S7	Sieved 60–80 µm + AM 1 h	PR101-T3	Sieved 60–80 µm + TiO_2 AM 4 h
PR101-S8	Sieved 60–80 µm + AM 4 h	PR101-T4	Sieved 60–80 µm + TiO_2 CM 30'
PR101-S9	Sieved 20–40 µm + CM 30'	PR101-T5	Sieved 60–80 µm + TiO_2 CM 1 h
PR101-S10	Sieved 20–40 µm + CM 1 h	PR101-T6	Sieved 60–80 µm + TiO_2 CM 4 h
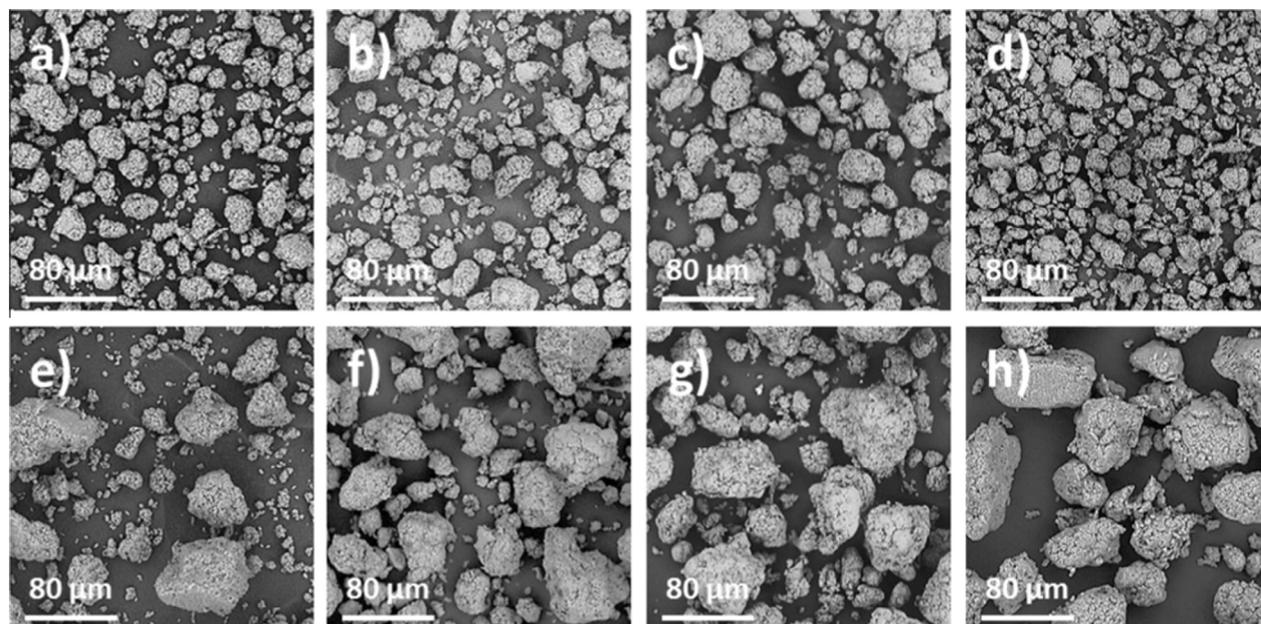
Fig. 6. AM micrographs of the sieved polymer at different times. (a) PR101-S1; (b) PR101-S3; (c) PR101-S4; (d) PR101-S5; (e) PR101-S2; (f) PR101-S6; (g) PR101-S7; (h) PR101-S8.
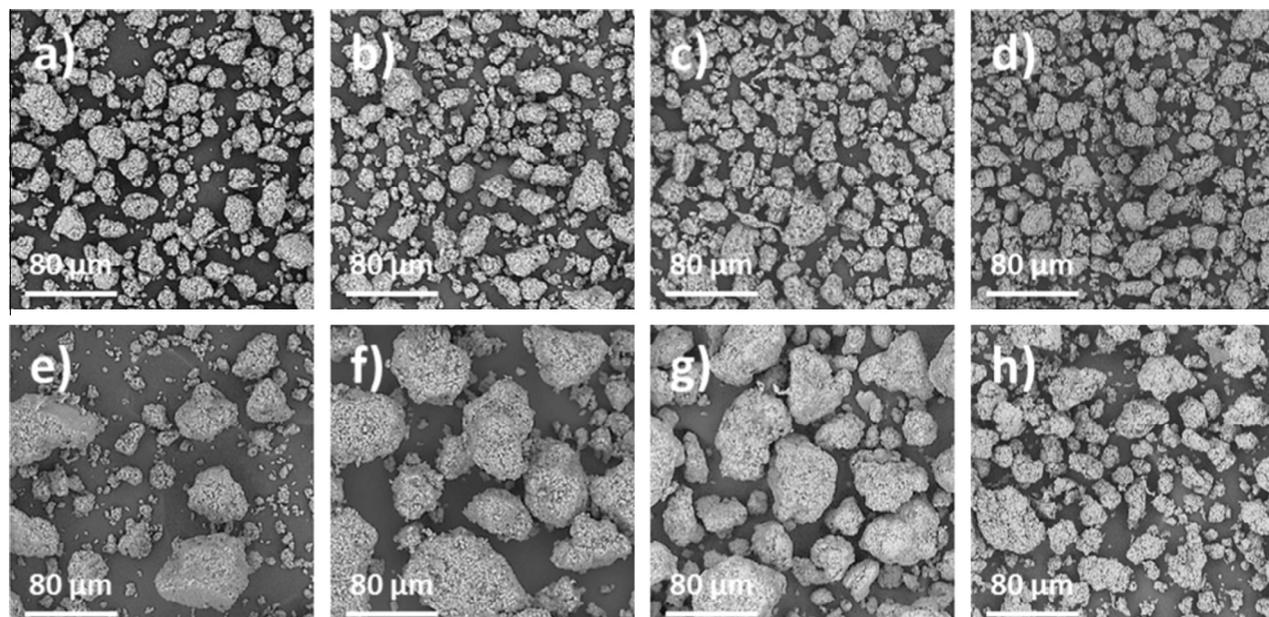
Fig. 7. CM micrographs of the sieved polymer at different times. (a) PR101-S1; (b) PR101-S9; (c) PR101-S10; (d) PR101-S11; (e) PR101-S2; (f) PR101-S12; (g) PR101-S13; (h) PR101-S14.

In these micrographs it is possible to notice the first effects of milling times. Polymeric particles sieved between 20 and 40 μm firstly present phenomena of union and finally after 4 h of AM they undergo milling process and their dimensions decrease. Regarding polymeric powder sieved 60–80 μm, particle surfaces start to deform and be more rounded; it is possible to confirm also the reduction in particle size distribution after the longest mixing time. In the subsequent Fig. 7 results of the cryomilled polymer are presented. The superficial embrittlement of particles due to low temperature causes a higher decrease in particle size distribution. The difference between AM and CM is clear: CM system is capable to decrease more particles dimensions due to the lower temperature given by liquid N_2 inside the milling environment [3,4]. The particle shapes are also influenced by the different equipments and by the temperature below the brittle–ductile transition [13]. Usually, CM offers more breaking of particles, while AM presents more plastic deformation of the surfaces. In the case of 20–40 μm sieved particles, the energy transferred by the crashes between balls, particles and vessels are lower. Results from micrographs 6 and 7, together with the purpose of the work, have led to the choice to mechanically mix with TiO_2 nanoparticles only the 60–80 μm

distributions. In fact, with this specific particle size distribution 60–80, the superficial plastic deformation of the polymeric particles is higher compared with the second studied range 20–40. So, the following mechanical union with TiO_2 nanoparticles can be favoured. Fig. 8 shows these new composite powders which can be sprayed by LP-CGS process [18–20]. It is possible to notice that after 30 min (Fig. 8a) only few titania particles are well mechanically mixed with the polymer. Therefore, this mixing time was not enough to anchor both particles and it was increased up to 4 h. In this other case (Fig. 8c), the particles size reduction was too high, particles were too much deformed and the initial morphology quite rounded and adequate for LP-CGS process was lost. One the other hand, it is possible to observe that after 1 h of AM mixing (Fig. 8b), TiO_2 nanoparticles are very well attached to the

Table 3
LP-CGS spraying conditions.

Spraying distance (mm)	Gun velocity (mm/s)	Temperature (°C)
10–50	100–500	50–500
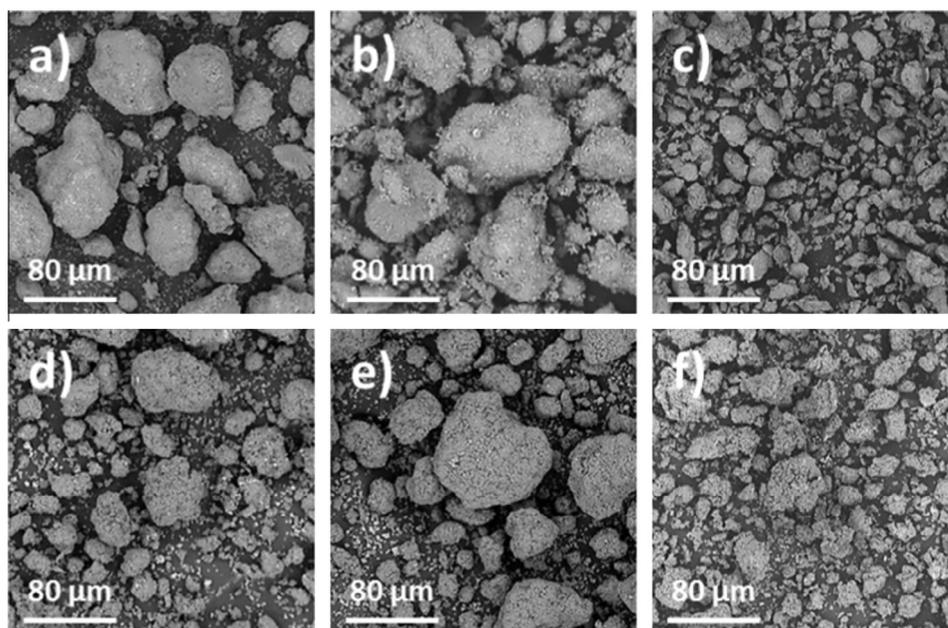
Fig. 8. Composite mixtures at various blending times by AM and CM. (a) PR101-T1; (b) PR101-T2; (c) PR101-T3; (d) PR101-T4; (e) PR101-T5; (f) PR101-T6.
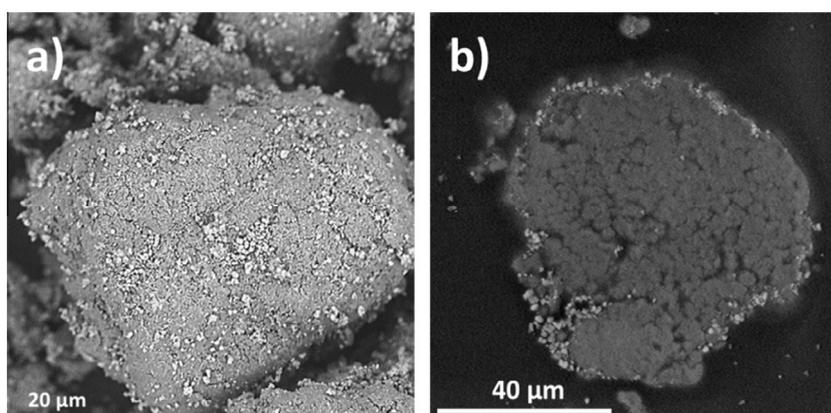
Fig. 9. SEM top surface micrograph (a) and SEM cross section micrograph (b) of PR101-T2 composite powder at higher magnifications.
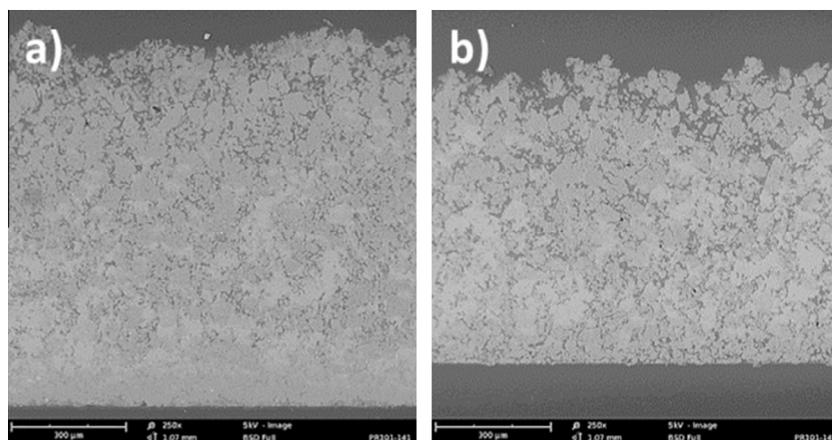
Fig. 10. SEM micrographs of coatings obtained by PR101-T2 (a) and PR101-T5 (b) blends.

polymeric surfaces and homogeneously distributed as well. For all these reasons, the optimal blending time by AM has been selected as 1 hour. This result has the same trend of a previous CPT study [2] in which the best composite mixture obtained by Low Energy Ball Milling method was achieved after 1 h of milling mechanism. The optimal composite powder, named PR101-T2, was compared with the same of 1 h by CM, PR101-T5. The difference is clear: in the second case it is present a higher embrittlement effect and this factor leads to a worse mechanical anchoring of titanium dioxide sub-micrometric particles onto the polymeric ones. In Fig. 9 it is possible to observe a micrograph at higher magnification of the best mechanically mixed composite powder, made from 60 to 80 μm sieved polymer and TiO_2 articles mixed for 1 h. In this case, particles are sufficiently deformed on the surface to let the ceramic nanoparticles be very well mechanically anchored. This powder presents also more rounded shape, which will be a good factor for LP-CGS spraying tests. Regarding CM process, the best mixture was also considered the one of 1 h because 30 min of mechanical milling are not enough for having a well anchoring and 4 h are too much because first particles deformation processes appear. For these reasons, powders PR101-T2 and PR101-T5 were the ones which were selected to be sprayed for the first time by Low Pressure Cold Gas Spray. Spraying conditions had to be found, good compromises between temperature, pressure and distances must be discovered and also good deposition parameters for the composite mixtures. The following Table 3 shows the specific parameters used for spraying these novel composite powders:

Once all these technical parameters were controlled and good deposition efficiency was obtained onto both stainless steel and polymeric substrates. The characterization presented in this work regards the second type of substrate, PS polystyrene polymer. The characterization of coatings cross sections is presented, while a second deeper investigation of mechanical properties and functional properties started to be evaluated. In Fig. 10a first coatings obtained with PR101-T2 powder are presented. On the other hand, in Fig. 10b a SEM micrograph of a coating manufactured with cryomilled PR101-T5 feedstock is shown as well. Fundamental coatings parameters such as thickness, porosity and superficial roughness were determined; they are shown in Table 4 below, together with the corresponding standard deviations:

Table 4
Coatings parameters.

	Thickness (μm)	Porosity (%)	Roughness Ra (μm)
PR101-T2	957.1 ± 20.8	12.0 ± 2.2	17.0 ± 1.4
PR101-T5	768.6 ± 19.3	9.8 ± 2.2	14.0 ± 2.6

It is possible to notice that CM coatings present lower thickness, porosity and roughness compared with AM ones. Considering that these powders possess the same particle size distribution after sieving (60–80 μm), the reason of this difference is related to the higher deformation and compacting of the material during the milling process. More dense and compacted starting particles give lower thickness and less porosity. Moreover, inside LP-CGS spraying process, particle dimensions are strictly related to the superficial roughness and subsequently final Ra values of CM coatings are lower too.

4. Conclusions

- Different ceramic–polymer composite powders were obtained and successively sprayed by Low Pressure Cold Gas Spray technique.
- The anchoring mechanism between polymer microparticles and ceramic nanoparticles during two different mixing processes such as Attrition and Cryogenic Milling was studied and explained. It was found that the mechanical anchoring of Attrition Milling was more efficient due to the plastic deformation of the surface of the polymeric particles. The behaviour of the polymer is similar to a rigid solid because the milling process temperature is below its Tg. This fact led to embrittlement effect, higher reduction of particle size and finally lower efficiency in the mechanical anchoring between polymeric particles and ceramic ones.
- The characterization of the different obtained composite powders was carried out. SEM, LS and XRD were fundamental characterization instruments to observe evolution and changes of the particles, especially during the mixing processes.
- The selected composite mixture is the one obtained sieving polymeric particles in the range 60–80 μm and milling them with TiO_2 inside Attrition Mill for 1 h. 30 min of milling time were not enough to achieve a proper anchoring among particles and 4 h are too much because of the increased number of fractured particles. Changes in particle size distribution and in shape were observed, while titania anatase crystalline phase was preserved.
- This well mechanical-bonded composite mixture which was later sprayed by Low Pressure Cold Gas Spray technology. First coatings were obtained, taking into account mechanical adhesion and CTE coefficient with the substrate, thickness, porosity and superficial roughness. Furthermore, these novel types of TiO_2 composite coatings can offer a perfect base for their applicability as photocatalysts materials.

Acknowledgements

References

[1] R. Quesada-Cabrera, A. Mills, C. O'Rourke, Action spectra of P25 TiO$_2$ and a visible light absorbing, carbon-modified titania in the photocatalytic degradation of stearic acid, Appl. Catal. B 150–151 (2014) 338–344.

[2] M. Robotti, M. Gardon, S. Dosta, A. Concustell, I.G. Cano, J.M. Guilemany, Self-cleaning, photocatalytic and superhydrophobic coatings obtained by Cold Gas Spray, Intell. Prop. Prot. IPP (2014).

[3] C. Suryanarayana, Mechanical alloying and milling, Prog. Mater Sci. 46 (2001) 1–184.

[4] P.J. Hubert, K. Kathiresan, K. Wakabayashi, Filler exfoliation and dispersion in polypropylene/as-received graphite nanocomposites via cryogenic milling, Polym. Sci. (2011) 2275.

[5] D.B. Witkin, E.J. Lavernia, Synthesis and mechanical behaviour of nanostructured materials via cryomilling, Prog. Mater Sci. (2006) 1–60.

[6] G. Zhang, A.K. Scharb, S. Tria, O. Elkedim, Tensile and tribological behaviors of PEEK/nano-SiO$_2$ composites compounded using a ball milling technique, Compos. Sci. Technol. 68 (2008) 3073–3080.

[7] M. Senna, V. Šepelák, J. Shi, B. Bauer, A. Feldhoff, V. Laporte, K.D. Becker, Introduction of oxygen vacancies and fluorine into TiO$_2$ nanoparticles by co-milling with PTFE, J. Solid State Chem. 187 (2012) 51–57.

[8] D. Olmos, C. Domínguez, P.D. Castrillo, J. Gonzalez-Benito, Crystallization and final morphology of HDPE: effect of the high energy ball milling and the presence of TiO$_2$ nanoparticles, Polymer 50 (2009) 1732–1742.

[9] J. González-Benito, G. González-Gaitano, Interfacial conformations and molecular structure of PMMA in PMMA/silica nanocomposites. Effect of high-energy ball milling, Macromolecule 41 (2008) 4777–4785.

[10] D. Olmos, E. Rodríguez-Gutiérrez, J. González-Benito, Polymer Structure and Morphology of Low Density Polyethylene Filled With Silica Nanoparticles, Wiley Online Library (2012).

[11] W. Mekprasart, W. Jarenboon, W. Pecharapa, TiO$_2$/CuPc hybrid nanocomposites prepared by low-energy ball milling for dye-sensitized solar cell application, Mater. Sci. Eng., B 172 (2010) 231–236.

[12] R. Amade, P. Heitjans, S. Indris, M. Finger, A. Haeger, D. Hesse, Defect formation during high-energy ball milling in TiO$_2$ and its relation to the photocatalytic activity, J. Photobiol. A: Chem. 207 (2009) 231–235.

[13] Y.G. Zhu, Z.Q. Li, D. Zhang, T. Tanimoto, PET/SiO$_2$ nanocomposites prepared by cryomilling, J. Polym. Sci., Part B: Polym. Phys. 44 (2006) 1161–1167.

[14] M. Fabián, G. Tyuliev, A. Feldhoff, N. Kostova, P. Kollár, S. Suzuki, F. Saito, V. Šepelák, One-step synthesis of nanocrystalline ZnO via cryomilling, Powder Technol. 235 (2013) 395–399.

[15] S. Amirkhanlou, M. Ketabchi, N. Parvin, Nanocrystalline/nanoparticle ZnO synthesized by high energy ball milling process, Mater. Lett. 86 (2012) 122–124.

[16] R.K. Sendi, S. Mahmud, Quantum size effect on ZnO nanoparticle-based discs synthesized by mechanical milling, Appl. Surf. 258 (2012) 8026–8031.

[17] D. Ma, Y.A. Akpalu, Y. Li, R.W. Siegel, L.S. Schadler, Effect of titania nanoparticles on the morphology of low density polyethylene, J. Polym. Sci., Part B: Polym. Phys. 43 (2005) 488–497.

[18] D.M. Chun, S.H. Ahn, Deposition mechanism of dry sprayed ceramic particles at room temperature using a nano-particle deposition system, Acta Mater. (2011) 2693–2703.

[19] J.B. Powers, Method for flame spraying polyethylene, 1955. Publication number: US2718473 A.

[20] M. Yamada, H. Isago, H. Nakano, M. Fukumoto, Cold spraying of TiO$_2$ photocatalyst coating with nitrogen process gas, J. Therm. Spray Technol. 19 (2010) 1218–1223.

[21] G. Bae, Y. Xiong, S. Kumar, K. Kang, C. Lee, General aspects of interface bonding in kinetic sprayed coatings, Acta Mater. 56 (2008) 4858–4868.

[22] E. Leivo, T. Wilenius, T. Kinos, P. Vuoristo, T. Mäntylä, Properties of thermally sprayed fluoropolymer PVDF, ECTFE, PFA and FEP coatings, Prog. Org. Coat. 49 (2004) 69–73.

[23] C. Mateus, S. Costil, R. Bolot, C. Coddet, Ceramic/fluoropolymer composite coatings by thermal spraying – a modification of surface properties, Surf. Coat. Technol. 191 (2005) 108–118.

[24] A.S. Alhulaifi, G.A. Buck, W.J. Arbegast, Numerical and experimental investigation of cold spray gas dynamic effects for polymer coating, J. Therm. Spray Technol. 21 (2012) 852–862.

[25] A. Moridi, S.M. Hassani-Gangaraj, M. Guagliano, M. Dao, Cold spray coating: review of material systems and future perspectives, Surf. Eng. 36 (2014) 369–395.

[26] Y. Xu, I.M. Hutchings, Cold spray deposition of thermoplastic powder, Surf. Coat. Technol. 201 (2006) 3044–3050.

[27] M. Gardon, C. Fernández-Rodríguez, D. Garzón Sousa, J.M. Doña-Rodríguez, S. Dosta, I.G. Cano, J.M. Guilemany, Photocatalytic activity of nanostructured anatase coatings obtained by cold gas spray, J. Therm. Spray Technol. 23 (2014) 1135–1141.

[28] M. Yamada, H. Isago, K. Shima, H. Nakano, M. Fukumoto. Deposition of TiO$_2$ Ceramic Particles on Cold Spray Process. International Thermal Spray Conference ITSC 2010, Proceedings.

[29] A. Fujishima, K. Honda, Electrochemical photolysis of water at a semiconductor electrode, Nature 238 (1972) 37–38.

[30] J.M. Guilemany, N. Cinca, L. Casas, E. Molins, Ordering and disordering processes in MA and MM intermetallic iron aluminade powders, J. Mater. Sci. 44 (2009) 2152–2161.

[31] N. Cinca, E. Hurtado, I.G. Cano, J.M. Guilemany, Mechanical milling of a nanostructured ductile iron powder under dry, wet and cryogenic atmospheres, Revista de Metalurgia 47 (2011) 197–204.

Paper 2: Photocatalysis

This second paper regards the powder production of micrometric ECTFE polymer and C-TiO$_2$ ceramic nanoparticles by Low Energy Ball Milling method. Mixing conditions were compared to the AM and CM parameters used in the previous paper. Each powder composition was sprayed by LP-CGS process and photocatalytic coatings were manufactured onto polymeric and metallic substrates. The manuscript already shows the first and innovative photocatalytic results of the composite products. The presence of anatase phase on the top surface of the coatings resulted to be one of the key-factors for the photocatalytic mechanism. NOx hazardous gases are degraded with high efficiency with both UV light and VIS light. Furthermore, photocatalytic performances of LP-CGS coatings resulted to be four times higher than commercial photocatalytic paint.

Photocatalytic abatement of NOx by C-TiO$_2$/polymer composite coatings obtained by low pressure cold gas spraying

M. Robotti [a,*], S. Dosta [a], C. Fernández-Rodríguez [b], M.J. Hernández-Rodríguez [b], I.G. Cano [a], E. Pulido Melián [b], J.M. Guilemany [a]

[a] CPT Thermal Spray Centre, Materials Engineering, Departament d'Enginyeria Química I Metal·lúrgica, University of Barcelona, Martí i Franquès, 1. 08028 Barcelona, Spain
[b] FEAM Grupo de Fotocatálisis y Espectroscopia Aplicada al Medioambiente, University of Las Palmas de Gran Canaria, Campus de Tafira, 35017 Las Palmas de Gran Canaria (Spain) Unit Associated to ICMS-CSIC (Seville), Spain

ARTICLE INFO

ABSTRACT

In the present work, we study the photocatalytic activity of carbon-modified TiO$_2$ (C-TiO$_2$)/polymer composite coatings obtained by low pressure cold gas spraying (LP-CGS). To produce the novel coatings, C-TiO$_2$ was mixed with a ductile material, the polymer ECTFE, by means of a low energy ball milling (LEBM) process. The LEBM system permits the mechanical anchoring of small TiO$_2$ aggregates around the large ductile polymeric particles. A well-bonded coating with good mechanical coupling was formed between the ball-milled mixture and the substrate. Photocatalytic tests showed that the LP-CGS nano-TiO$_2$ coatings actively photodegraded NO and the by-product, NO$_2$. Compared to commercial paint, the as-prepared coatings presented here enhanced photocatalytic performance.

© 2015 Elsevier B.V. All rights reserved.

1. Introduction

Indoor air pollution and urban air quality are considered to be two of the world's worst toxic pollution problems. According to the 2014 WHO report, in 2012 air pollution caused the deaths of around 7 million people worldwide [1]. In many urban areas, concentrations of atmospheric air pollutants such NOx or VOCs reach one ppm [2,3]. Of the technologies currently available to reduce the presence of these compounds in air, photocatalysis with TiO$_2$ semiconducting materials exhibits some highly attractive characteristics, such as low cost, environmentally-friendly behaviour and reduced toxicity. Small particles of TiO$_2$, in the range of 5–50 nm, catalyse the oxidation of adsorbed molecules in the presence of UV light [4,5]. Unfortunately, bare TiO$_2$ utilizes only a very small part (about 3%) of the solar light arriving at the earth's surface: the UV range. However, the visible part ($\lambda > 400$ nm) of solar radiation may also induce photocatalysis if the titania is modified with

non-metal elements [6]. Of these, nitrogen and carbon have been reported to produce the most active photocatalysts [7]. However, up until now, the nature of the carbon-induced modifications to the TiO$_2$ electronic band structure has remained unclear and the resultant enhancement of photo-catalytic activity has been attributed to either band gap narrowing [8–11] or the formation of a localized mid-gap state [11–13] in the TiO$_2$ band gap. In this work, carbon-doped TiO$_2$ (C-TiO$_2$) vlp7000 of Kronos International Inc. [14] was used as a visible sensitive C-TiO$_2$ to prepare photoactive coatings to remove NOx from air. Photo-TiO$_2$ must be immobilized in different construction materials for the photo-abatement of atmospheric NOx to be effective. Recently, different construction materials, such as ceramic tiles, blocks, paints and different concretes, with photocatalytic activity have become commercially available [15,16]. Of all these construction materials, paints have several advantages when used for immobilizing photo-TiO$_2$, since almost all surfaces in urban areas can be painted. However, paints can produce detrimental effects on the photoactivity of TiO$_2$, probably due to a masking effect [17]. Moreover, the organic components in paints can become photocatalytically degraded [18]. For these reasons, the main idea of this work is to immobilize TiO$_2$ by depositing fine particles of it onto an appropriate substrate to form a coating that maintains the original photocatalytic

* Corresponding author. Tel.: +34 934031164; fax: +34 934031164.
E-mail address: mrobotti@cptub.eu (M. Robotti).

properties of the TiO$_2$. To this end, we prepared coatings by means of low pressure cold gas spraying (LP-CGS). LP-CGS is highly competitive, fast and has a low cost; it also has the benefit of being portable. From a technical point of view, LP-CGS uses a lower particle velocity than high pressure CGS and does not require high temperatures. Unfortunately, this technology does not allow the direct spraying of a nano-powder, mainly due to the difficulty of getting the powder itself to flow or because of static agglomeration of the extremely fine particles. These factors led to the idea of developing an innovative kind of composite material; a second polymeric material, ECTFE, is used and mixed with the C-TiO$_2$. The main objective of the second polymeric material is form a softer part of the composite mixture; accommodating the titania nanoparticles around its surface, becoming deformed during the spraying process and finally promoting the formation of the coating. In this way, the need to spray a brittle ceramic material at high kinetic energies can be avoided [19]; this is the reason for the choice of a polymeric material, over other kinds of ductile materials such as aluminium or copper. During the LP-CGS process, it is possible to change different parameters such as the rate of feed of the feedstock, gas heating temperature, number of cycles, distance between cycles and pressure. Temperature and pressure are the most important features that permit the so-called *cer-pol* mixture to maintain its phases and the polymer particles to deform on impact. As mentioned above, LP-CGS presents many advantages over high-pressure CGS; especially in the case of this study in which a polymeric-ceramic composite material is used. LP-CGS does not require high pressures or temperatures that could melt the polymeric particles and produce clogging inside the nozzle or phase transformations of the TiO$_2$ anatase. Deposition can be performed both in air and in a nitrogen atmosphere; and the temperature of the substrate does not reach high temperatures. In this way, the appearance of internal stresses and deformations, as well as oxidation processes, are avoided. This new type of technology is also environmentally friendly because no dangerous gases or chemically aggressive waste is released during the procedure. The use of low pressures, along with the absence of a Duval nozzle, does not create high compression and expansion of the heated gas. This is the reason why LP-CGS transmits less kinetic energy to the particles and so they have less velocity in the flux. Another advantage of this methodology is the possibility of depositing multi-component coatings, varying the thickness of the layers. Such multilayer deposition can be useful as one material can act as a bond coat and improve the adhesion of another external layer. LP-CGS is also performed using portable and compact equipment, which is of practical importance for industrial enterprises and offers increased possibilities as well as economic advantages. Through this type of technology it is possible to spray materials which possess an elastic limit, i.e., they are able to deform. The spraying parameters can be adjusted in order to achieve the best equilibrium between distance, velocity, the capacity to transmit kinetic energy to the particles, deformation at impact with the substrate, the number of layers, and the thickness of the final coatings. Using LP-CGS, it is possible to deposit materials which undergo stresses above their elastic limit, and which in this way show plastic behaviour and deform during impact with the substrate. One of the purposes of this paper is to present a new deposition strategy for composite materials made of a polymer matrix and ceramic nanoparticles. This work represents not only an innovative approach, but also a new challenge; as the aim is to achieve a coating sprayed by LP-CGS that contains a ceramic and brittle material: TiO$_2$. The main aim is to achieve a composite coating material with multifunctional (self-cleaning, de-polluting, biocidal and photocatalytic) properties, to be sprayed onto different building materials.

2. Material and methods

2.1. Powder production, production of coatings and their characterization

Different powders were analysed: the polymer ECTFE, C-TiO$_2$ vlp7000 and three mixtures of the two obtained by low energy ball milling (LEBM). Laser scattering (LS 13 320, Universal Liquid Module) measurements were taken to determine the particle size distribution of the pure materials and their mixtures. The powders were ball-milled using a planetary mill (PM400 RETSCH) under different mixing conditions. The mixtures contained 10% by volume of C-TiO$_2$, and were produced at three different milling times: 1, 4 and 8 h, while maintaining a constant 1:1 ratio of volume/balls. Slow rates of revolution and ZrO$_2$-Y$_2$O$_3$ mixing balls with a diameter of 5 mm, mixed only the raw materials while avoiding a large reduction in the volume of the polymer particles. The coatings were deposited by means of LP-CGS Spray equipment (Dymet 423). The composite powders and coatings obtained were mounted in an epoxy resin (EpoFix, Struers) and metallographic preparation was then carried out. The cross sections were analysed using an optical microscope (Leica DMI 5000M) and observed by SEM (Pro-X, Phenom); while the phase compositions were analysed using an X'Pert PRO MPD diffractometer (PANalytical) and the RAMAN technique. Finally, the surface of the coatings was deeply studied in-depth using confocal measurements (Leica DCM3D, Leica microsystems) and the image analysis software Sensoscan. The main aim was to achieve a composite coating material with photocatalytic properties to be sprayed onto different building materials [19].

2.2. Photocatalytic experimental set-up

Fig. 1 is a schematic representation of the configuration for the photoactivity tests. The desired concentration of NOx was obtained by dilution with air of a 100 ppm concentration of NO (supplied by Air Liquide) using mass flow controllers. To add humidity, an extra air line was used which passed through a thermostatically controlled water bath. Humidity levels were controlled using a Rotronic Hygropalm probe. The total work flow was 1.2 L/min at 1 atm. The air stream contained 500 µg/L of NO and 40 µg/L of NO$_2$. The tests began after 30 min of adsorption onto the deposited photocatalyst in darkness, followed by illumination for 5 h. The light source employed was a 10 W/m^2 OSRAM Ultra Vitalux 300 W lamp. A SCHOTT filter (cut-off wavelength: 420 nm) was placed between the reactor and the lamp for the tests with visible light. NOx was quantified using a HORIBA APNA-370 N/S analyser. The results are expressed as percentages of degraded NO ([NO]/%) and selectivity of NO degradation to ionic species (S):

$$\frac{[NO]}{\%} = \frac{[NO]_{in} - [NO]_{out}}{[NO]_{in}} \times 100$$

$$S = 1 - \left(\frac{[NO_2]_{out}}{[NO]_{in} - [NO]_{out}} \right)$$

where [NO]$_{in}$ is the NO molar concentration after 30 min of adsorption, and [NO]$_{out}$ and [NO$_2$]$_{out}$ are the molar concentrations at the end of the illumination period.

3. Results and discussion

3.1. Characterization of powders and coatings

Before spraying, the powder particle size needs to be adjusted and characterized; it is fundamental to know the particle size
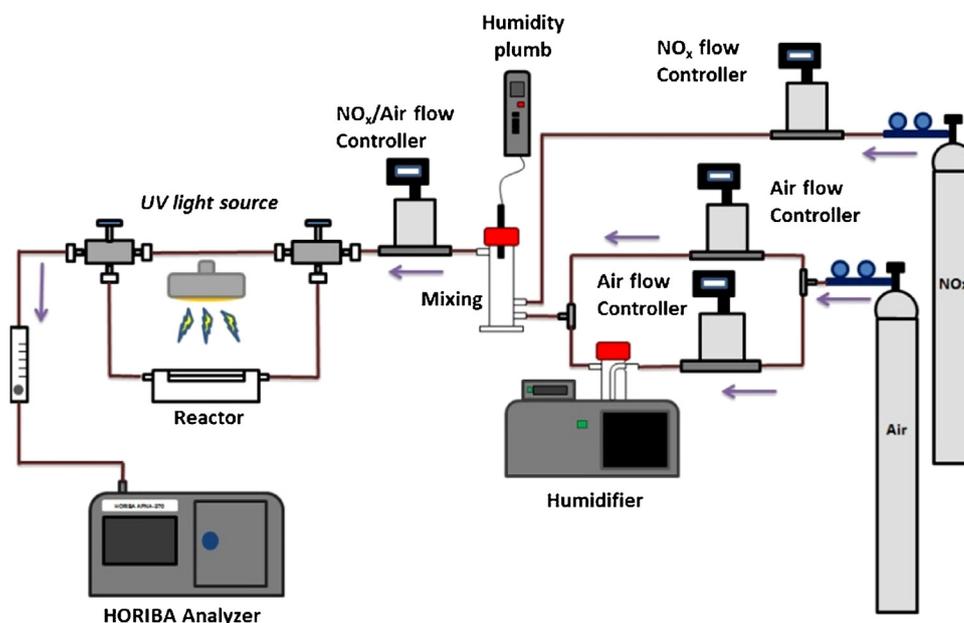
Fig. 1. Schematic representation of the photoactivity tests for NOx gases.
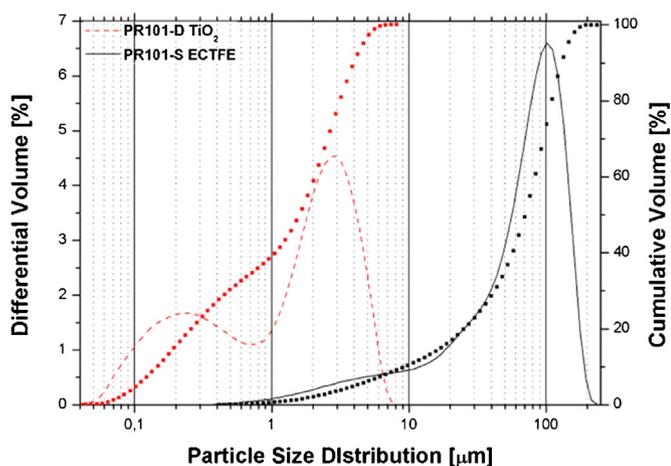
Fig. 2. Particle size distribution of the two different starting powders TiO_2 and polymer ECTFE.

Fig. 3. SEM micrograph of ECTFE polymeric powder (a) and of TiO_2 ceramic powder (b) are shown.

distribution, the morphology and the thermal properties of the materials that pass through the gun. The particle size distribution and cumulative volume of each powder were obtained using the laser scattering (LS) technique, as shown below:

As can be observed, C-TiO_2 presents a main peak centred on 3 μm and a second which consists of a tail of finer submicron particles. Meanwhile, the polymer shows a wide range of particle size, from 1 μm up to 110 μm (Fig. 2).

From the SEM top surface observation of ECTFE (Fig. 3a) it can be concluded that these polymeric particles are rough and possess an irregular shape. This intrinsic characteristic of the material could be useful inside the gas flow for the spraying process and also in the final properties of the coating produced. This soft and ductile material was mixed with the C-TiO_2; this nano-material is made of very fine particles (Fig. 3b) which readily agglomerate due to electrostatic phenomena [1]. The SEM free surface micrographs below illustrate how large quantities of nano-TiO_2 are present in small areas. The small dimensions of this powder coupled with its volatile brittle behaviour make it difficult to spray this material by LP-CGS. Faced with these problems, we decided to mix this powder feed

with a ductile one. Fig. 4 shows the SEM top surface structure of the *cer–pol* mixture obtained after 1 h of LEBM. Different magnifications allowed us to study the anchoring mechanism between nano TiO_2 and ECTFE accurately. At higher magnifications, it is possible to see that the finest ceramic particles have a greater tendency to form the composite; especially together with the finest particles of the polymer [19].

These micrographs permit us to comprehend the effect of an important parameter: milling time. The first mixture, milled for 1 h, does not present particular phenomena of the particles, but it is already possible to see a good mechanical union between the two different materials. The second mixture, milled for 4 h, shows that as the milling time increases, the polymeric particles start to deform. At high magnifications, it is possible to see the deformed surface of the particles. Increased mixing time is an advantage in this specific case, because it helps the mechanical anchoring of finer ceramic particles around the polymeric ones. In the last two micrographs, it is possible to observe an even higher deformation of the ECTFE particles; these phenomena are due to the impacts between the balls and materials, and moreover are due to the energy involved in the process, which can be transferred from the balls and walls of the vessel directly to the micrometric materials.

Fig. 5 illustrates the particle size distribution of the three different ball-milled powders. It is possible to observe the main peak of ECTFE particles and a tail of micrometric C-TiO_2. These novel
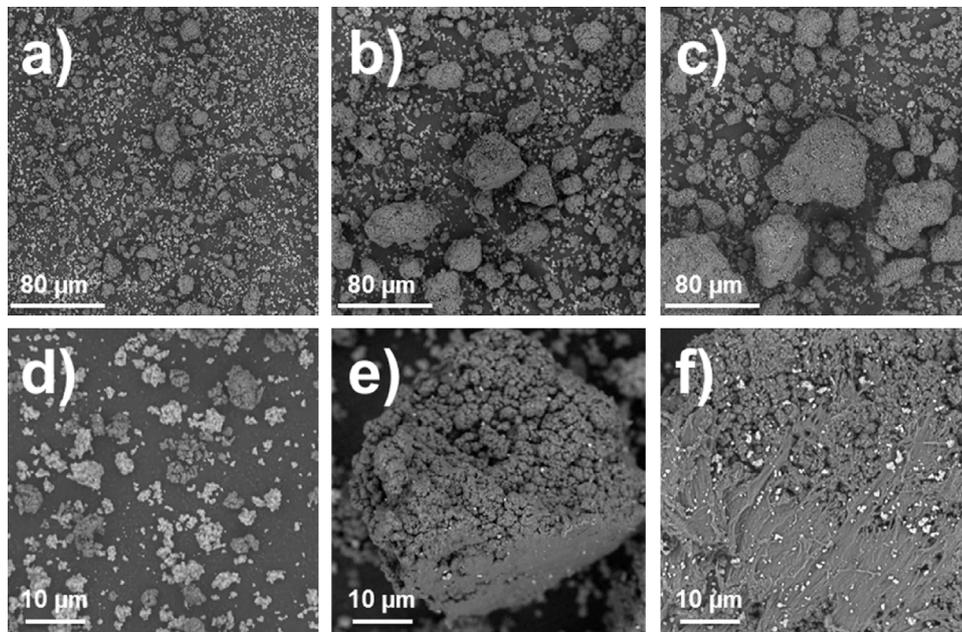
Fig. 4. SEM secondary electrons micrographs of TiO₂ and ECTFE BM 1 h (a and d), BM 4 h (b and e), BM 8 h (c and f) mixed powder at different magnifications.
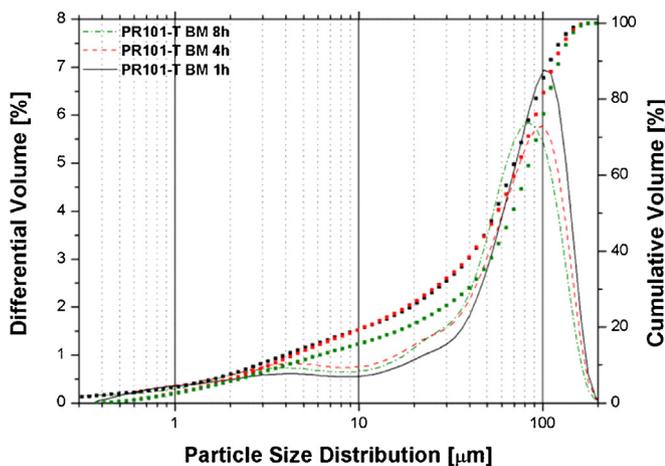
Fig. 5. Particle size distribution of the three composite mixtures.

Fig. 6. SEM top surface of the coatings.

Table 1
LP-CGS spraying parameters.

Spraying distance [mm]	Gun velocity [mm/s]	Temperature [°C]	Feed rate [g/min]
10–50	100–500	100–400	19.93

ceramic-polymeric materials were thermally sprayed using LP-CGS. Table 1 shows the specific parameters used.

The spraying conditions play an important role and it is vital to find the most appropriate ones for the specific final application. Thickness, adhesion, roughness and porosity are only a few of the parameters that depend on the spraying conditions. Once a suitable composite material is coated onto carbon steel, the substrate was changed in order to study the formation of the coating on other kinds of materials. Both stainless steel and polymeric polystyrene substrates were used. Fig. 6 illustrates how polymeric (100 × 50 × 5 mm) substrates were coated.

In this specific case, a polystyrene substrate had a coefficient of thermal expansion (CTE) that was more similar to that of the *cer-pol* composite powders than that of simple stainless steel substrate

was. Characterization of the coatings obtained is an important laboratory procedure to understand how the material adheres to the substrate, to establish the thickness of the coatings and to see how the particles are deformed. For all these reasons, different techniques were used to characterize cross section of the deposited films and their top surface. The first method was optical confocal microscopy; images of the top surface of the coatings gave the results illustrated in Fig. 7a.

Even SEM micrographs of the cross section of the materials produced were taken (Fig. 7b). It is possible to see that the coatings are well-adhered to the substrate. There are also a considerable number of pores, which could be useful for different final applications of the product. Interconnected pores close to surface can give interesting superficial properties to the composite material. The superficial roughness was studied not only via cross section micrographs, but also through SEM top surface micrographs. It is possible to observe that on the surface of the coating there are some peaks that create the final roughness. These peaks of material are due to the process of the formation of the coating itself; the first particles that impact the surface deform onto it and form a base for the particles that
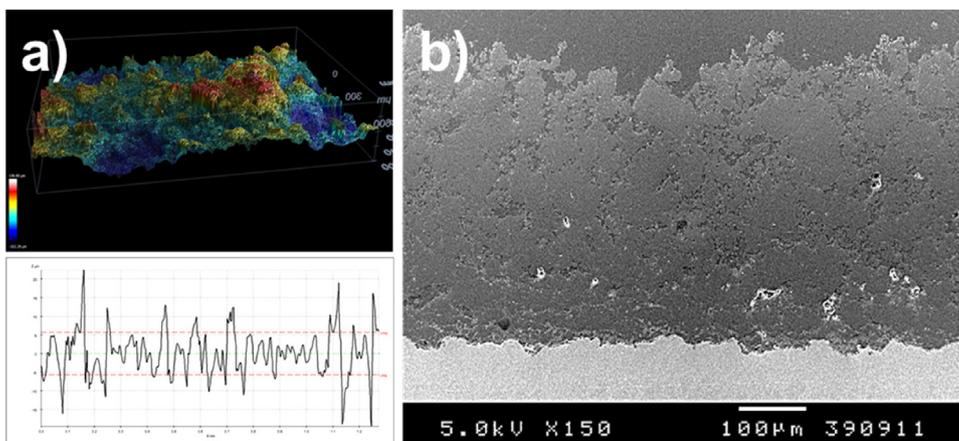
Fig. 7. OM confocal top surface of the coating (a) and SEM cross section (b).
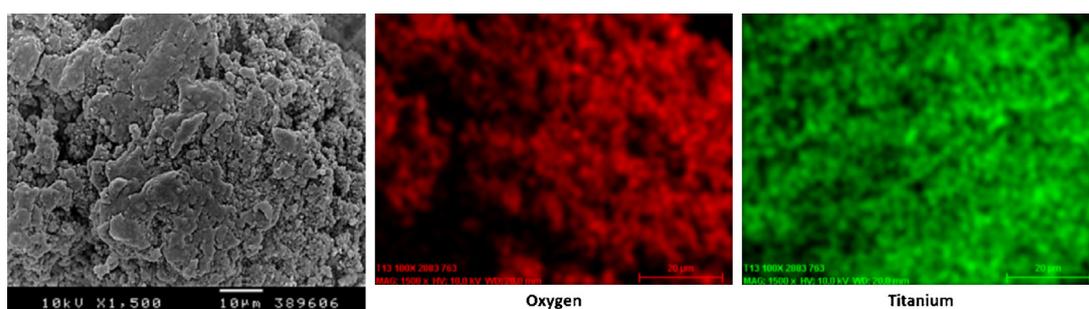
Fig. 8. SEM-EDS microanalysis of the surface.

will follow and which are still inside the gas flow. Those particles, which arrive at the surface later, impact on the initial deformed ones and attach onto them very well. Thus, larger particles impact onto the substrate, deform and represent the material onto which the following particles impact, deform and grow, forming column-like structures on the upper part of the coating. Fig. 6 shows another key factor of this work; this micrograph is extremely important because it shows the well-dispersed submicron particles and nano-particles, and moreover they are well embedded and anchored inside the polymeric and deformed matrix. This rough surface is an innovative surface and it is suitable for many scientific applications [4]. This kind of new composite ceramic-polymeric material represents a future trend for other studies and products; starting from cheap and useful nanoceramic materials such as TiO_2 [1], it is possible to exploit all the properties of the mixture and spray it using LP-CGS without modifying the original characteristics of the mixture. The characterization process continued with the study of the surface of the coatings. EDS studies were carried out, as presented in Fig. 8:

These micrographs demonstrate that nanoceramic TiO_2 is still present inside the coatings and particularly on the surface of them, which is the most important area; where the photocatalytic reactions take place. The more active C-TiO_2 particles are present on the top surface, the greater is the photocatalytic process [4]. Another fundamental step in the coating characterization consists of studying the phases present in the material. Especially in this case study, it is important to understand if there is a phase change in the titania structure. The milling mixing method, as well as the spraying process, could easily cause phase changes in the material. The aim of this work is to avoid phase changes due to impact temperatures. The main idea, therefore, is to maintain both the nanostructure and the chemical phase of TiO_2, even in the final composite material. The analysis which can
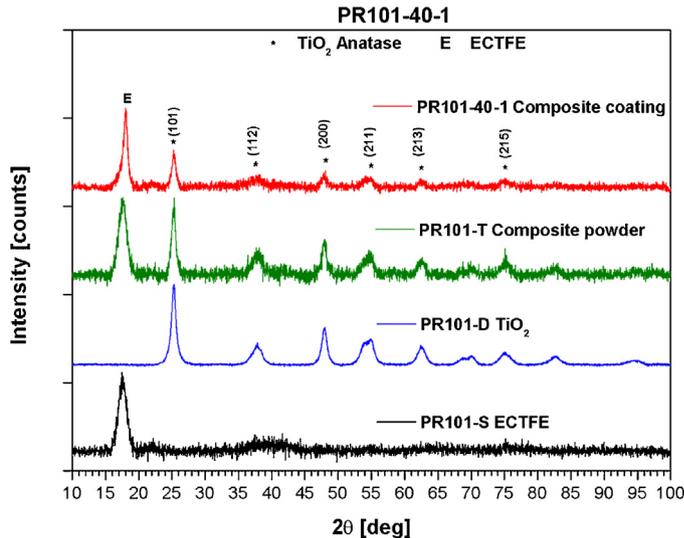
Fig. 9. XRD X-ray diffraction of ECTFE, TiO_2, mixture PR101-T and the obtained coating.

show the phases present in the coating is X-ray diffraction, XRD (Fig. 9).

The XRD patterns confirmed the maintenance of the anatase phase among the original powder, the mixture and the final product. The use of a low-temperature spraying technique such as LP-CGS avoids the phase transformation from anatase to rutile. Another important surface characterization technique is Raman spectroscopy; as can be observed in Fig. 10, this shows the presence of the TiO_2 anatase phase on the top surface of the coating. The four characteristic peaks of anatase are on in the left part of the
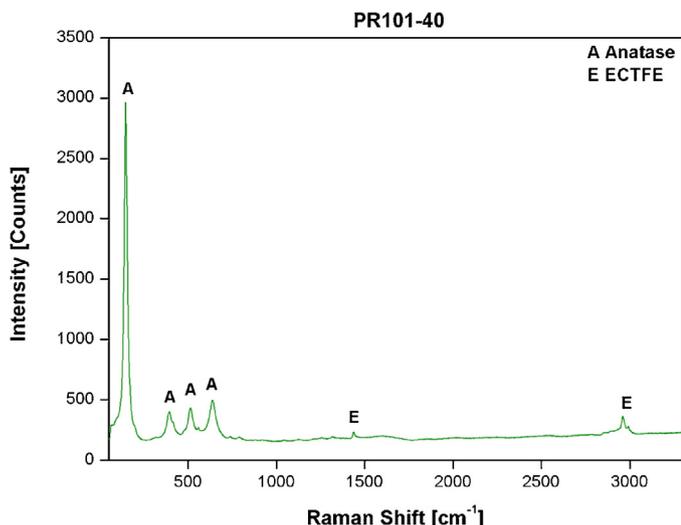
Fig. 10. Raman spectroscopy of the specimen.

Fig. 12. Photoactivity of C-TiO$_2$ sample on NO photodegradation and selectivity to transform NO$_2$ to ionic species. C-TiO$_2$ sample underwent cleaning processes between photocatalytic tests.

graph; while smaller ECTFE peaks can be seen at higher wavenumber Raman shifts.

The experimental work related to coating production demonstrated that is feasible to build up composite coatings containing nanostructured anatase particles on the top surface of the coating by means of LP-CGS. Next, proof of concept is required to demonstrate the capacity of these surfaces to degrade contaminants.

3.2. Photocatalytic tests

3.2.1. Nitrogen oxide (NOx) degradation test

In Fig. 11, it is possible to observe the photocatalytic NOx degradation in the three different case studies. Results with UV–vis light are satisfying, with degradation percentages reaching 90% and selectivity values higher than 0.8. When UV filter is applied, the NOx degradation and selectivities are lower; this phenomenon is due to the lower quantity of energy that C-TiO$_2$ coatings receive and the difficulties that photochemical reactions take place.

3.2.2. Photocatalyst stability

Quesada-Cabrera et al. [20] observed a loss of efficacy of C-TiO$_2$ samples under visible light, due to the photo-instability of the organic sensitizer. In the present work, photocatalyst stability was verified by testing the sample to different experiments of photoactivity under both UV–vis and VIS radiation. Between each test, the sample underwent cleaning procedures. These cleanings consisted in washes with water followed by 48 h of UV lighting in presence of air stream.

Fig. 13. NOx abatement comparison among produced coating and commercial paint.

Fig. 12 proves that the photoactivity under UV–vis light remains practically unchanged after a long period of time and several lighting washing cycles. Inside the visible light range, the C-TiO$_2$ material shows a decreasing capacity to oxidise NOx species after each cleaning lighting cycle. Thus, the photo-instability of the organic sensitizer of the photocatalyst is confirmed.

Fig. 11. NO degradation [%] (bars) and selectivity (▲) to transform NO to ionic species by the obtained coatings both with UV–vis (a) and vis lights (b).

3.2.3. Comparative test with commercial paint

Finally, Fig. 13 shows the results of NOx photocatalytic abatement by the 8 h LEBM coating compared with those obtained by commercial Salud Activa photocatalytic paint.

The steady-state photoactivity achieved with paint was 26.6% of NO degradation and the selectivity was 0.65. Thus, the efficiency of the coating prepared by LP-CGS is higher than that achieved with the commercial paint. These positive results regarding this final proof of concept confirms that novel feedstock formulations can be used in LP-CGS to achieve functionally active surfaces for many different fields of application, such as photocatalysis, biofouling, solar energy and photoelectrochemistry among others.

4. Conclusions

The case study presented here demonstrates that LEBM can mechanically mix nanometric C-TiO$_2$ particles with ductile polymeric ones, leading to novel composite powders. These new composite mixtures represent suitable feedstocks for LP-CGS. This spraying process represents a successful technique for building up coatings using the composite feedstock. Well-bonded micrometric coatings of the polymer ECTFE and C-TiO$_2$ anatase were sprayed onto carbon steel and PS substrates. OM, SEM micrographs demonstrated the thickness, porosity and surface area of the sprayed coatings.

The presence of functionally active nanoparticles in the top surface of the coating was confirmed by energy dispersive spectroscopy and Raman spectroscopy. Furthermore, XRD demonstrated the conservation of the fundamental photocatalytic anatase phase of TiO$_2$. Proof of concept at the lab scale demonstrated that the LP-CGS composite coatings act effectively as photocatalysts degrading NO and NO$_2$ pollutants in the gaseous phase using both UV and visible light. The yellow/brown organic species responsible for the visible light photocatalytic activity of the C-TiO$_2$ powder are readily photobleached in air, upon exposure to UV light. Finally, comparative tests with commercial photocatalytic paint showed that the as-prepared coatings presented here had enhanced photocatalytic performance. This novel line of powder and coating production through LP-CGS represents a promising direction for many ceramic oxide active nanoparticles.

Acknowledgements

References

[1] 7 Million Premature Deaths Annually Linked to Air Pollution, WHO report, March 2014.

[2] P. Qiu, H. Tian, C. Zhu, K. Liu, J. Gao, J. Zhou, An elaborate high resolution emission inventory of primary air pollutants for the Central Plain Urban Agglomeration of China, Atmos. Environ. 86 (2014) 93–101.

[3] B. Zhao, S.X. Wang, H. Liu, J.Y. Xu, K. Fu, Z. Klimont, J.M. Hao, K.B. He, J. Cofala, M. Amann, NOx emissions in China: historical trends and future perspectives, Atmos. Chem. Phys. 13 (2013) 9869–9897.

[4] K. Nakata, A. Fujishima, TiO$_2$ photocatalysis: design and applications, J. Photochem. Photobiol. C. 13 (2012) 169–189.

[5] A.L. Linsebigler, G. Lu, J.T. Yates, Photocatalysis on TiO$_2$ surfaces: principles, mechanisms, and selected results, Chem. Rev. 95 (1995) 735–758.

[6] L.G. Devi, R. Kavitha, A review on non metal ion doped titania for the photocatalytic degradation of organic pollutants under UV/solar light: role of photogenerated charge carrier dynamics in enhancing the activity, Appl. Catal. B: Environ. 140–141 (2013) 559–587.

[7] M.V. Dozzi, E. Selli, Reviews, J. Photochem. Photobiol. C: Photochem. 14 (2013) 13–28.

[8] H. Wang, P. Lewis James, Effects of dopant states on photoactivity in carbon-doped TiO$_2$, J. Phys. Condens. Matter 17 (2005) L209–L213.

[9] S.U.M. Khan, M. Al-Shahry, W.B. Ingler Jr., Science 297 (2002) 2243–2244.

[10] E. Borborini, A.M. Conti, I. Kholmanov, P. Piseri, A. Podestà, P. Milani, C. Cepek, O. Sakho, R. Macovez, M. Sancrotti, Nanostructured TiO$_2$ films with 2 eV optical gap, Adv. Mater. 17 (2005) 1842–1846.

[11] C. Xu, Y.A. Shaban, W.B. Ingler Jr., S.U.M. Khan, Nanotube enhanced photoresponse of carbon modified (CM)-n-TiO$_2$ for efficient water splitting, Sol. Energy Mater. Solar Cells 91 (2007) 938–943.

[12] X. Wang, S. Meng, X. Zhang, H. Wang, W. Zhong, Q. Du, Multi-type carbon doping of TiO$_2$ photocatalyst, Chem. Phys. Lett. 444 (2007) 292–296.

[13] Y. Li, D.S. Hwang, N.H. Lee, S.L. Kim, Synthesis and characterization of carbon-doped titania as an artificial solar light sensitive photocatalyst, Chem. Phys. Lett. 404 (2005) 25–29.

[14] J. Orth-Gerber, H. Kisch, Titanium dioxide photocatalyst containing carbon and method for its production, U.S. Pat. Appl. Publ. US 2,005,226,761 (2005), p. 19.

[15] R. Cucitore, S. Cangiano, L. Cassar, High durability photocatalytic paving for reducing urban polluting agents, WO/2006/000565 (2006).

[16] Y. Murata, H. Tawara, H. Obata, K. Murata, NOx-cleaning paving block, EP0786283 (2003).

[17] C. Águia, J. Ângelo, L.M. Madeira, A. Mendes, Influence of photocatalytic paint components on the photoactivity of P25 towards NO abatement, Catal. Today 151 (2010) 77–83.

[18] C. Águia, J. Ângelo, L.M. Madeira, A. Mendes, Influence of Paint components on photoactivity of P25 titania toward NO abatement, Polym. Degrad. Stab. 96 (2011) 898–906.

[19] M. Robotti, M. Gardon, S. Dosta, A. Concustell, I.G. Cano, J.M. Guilemany, Self-cleaning, photocatalytic and superhydrophobic coatings obtained by Cold Gas Spray, in: Intellectual Property Protection IPP, March 2014.

[20] R. Quesada-Cabrera, A. Mills, C. O'Rourke, Action spectra of P25 TiO$_2$ and a visible light absorbing, carbon-modified titania in the photocatalytic degradation of stearic acid, Appl. Catal. B: Environ. 150–151 (2014) 338–344.

Additional experiments were carried out on the polymeric-ceramic composite coatings in order to test their multifunctional properties.

Photocatalytic NOx degradation:

The standard NOx concentration used in all experiments was 500 ppb. In order to study the photocatalytic response of the composite coatings in a wider working range, 250 and 750 ppb initial gas concentrations were also selected. Graph on Fig. 24 demonstrates that lower and higher NOx concentrations do not represent a problem for LP-CGS coatings. The NOx degradation and selectivity values are kept high.
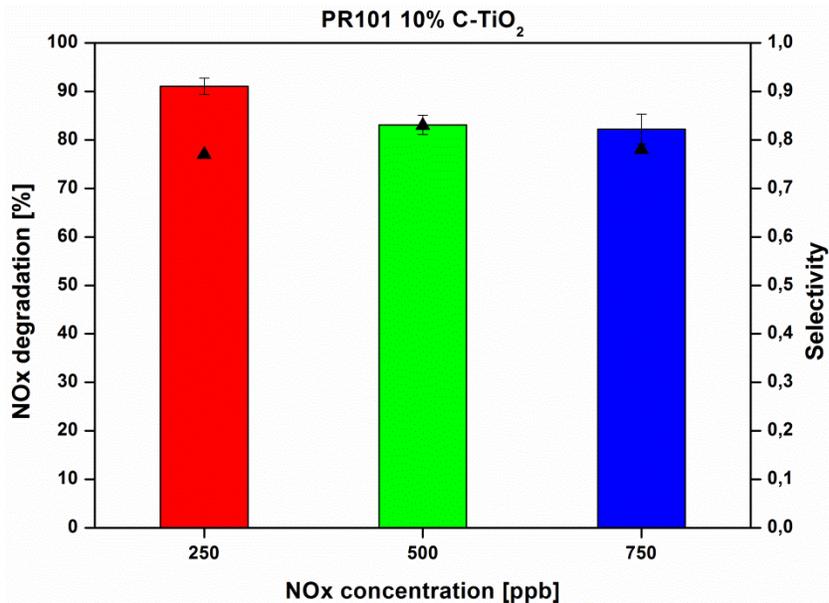
Fig. 24 Photoactivity of LP-CGS coatings toward different NOx concentrations

The higher photoactivity of carbon doped titanium dioxide was confirmed through another photocatalytic experiment. Two mixtures made by ductile polymer and P25 TiO_2 and SnO_2 catalysts were produced with the same milling conditions and tested in heterogeneous photocatalysis. Fig. 25 confirms that the doping method is really capable to increase the photocatalytic performances compared to a commercial P25 TiO_2 which possesses only 80% of anatase crystalline phase. The catalyst with lower photocatalytic activity resulted to be SnO_2 and this fact is related to its higher band gap energy compared to the other ones. The high is the

energy difference between valence and conduction band, the high is the quantity of energy that photons of light should give to promote the electron transfer to the conduction band and consequently the photocatalytic reactions.
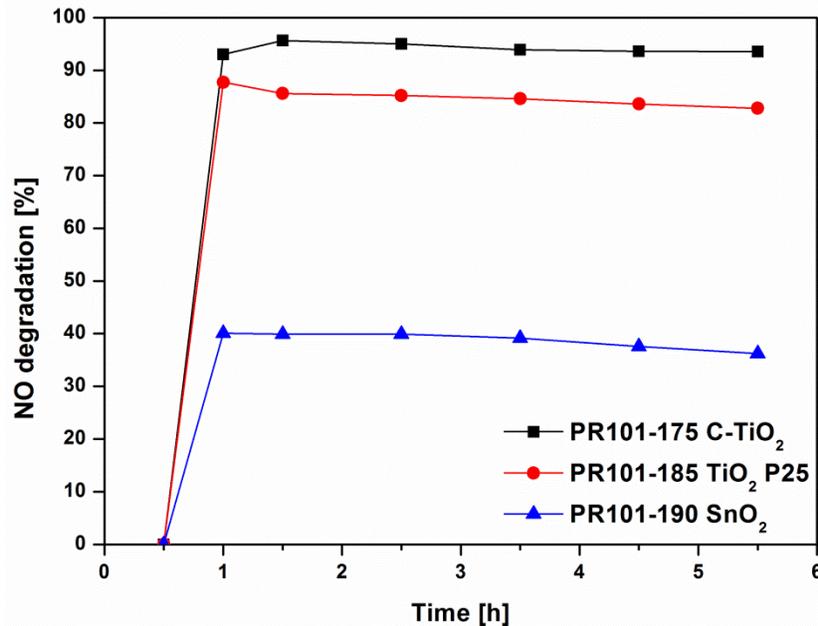
Fig. 25 Comparison among different catalyst materials (C-TiO$_2$, P25 TiO$_2$ and SnO$_2$)

In Fig. 26 it is reported the photocatalytic activity under UV and VIS light after 5 hours of experiment. Two coating deposition technique are compared: conventional dip coating and LP-CGS. With UV light it is possible to notice that these techniques gave similar results using C-TiO$_2$ catalyst. Elimination of NOx is very high and rapid. The second studied catalyst P25 TiO$_2$ gave lower results due to its lower content of crystalline anatase phase compared to C-TiO$_2$. The performances of these deposited coatings were compared with two commercial paints and the efficiencies are three and four times higher with UV light. Photocatalytic results with VIS light resulted to be even better. LP-CGS coatings are able to main high NOx degradation levels thanks to its carbon doping. Dip coating present a significant decrease, which is still studied and probably it is due to a loss of carbon doping from the TiO$_2$. Commercial paints are almost not active in the visible light range.
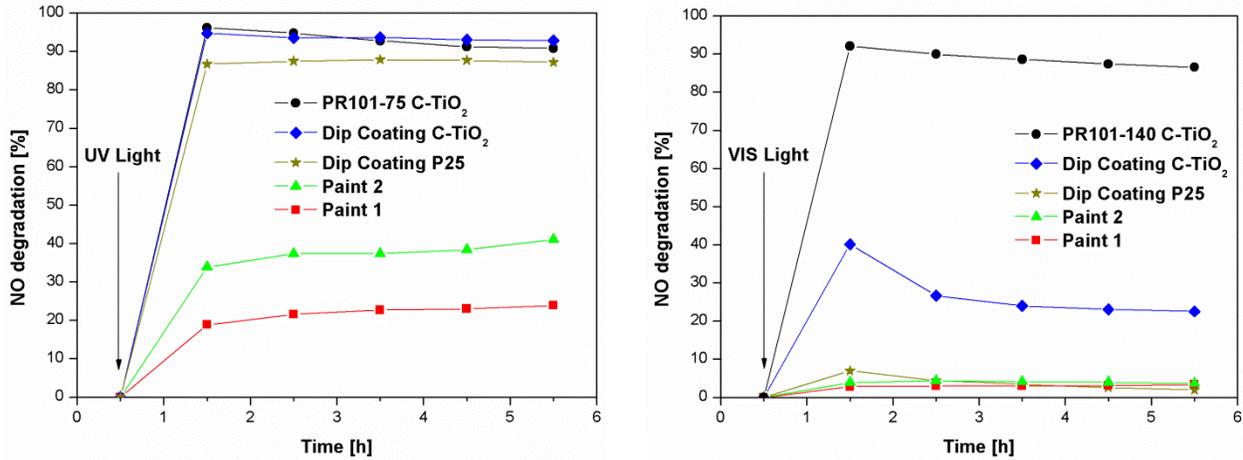
Fig. 26 UV - VIS light comparison after 5 hours test

These experiments were extended up to 24 hours to study the photocatalytic durability of the manufactured products. These types of tests are the ones which get closer to a possible real application. The results are reported in Fig. 27 and follow the same trend of the previous ones of 5 hours.
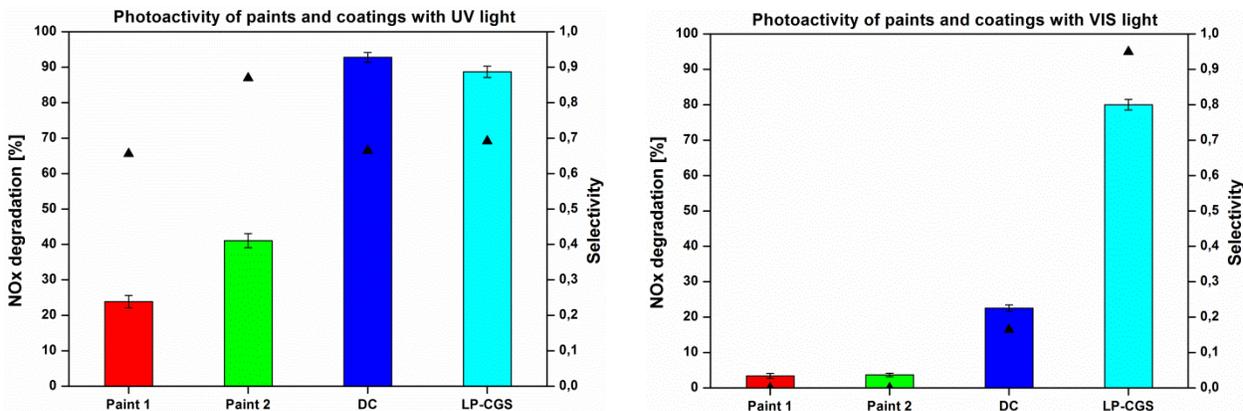
Fig. 27 UV - VIS light comparison after 24 hours test

These important results increase the value of LP-CGS manufactured coatings, especially for outdoor and indoor applications in the smart cities field of the near future. In fact, these materials can be applied in photocatalytic areas, i. e. quarters of cities, in particular in the buildings facades, roofs, pedestrian zones and indoor environments such of offices or houses to purify the contaminated air. Fig. 28 reports the results obtained from the different compositions resulting from the LEBM milling system. The volume quantity of carbon doped titanium dioxide was

76

increased up to 50% in order to boost even more the presence of this photocatalytic material inside the final coating.
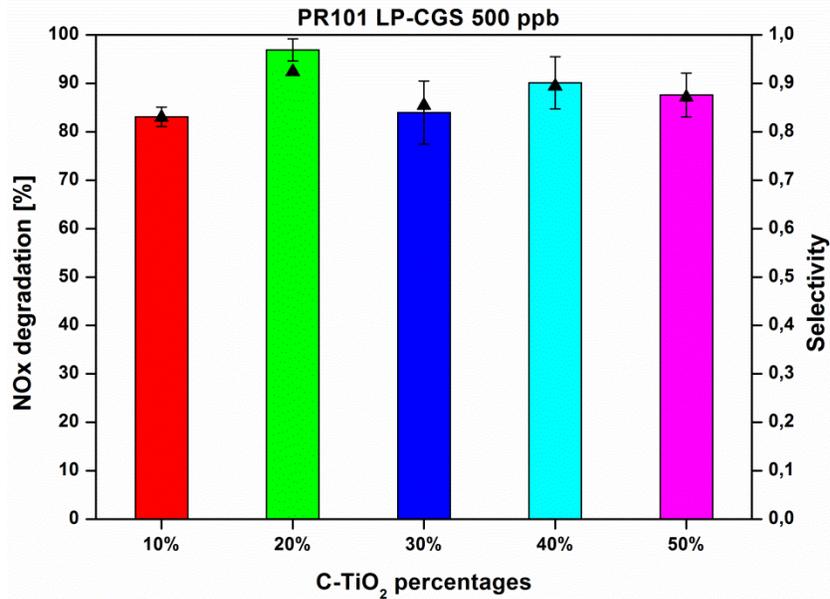
Fig. 28 NOx abatement of different C-TiO$_2$/polymer composite LP-CGS coatings

All the various compositions were sprayed by LP-CGS and gave excellent photocatalytic results toward NOx gases. It is possible to notice a slight increasing trend that follows the percentage of the catalyst material. Once passed the 40%, there reduction occurs; this fact is also related to the deposition efficiency of the composite powder by LP-CGS process. In fact, all the percentages of C-TiO$_2$ in the final coatings were confirmed by EDS, but the last one of 50% which was slightly lower. This phenomenon is strictly related to the spraying process, in particular increasing the percentage of ceramic material the deposition efficiency decreased because the ceramic particles not mechanically blended increased and gave as result erosion phenomena during the spraying deposition.

Contact angle results:

Static contact angles of LP-CGS sprayed coatings were determined during this PhD thesis. Fig. 29 reports the images of 5 µl droplets of ultrapure Milli-Q water in function of the time.
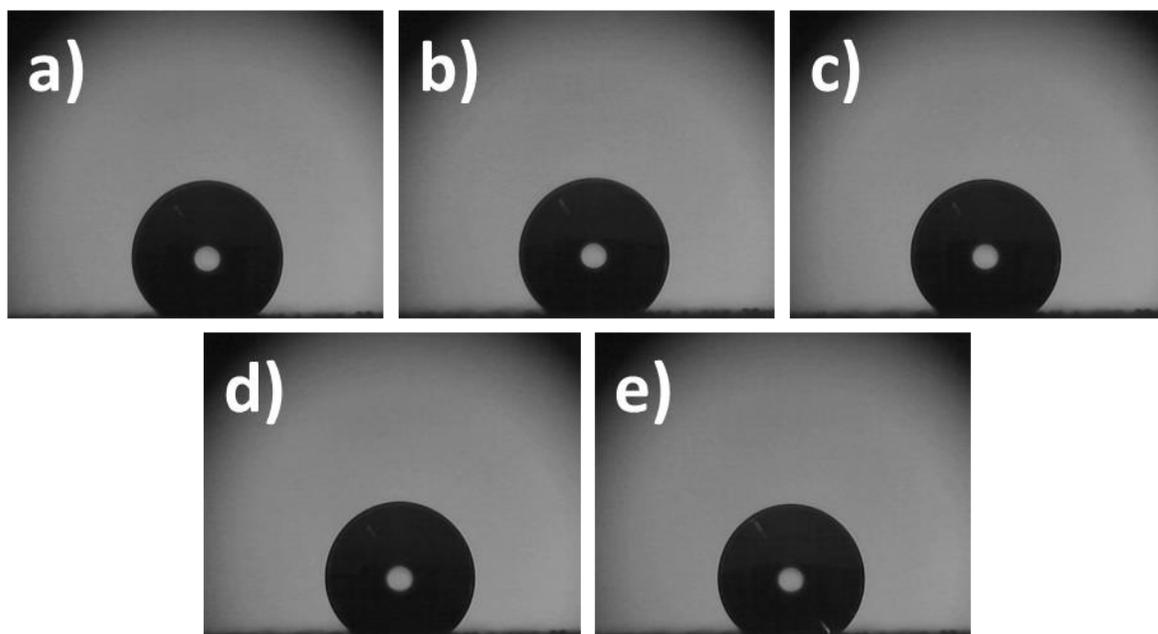
Fig. 29 Water droplets versus time: a) 0.5 min; b) 1 min; c) 2 min; d) 3 min and e) 5 min

There is no significant change of the static contact angles with the time. Contact angle from 90° to 150° determine hydrophobic surfaces, while layers having angles higher than 150° are considered superhydrophobic. As confirmed in Tab. 7, the coatings resulted to be hydrophobic, with an average value of 134.5°.

Tab.7 Static contact angles and standard deviation in function of time

Time [min]	Static contact angle [°]	Standard deviation [°]
0.5	136.1	3.9
1	134.9	2.6
2	134.5	2.4
3	133.9	2.3
5	133.2	2.6

These results increase the functionality of the coatings because they achieve a self-cleaning property. This property is highly interesting for the photocatalytic application of these composite materials. Usually, the active surface accumulates residual products from the photocatalytic reactions (e.g. organic molecules, nitrates, etc.), but with just small quantity of water the surface can be cleaned and the accumulated species can be removed. That means that from the

combination of common rain and LP-CGS advanced coatings, a surface cleaning process can take place. After that, the photocatalytic area will be active again and the hazardous gas degradation process can continue.

Taber test experiment:

Taber rotary platform abrasion test was carried out onto LP-CGS composite coatings to characterise the wear resistance of these materials. Abrasive CS10 wheels, specific to evaluate organic coatings and paints, were used during the experiment.
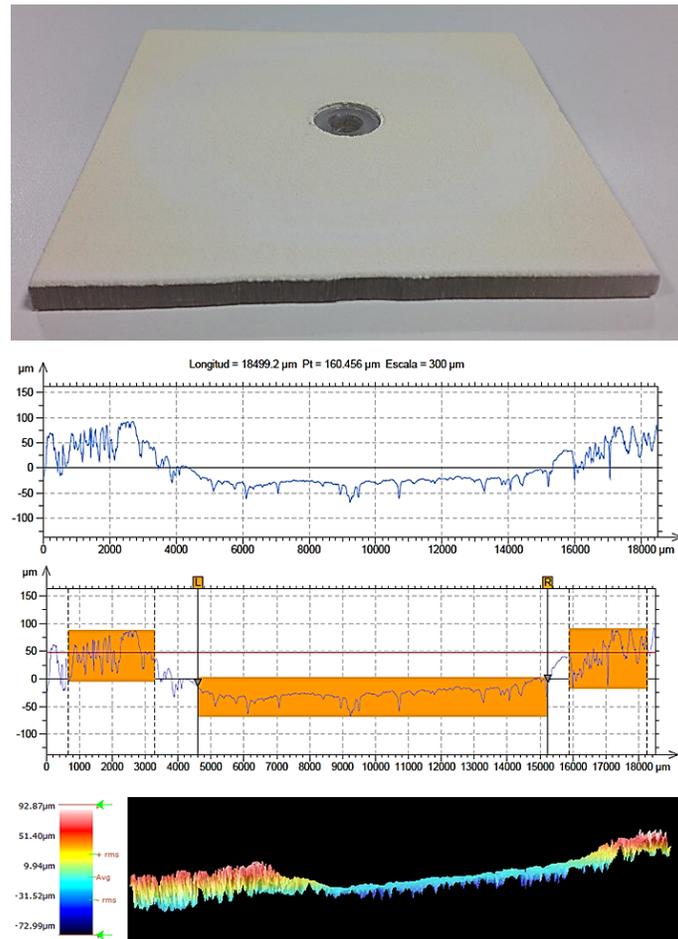
Fig. 30 Wear track reconstruction by confocal optical microscope

This Fig. 30 shows the wear track profile and 3D confocal optical microscope image of the surface of the coating after 2000 cycles of Taber test (PR101-175 sample). All values at each step (500, 1000, 1500 and 2000 cycles) and at two different weights, i.e. 4.9 and 9.8 N, were analysed. The result is reported in Fig. 31 below.
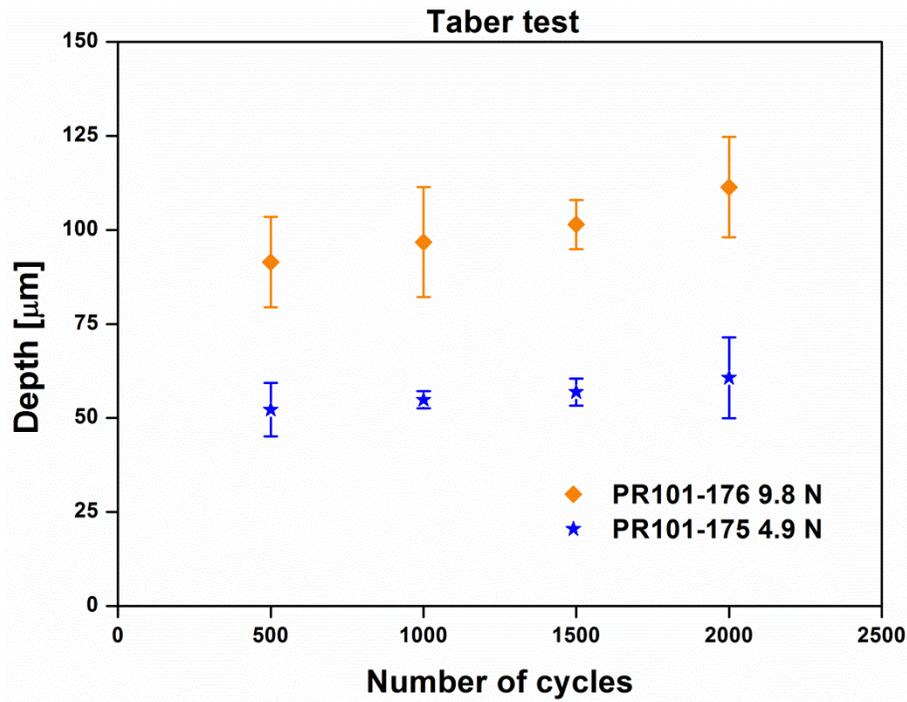
Fig. 31 Wear track depth vs number of cycles during abrasion Taber test

The values of the samples tested with different conditions gave as result linear trends. In the most abrasive case with the weight of 9.8 N, the coatings lost 100 µm in depth, which is acceptable considering that the coating thickness can vary between 200 and 900 µm depending on the spraying conditions.

This third paper focuses on the photoelectrocatalytic properties of three different titanium dioxide powders thermally sprayed by APS technique. Differences in composition between starting feedstocks powder and deposited coatings were analysed. Particular attention was dedicated to the percentage of crystalline phases (anatase and rutile) and their consequential effect on the photocatalytic properties. It was discovered that the sum of crystalline titanium dioxide phases is the main responsible of the photocatalytic water purification process. On the other hand, amorphous phases present inside the final coatings do not have significant effect on this functional characteristic of the APS coatings. The manufactured photoanodes were able to degrade and purify water from AO7 azo dye in 3 hours. This second research based on photocatalytic titanium oxide functional materials represents a new trend to follow in the near future, especially for the smart cities sector.

Influence of atmospheric plasma spraying on the solar photoelectro-catalytic properties of TiO$_2$ coatings

Sergi Dosta [a,*], Marco Robotti [a], Sergi Garcia-Segura [b,**], Enric Brillas [b], Irene Garcia Cano [a], Josep Maria Guilemany [a]

[a] CPT Thermal Spray Center, Materials Engineering, Departament d'Enginyeria Química I Metal·lúrgica, Universitat de Barcelona, Martí i Franquès 1, E-08028 Barcelona, Spain
[b] Laboratori d'Electroquímica dels Materials i del Medi Ambient, Departament de Química Física, Facultat de Química, Universitat de Barcelona, Martí i Franquès 1, E-08028 Barcelona, Spain

ABSTRACT

Titanium dioxide is a widely available material which possesses outstanding properties, chemical stability and low cost. This paper reports the synthesis of nine TiO$_2$ coating from three commercial TiO$_2$ rutile and anatase and TiO$_{2-x}$ sub-oxide powders onto Inconel alloy substrates by means of atmospheric plasma spray (APS). The influence of this thermally-activating technique on TiO$_2$ powder feedstocks, the role of its spraying conditions as well as the importance of the final active behavior of the coatings were studied. The performance of the coatings as photoanodes in the solar photoelectrocatalysis (SPEC) treatment of a model azo dye was explored. APS spraying parameters were selected in order to achieve a well-bonded coating, a determined thickness and a specific surface roughness. Moreover, Argon feeding gas of plasma torch played an important role in the quick melting process, particularly related to the heat transferred to the TiO$_2$ particles and the achievement of non-stoichiometric TiO$_2$. The prepared coatings were coupled to an air-diffusion cathode inside a photoelectrochemical cell and directly exposed to sunlight irradiation. Through XRD, SEM and surface characterization of the different coatings, the properties of the best TiO$_2$ material for the dye degradation by SPEC were elucidated.

© 2016 Elsevier B.V. All rights reserved.

1. Introduction

Titanium dioxide (TiO$_2$) is one of the materials of the next future due to their mechanic characteristics, biocompatibility and high stability and photocatalytic properties [1]. Taking advantage of such photocatalytic properties, TiO$_2$ can be employed in a wide spectrum of different advanced functional material applications such as auto-cleanable surfaces or decontamination devices to improve environmental quality [1–3]. The photocatalytic properties of TiO$_2$ are related to its semiconductor condition. When TiO$_2$ is irradiated with UV light, the transition of an electron from the filled valence band to the empty conduction band is promoted by Reaction (1), with an energy band gap of 3.2 eV, generating highly oxidative holes (h$_{vb}^+$) and reductive electrons (e$_{cb}^-$) [1,4]. The holes thus formed can react with water either from air humidity or from an aque-

ous media generating hydroxyl radical ($^\bullet$OH) from Reaction (2), the second most oxidizing species known after fluorine [3–5].

$$TiO_2 + h\nu \rightarrow e_{cb}^- + h_{vb}^+ \qquad (1)$$

$$h_{vb}^+ + H_2O \rightarrow {}^\bullet OH + H^+ \qquad (2)$$

However, the photocatalytic activity is strongly lost due to the fast recombination of electrons promoted to the valence band either with unreacted holes by Reaction (3), returning to the ground state [4,5].

$$e_{cb}^- + h_{vb}^+ \rightarrow TiO_2 + heat \qquad (3)$$

It is known that the specific area of TiO$_2$ irradiated plays an important role on its photocatalytic efficiency. A higher area allows a major promotion of Reaction (1) to compensate the efficiency lost by Reaction (3) and hence, TiO$_2$ nanoparticles present better photocatalytic performances than bigger shapes [1,6]. Despite this advantage, the problematic manipulation of TiO$_2$ nanoparticles along with their possible health hazardous effects [7,8], and the difficult recovery after usage [9,10] have avoided the application of these functional photocatalytic materials [2]. Supporting

the nanoparticles onto substrates has been proposed as a possible solution to the aforementioned handicap [11–13]. However, the considerable diminution of exposed area to UV illumination owing to the formation of nanoparticles conglomerates mined the photocatalytic efficiency of the resulting coating [14,15].

During the last years, photoelectrocatalysis (PEC) has been considered a valuable advanced oxidation process (AOP) to solve the nanoparticles handicaps and the loss in photocatalytic efficiency of easily operable surfaces of TiO$_2$ such as thin-films [16–21], nanotubes [22–26], or coral structures [27,28]. The application of either a constant bias anodic potential [17,22] or a low constant anodic current density (j_{anod}) [19,29] to the TiO$_2$ subjected to UV illumination in PEC allows extracting the photoinduced electrons by an external electrical circuit, thus inhibiting the recombination Reaction (3) and consequently, improving the photocatalytic performance [16,29,30]. Nevertheless, to homogenize the electric distribution onto the TiO$_2$ surface, it is highly recommended the use of a conductive substrate like a metal in contact with TiO$_2$. The preparation of stable TiO$_2$ coatings by affordable technologies is the last challenge to overcome [17,19,21,29]. In this context, atmospheric plasma spray (APS) is a technique that produces highly stable coatings, particle by particle from molten, semi-molten or solid particles onto a substrate. Previous studies have shown that it possesses ability enough to coat large areas in short manufacturing time with an excellent specific surface layer, which is expected to improve the photocatalytic performance of TiO$_2$ [31,32]. The control of the synthesis parameters in APS is fundamental since they directly affect the surface characteristics and the phase composition of the coatings, thus allowing modulating the intrinsic properties of prepared TiO$_2$ [33].

The main aim of the present work is to prove the applicability of APS to obtain highly stable TiO$_2$ coatings with a wide range of structural characteristics for their application as photoanodes. The influence of the synthesis parameters on the photoelectrocatalytic performances of the different TiO$_2$ coatings was evaluated by means of the decolorization efficiency of a solution of a model azo dye like Acid Orange 7 (AO7) using natural solar light as inexpensive and renewable UV source in the so-called solar photoelectrocatalysis (SPEC) process.

2. Experimental

2.1. APS technology and TiO$_2$ coating

Thermal spray processes represent advanced techniques for coatings manufacturing. Inside this wide field, APS is known as particle-by-particle depositing method of molten, semi-molten or solid micrometric materials onto a substrate. The powder feedstock material to be sprayed is accelerated by means of a high energetic stream. The high temperatures (5000–20000 °C) and particles velocities (100–600 m s^{-1}) of the plasma jet permit to melt materials with a high melting point. During the permanence time of the particles in the hot zone of plasma jet, mixing and homogenization phenomena occur and facilitate the following deposition and coating build-up steps. The quality of coatings strongly depends on spraying parameters such as powder particle size distribution, velocities, stand-off distance, gas stream temperature, transferred heat, coefficient of thermal expansion, heat and mass flows. Particles deformation in-flight behavior of the sprayed particles is fundamental to achieve good bonding, desired thickness and final top surface roughness of the products.

To prepare the TiO$_2$ coatings, an APS A-3000 system with an F4 plasma torch was used, together with an ABB three-dimensional 3D robot. This facility permits to reach high deposition efficiencies, coat large areas of different substrates in low manufacturing

Table 1
Spraying conditions values for different samples.

Sample	Intensity [A]	Ar/H$_2$ ratio	Distance [mm]
A1	400	2.9	140
A2	600	2.9	120
A3	600	3.4	100
B1	400	2.9	140
B2	600	2.9	120
B3	600	3.4	100
C1	400	2.9	140
C2	600	2.9	120
C3	600	3.4	100

time and produce specific surface active layers. Different Ar/H$_2$ gas mixtures were used and they influence the heat transferred to the particles during their permanence inside the plasma. The Ar/H$_2$ ratios were modified, together with the plasma intensity, in order to change the phase composition of the coatings.

2.2. Chemicals

TiO$_2$ rutile (Powder A) and anatase (Powder C) commercial powders were both supplied by Sulzer Metco, whereas TiO$_{2-x}$ sub-oxide (Powder B) commercial powder was supplied by Starck Amperit. These nano-agglomerated powders were used as starting feedstocks to manufacture the final coatings using Inconel alloy as substrate. Table 1 summarizes the spraying conditions that were used to obtain the final TiO$_2$ coatings.

Pure azo dye AO7 was purchased from Acros Organics and used as received to test the photocatalytic activity of the synthesized TiO$_2$ coating by APS. Sodium sulfate used as background electrolyte to improve the conductivity of test solutions was of analytical grade supplied by Fluka. Synthetic dye solutions were prepared with high-purity water obtained from a Millipore Milli-Q system with resistivity >18 MΩ cm at 25 °C and their pH was adjusted to 7.0 with analytical grade sulfuric acid or analytical sodium hydroxide, both supplied by Merck.

2.3. SPEC tests

The photoelectrochemical reactor consisted in an undivided, open and cylindrical cell with a double jacket in which external water circulated to maintain the solution temperature at 35 °C using a Thermo Electron Corporation HAAKE DC 10 thermostat to avoid water evaporation under sunlight exposition as described in previous work [29]. These trials were carried out under vigorous stirring with a magnetic bar at 800 rpm to ensure homogenization and the transport of reactants toward/from the TiO$_2$ coating used as electrode. The different synthesized TiO$_2$ coatings were used separately as photoanodes with 5 cm^2 electroactive area exposed to sunlight and tilted 41° from the solution surface to better collect the direct sun rays in our laboratory of Barcelona (latitude: 41° 21′N, longitude: 2° 10′E). The cathode was a 3 cm^2 carbon-PTFE air-diffusion electrode supplied by E-TEK and mounted as described elsewhere [34]. This cathode was fed with air pumped at 300 mL min^{-1} to generate H$_2$O$_2$ from Reaction (4). At the anodic current density of j_{anod} = 1.0 mA cm^{-2}, 1.66 mM of H$_2$O$_2$ were detected in solution after 180 min of treatment, indifferently of the photoanode used. This concentration represents about a 60% of the 2.76 mM H$_2$O$_2$ expected for a 100% current efficiency, probably due to its oxidation to O$_2$ gas at the TiO$_2$ photoanode yielding the weaker oxidant HO$_2^\bullet$ as intermediate from Reactions (5) and (6) [5,14]. This cathode was chosen because it prevents any possible reduction of the azo dye and its by-products [5].

$$O_2 + 2H^+ + 2e^- \rightarrow H_2O_2 \tag{4}$$

$$H_2O_2 \rightarrow HO_2{}^\bullet + H^+ + e^- \quad\quad (5)$$

$$HO_2{}^\bullet \rightarrow O_2 + H^+ + e^- \quad\quad (6)$$

The electrochemical assays were performed with 100 mL of solutions containing 0.050 M Na_2SO_4 as background electrolyte at pH 7.0 and constant j_{anod} = 1.0 mA cm^{-2} provided with an Amel 2053 potentiostat-galvanostat, as optimum operational parameters determined in previous work [29]. The experiments were made in sunny and clear days during the summer of 2014, with similar average irradiance of 31.0 W m^{-2} between 300 and 400 nm, as measured with a Kipp & Zonen CUV 5 radiometer.

2.4. Apparatus and analytical procedures

The particle size distribution of the three different feedstocks A (100% TiO_2 rutile), B (TiO_{2-x}) and C (100% TiO_2 anatase) commercial powders were measured by laser scattering using a Beckman Coulter LS 13 320 equipment. TiO_2 coating samples were cut and mounted in a conductive phenolic resin (Konductomet, Buehler) followed by the metallographic preparation. Optical microscope (DMI 5000 M, Leica) images of the cross section have been carried out in order to measure the thickness of the coatings. Afterwards, cross-section areas of the coatings as well as their surface morphologies have been studied by scanning electron microscopy (SEM) (JSM-5310, JEOL). Phase composition and quantification of feedstock powders were analyzed with an X'Pert PRO MPD diffractometer (PANalytical). The phase analysis of the different coatings were performed by X-ray diffractometry (XRD) using a Siemens D500 system type Bragg-Brentano θ/2θ by applying a Cu Kα$_1$ radiation ($\lambda(\alpha_1)$ = 0.15406 nm) at 45 kV and 40 mA current. The ratio between the obtained crystalline phases was determined using the calculation support of X'pert HighScore Plus software. A Matrox Inspector software image analyzer was used to quantify the porosity percentage of the coatings. The photocatalytic surface of the TiO_2 coatings was measured with a Mitutoyo Surftest 301 equipment and its adhesion was measured with a Servosis MCH-102ME system through the ASTM C633 standard. Both 2D and 3D roughness parameters were analyzed using a confocal microscope LEICA DCM3D system with an objective of 10X magnification. Sensoscan image analysis was used for such data and surface roughness Sa and Sq parameters were obtained through a LeicaScan Mountain software.

Linear sweep voltammetry (LSV) was carried out with a conventional three-electrode one-compartment cell thermostated at 25 °C using an Ecochemie Autolab PGSTAT100 potentiostat-galvanostat controlled by an Autolab Nova 1.5 software. The working electrode was the A3 TiO_2 coating, the counter electrode was a Pt wire and the reference electrode was a Ag/AgCl/KCl(sat.) electrode ($E°$ = 0.197 V/SHE). The linear sweep voltammograms were recorded for a 0.050 M Na_2SO_4 solution of pH 7.0 at anodic potential (E_{anod}) from 0 to 2.4 V and a scan rate of 1 mV s^{-1} under an Ar atmosphere after previous bubbling of this gas through the solution for 30 min. The analysis was conducted in the dark and under natural sunlight irradiation.

The pH of dyes solutions was controlled and adjusted using a Crison GLP 22 pH-meter. The photoelectrocatalyic performance of the TiO_2 coatings was monitored from the decay of the absorbance of the AO7 solution at the maximum wavelength (λ_{max}) = 484 nm, measured on the spectra recorded with a Shimadzu 1800 UV–vis spectrophotometer at 35 °C. The percentage of color removal or decolorization efficiency was calculated from the absorbance at initial time (A_0) and at time t (A_t) at the λ_{max} = 484 nm from the expression [5,34]:

$$\% \ Color \ removal = \frac{A_0 - A_t}{A_0} \times 100 \quad\quad (7)$$
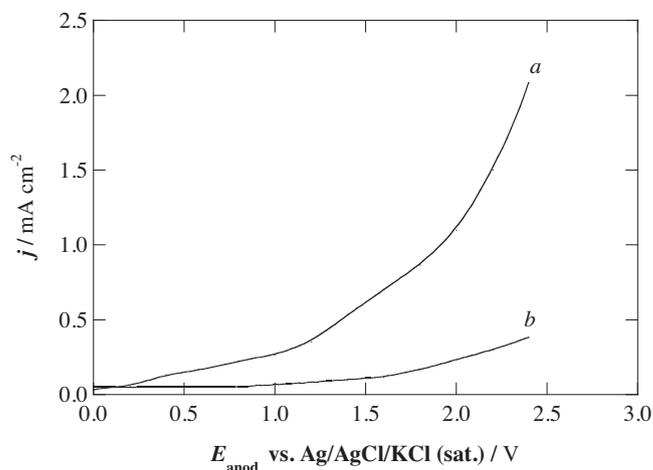
Fig. 1. Linear sweep voltammograms recorded for the TiO_2 coating A3 immersed in a 0.050 M Na_2SO_4 solution at pH 7.0 and 25 °C (a) under sunlight illumination and (b) in the dark. Initial anodic potential: 0 V, final anodic potential: 2.40 V. Scan rate 1 mV s^{-1}.

The AO7 concentration was followed during the photoelectrocatalytic treatments by reversed-phase high-performance liquid chromatography (HPLC) using a Waters 600 LC fitted with a Spherisorb ODS2 5 μm, 150 mm × 4.6 mm, column at 35 °C coupled to a Waters 996 photodiode array detector set a 484 nm. The chromatograms displayed a well-defined peak with retention time of 7.6 min after injection of 20 μL of sample into the LC using a mobile phase of 30:70 (v/v) acetonitrile/water mixture with 2.4 mM n-butylamine at 0.6 mL min^{-1}.

3. Results and discussion

3.1. Influence of crystalline and non-stoichiometric phases on SPEC performance

An initial blank experiment without any TiO_2 coatings did not undergo any loss of color of 100 mL of a 0.43 mM AO7 solution in 0.050 M Na_2SO_4 at pH 7.0 and 35 °C when 2 mM H_2O_2 was added to it either in the dark and under solar irradiation, indicating that the azo dye does not react with H_2O_2 electrogenerated at the cathode under SPEC conditions. Our previous work [29] evidenced a poor color loss by electrochemical oxidation in the dark and by direct photocatalysis under natural sunlight irradiation, where less than 45% and 20% decolorization were attained after 300 min of treatment, respectively. The present study was then focused on the photoelectrocatalytic response of the new TiO_2 coatings prepared by APS.

Taking into account that the use of galvanostatic experiments in photoelectrochemistry is problematic, since it does not allow to distinguish between photocurrents produced by light generating charge carriers and dark currents, comparative current density-E_{anod} curves for the A3 semiconductor anode in the background electrolyte at pH 7.0 were recorded in the dark and under natural sunlight illumination by means of LSV. As can be seen in Fig. 1, the photocurrent upon irradiation of the TiO_2 anode by sunlight (curve a) increased up to 6-fold compared to the current in the dark (curve b), thereby demonstrating the photoelectrocatalytic nature of the process under solar illumination.

To assess the photoelectrocatalytic efficiency of the prepared TiO_2 coatings, the above AO7 solution was degraded at j_{anod} = 1.0 mA cm^{-2} and the azo dye abatement was followed by HPLC for 180 min, time in which an almost complete removal of this compound (94%) was attained for the best coating performance,
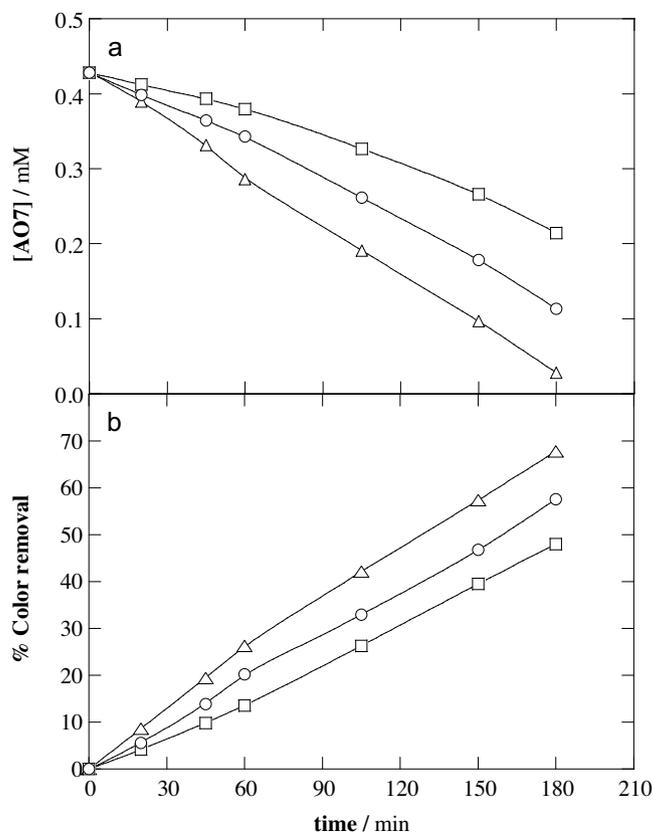
Fig. 2. (a) Acid Orange 7 (AO7) abatement followed by HPLC and (b) percentage of color removal measured by UV–vis at $\lambda_{max} = 484$ nm vs. time of the photoelectrocatalytic treatment of a 0.43 mM azo dye solution with 0.050 M Na$_2$SO$_4$ at pH 7.0 and 35 °C under natural sunlight irradiation by applying $j_{anod} = 1.0$ mA cm^{-2} for the TiO$_2$ coatings: ($\triangle$) A3, ($\square$) B3 and ($\bigcirc$) C3.

Table 2
Crystalline and non-stoichiometric phases inside the prepared TiO$_2$ coatings.

Sample	Anatase [%]	Rutile [%]	Ti$_3$O$_5$ [%]	Ti$_7$O$_{13}$ [%]	Ti$_9$O$_{17}$ [%]
A1	2.0	13.0	38.0	18.0	29.0
A2	3.0	18.2	16.2	25.3	37.4
A3	4.0	20.0	18.0	23.0	35.0
B1	2.0	11.0	12.0	29.0	46.0
B2	3.0	10.0	10.0	28.0	49.0
B3	4.0	11.0	12.0	30.0	43.0
C1	3.0	13.0	12.0	26.0	46.0
C2	2.0	12.1	26.3	24.2	35.4
C3	4.0	12.9	11.9	28.6	42.6

as shown Fig. 2a. In all these trials, the solution pH was continuously regulated to its initial value of 7.0 by adding small volumes of 0.5 M NaOH. Fig. 2b highlights that the changes of the percentage of color removal at $\lambda_{max} = 484$ nm in such SPEC treatments showed significant differences of the photoelectrocatalytic activity depending on the synthesized coatings, leading to different decolorization kinetics. For this reason, the phase distribution of the TiO$_2$ coatings was analyzed by XRD as one of the feasible parameters that could explain their photoelectrocatalytic efficiency.

As stated above, the spraying conditions and the feedstock powder used could affect the final distribution of titanium oxide phases in the coating [31–33]. Consequently, it is possible to control the phase distribution in the coatings from the selection of spraying parameters. The XRD spectra of Fig. 3 evidence that the same final phases were found in all the coatings, indistinctly of the starting powder material (TiO$_2$ rutile, TiO$_{2-x}$ sub-oxide or TiO$_2$ anatase) and conditions tested. However, different proportion of phases were formed depending on the experimental conditions, as can be seen in Table 2. The formation of new phases could be justified

by the high temperatures of plasma that are able to promote the feedstock powder phase transformation [31–33]. Greater spraying temperature then made feasible to obtain a higher quantity of different sub-oxides or phases.

The results on the characterization of the synthesized titanium dioxide showed a predominance of non-stoichiometric phases (over 75%) in front of crystalline phases (anatase and rutile). The most influencing spraying parameter on the degree of crystallinity was the Ar/H$_2$ ratio of the plasma stream, since a greater Ar flow resulted in an increase of the percentage of crystalline phases. The melting and rapid solidification enhanced their presence and avoided the evolution to the rutile phase. Moreover, anatase appeared as a high-T metastable phase in a lower percentage in all coatings. When producing coatings through powders A (rutile) and C (mainly anatase), the same effect was observed. The proportion of sub-oxides increased rapidly when being sprayed, whereas there was some rutile (in the case of powder C) or anatase (in the case of powder A) coming from the rutile/anatase transformation during solidification. Finally, in the case of powder B (rutile and sub-oxides), the percentage of rutile was reduced due to an increase of the sub-oxide content during rapid solidification along with the transformation to anatase, because of the melting and resolidification process that led to similar percentages of this phase in all the coatings obtained through powders A and C.

The direct assessment of the phase distribution on the photoelectrocatalytical behavior of the coating on the color removal of the AO7 solution evidenced the noticeable higher photocatalytic character of the crystalline phases, as can be easily deduced from Fig. 4. It is important to remark that the crystalline phases of rutile and anatase present considerably lower band gaps ($\leq$3.2 eV) than those of the non-stoichiometric phases ($\geq$3.2 eV), thereby being
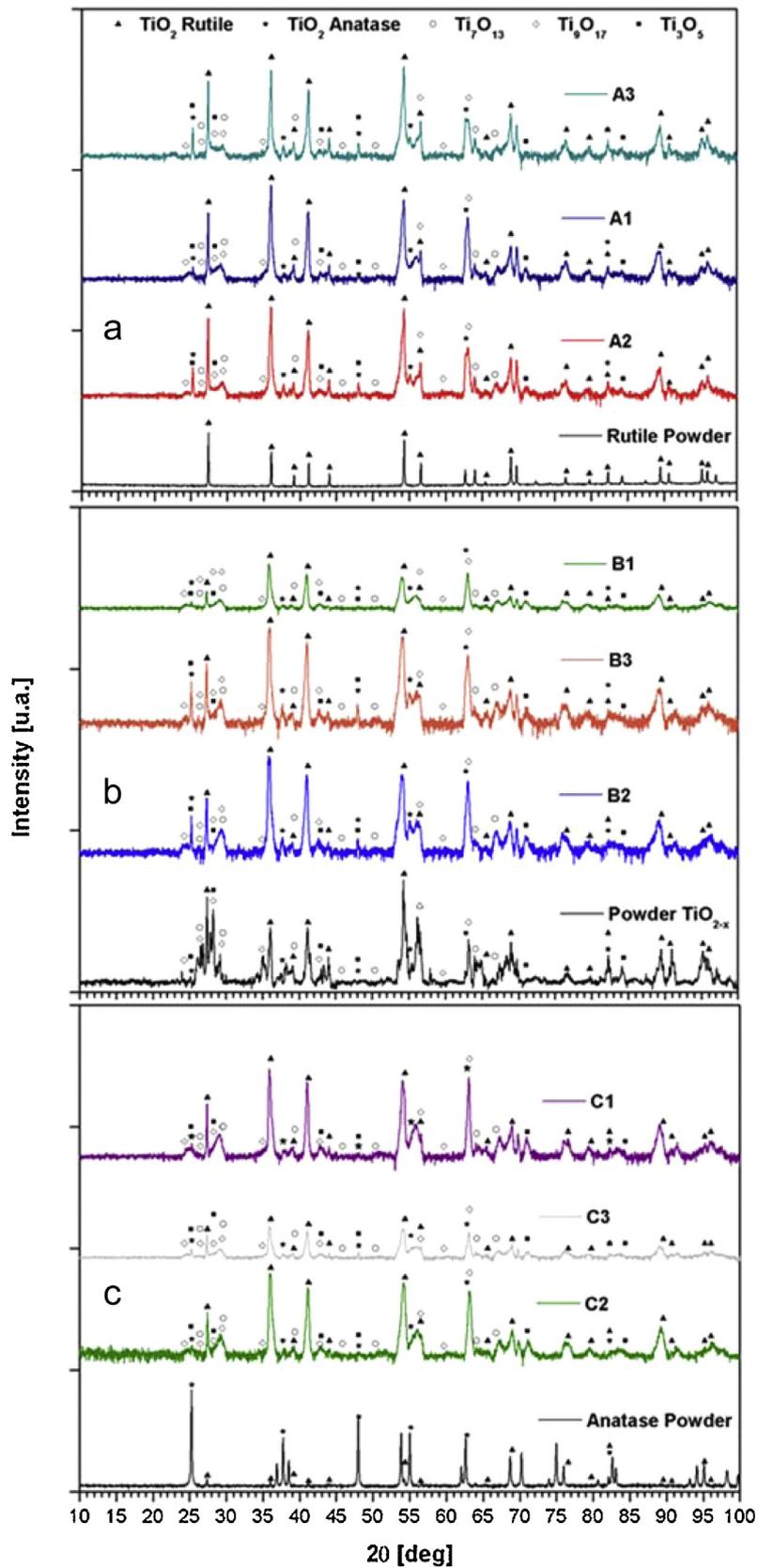
Fig. 3. X-ray diffractograms of the prepared TiO_2 photoanodes by atmospheric plasma spray (APS) technology using as precursor: (a) rutile powder, (b) TiO_{2-x} sub-oxide powder or (c) anatase powders, under the spraying conditions collected in Table 1.
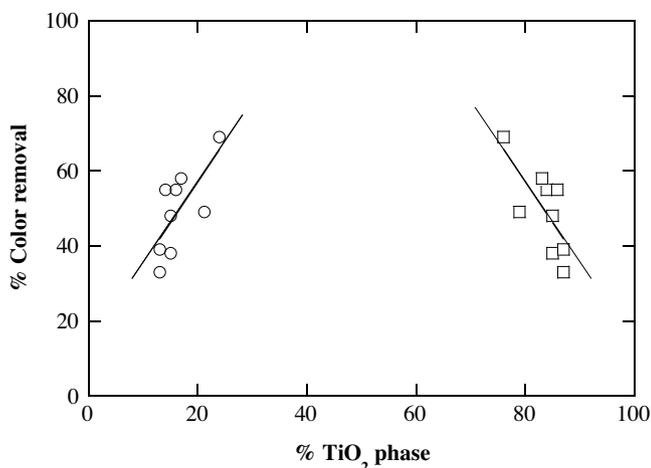
Fig. 4. Percentage of color removal at $\lambda_{max} = 484$ nm for 100 mL of a 0.43 mM Acid Orange 7 solution with 0.050 M of Na_2SO_4 at pH 7.0. and 35 °C under solar photoelectrocatalysis (SPEC) by applying $j_{anod} = 1.0$ mA cm^{-2} for 180 min in function of: (○) the percentage of crystalline phases of TiO_2 and (□) the percentage of amorphous phases of TiO_2.

easier the photo-promotion of the valence band electrons to the conductive band from Reaction (1) [1,23]. Nonetheless, titanium sub-oxides improve the electrical behavior of the coatings enhancing the recombination Reaction (3) between electrons and holes, although they are also able to increase the conductivity of the pre-

pared materials, which is a functional property of interest for their application as photo-anodes.

3.2. Relationship between structural characteristics and photoelectrocatalytic response

The photoelectrocatalytic performance of the synthesized TiO_2 coatings is not expected to be exclusively related to their chemical composition but also to other important microstructural characteristics. The contribution and relevance of each measurable property on the photoelectrocatalytical response of prepared materials was then explored.

First of all, coatings micrographs were obtained by SEM. Fig. 5 highlights the cross section micrographs of the coatings synthesized using the three different feedstocks of A (TiO_2 rutile), B (TiO_{2-x}) and C (TiO_2 anatase). The most noticeable difference was associated to the thickness achievable under the same conditions for the different powders, being the thinner coatings those obtained with anatase powder. This effect is due to the stockpowder used. The powder morphology, apparent density and intern porosity affected the powder interaction with the flame torch of APS and influenced directly the efficiency of the coating formation and its thickness. Nevertheless, the coatings presented the same types of TiO_2 phases regardless of the feeding powder, as pointed out above.

It is also remarkable that lower energetic spraying conditions led to a lower melting of the particles and consequently, to higher roughness and porosity in the coatings. On the contrary, higher energetic spraying conditions melted better the particles.
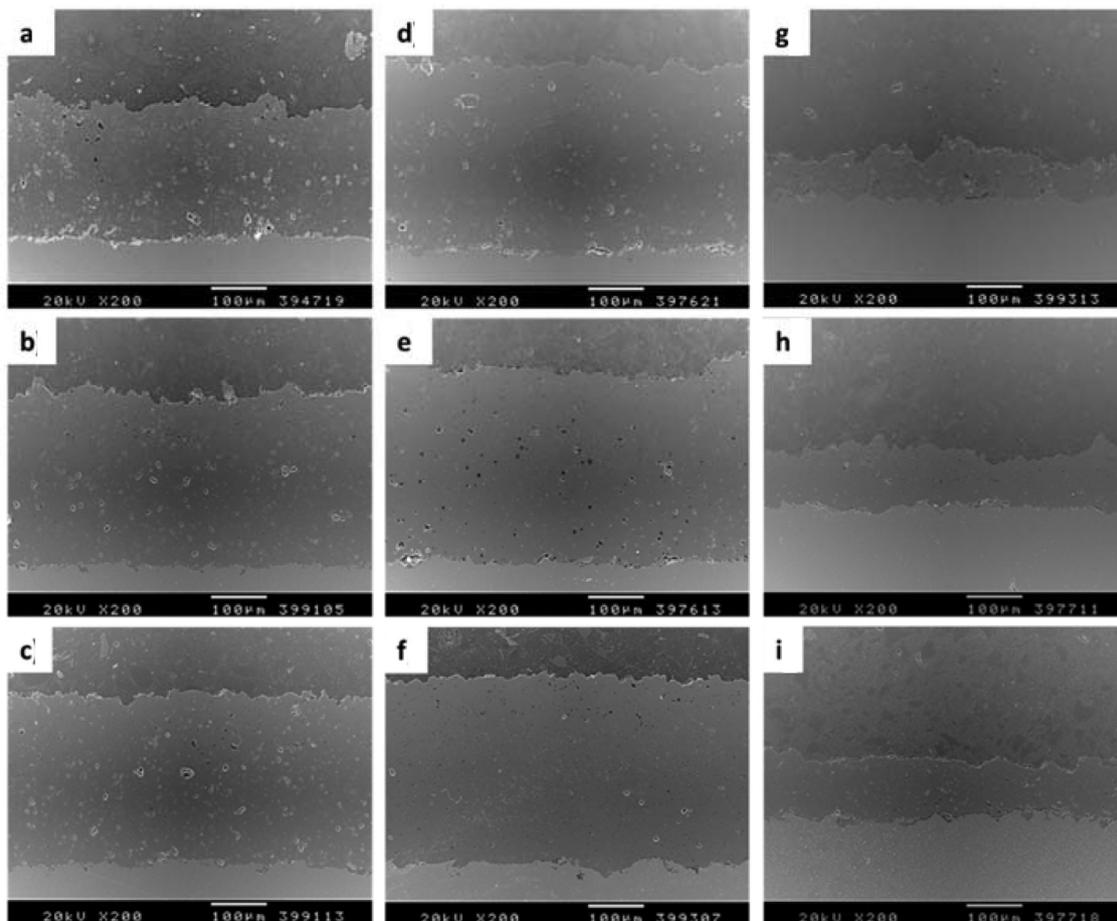
Fig. 5. Cross section scanning electron microscopy (SEM) micrographs of the TiO_2 coatings obtained by APS. Sample: (a) A1, (b) B1, (c) C1, (d) A2, (e) B2, (f) C2, (g) A3, (h) B3 and (i) C3.
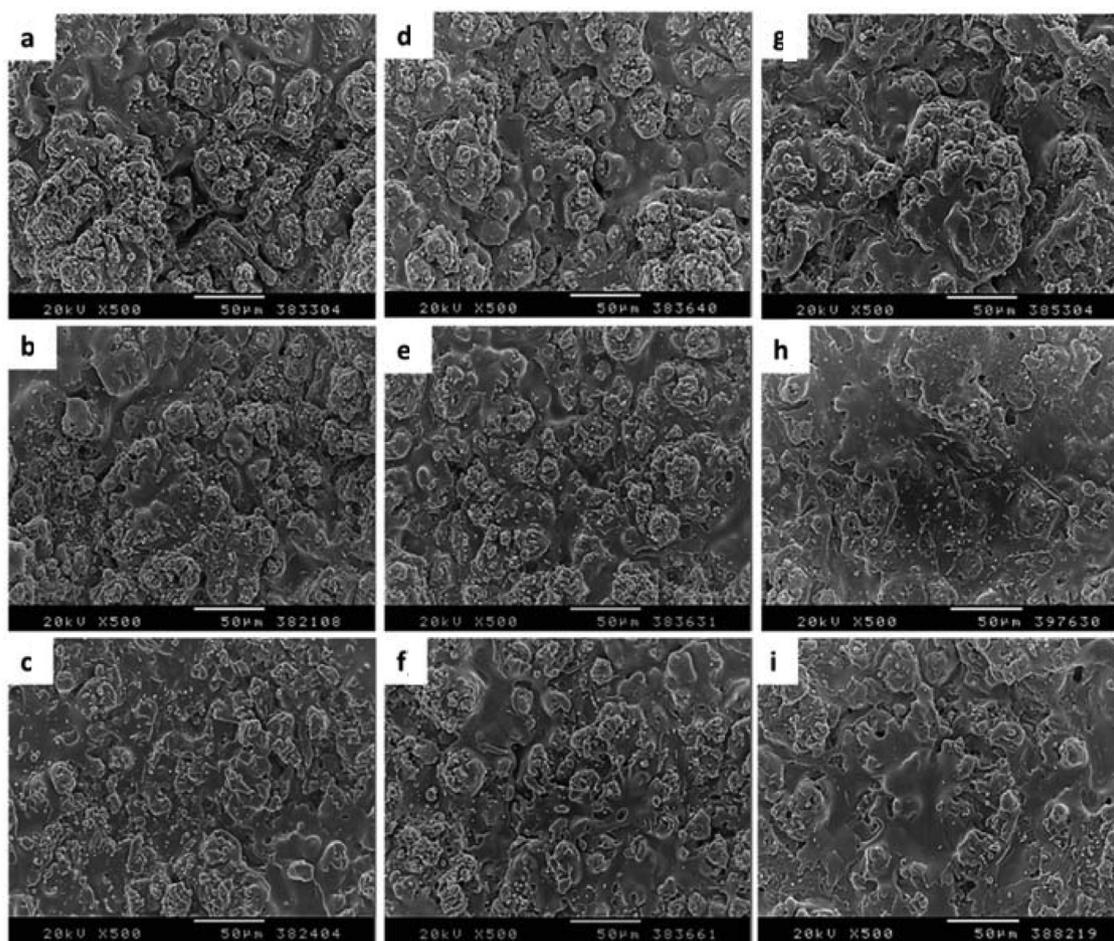
Fig. 6. SEM images of the free-surface of the TiO$_2$ coatings prepared by APS. Sample: (a) A1, (b) B1, (c) C1, (d) A2, (e) B2, (f) C2, (g) A3, (h) B3 and (i) C3.

Table 3
Experimental parameters determined for each prepared TiO$_2$ coating.

Sample	Thickness [μm]	Porosity [%]	Roughness Ra [μm]	Sa [μm]	Sq [μm]
A1	257.9 ± 9.9	9.5 ± 2.6	4.8 ± 0.1	4.9 ± 0.5	6.3 ± 0.7
A2	275.5 ± 9.5	11.4 ± 3.0	8.1 ± 0.4	6.1 ± 0.4	7.8 ± 0.5
A3	231.5 ± 15.5	9.9 ± 3.3	10.4 ± 0.4	7.7 ± 0.5	9.9 ± 0.7
B1	284.0 ± 6.9	10.1 ± 2.5	6.0 ± 0.2	4.7 ± 0.3	6.2 ± 0.3
B2	310.6 ± 17.7	6.9 ± 3.7	7.9 ± 0.9	5.4 ± 0.2	6.9 ± 0.2
B3	317.7 ± 24.7	5.6 ± 1.9	11.5 ± 3	6.1 ± 0.1	7.7 ± 0.1
C1	102.2 ± 14.8	11.3 ± 3.0	9.3 ± 0.5	7.4 ± 0.1	9.6 ± 0.1
C2	102.1 ± 15.4	9.6 ± 4.3	10.1 ± 0.6	7.0 ± 0.2	9.1 ± 0.3
C3	124.5 ± 14.1	14.4 ± 4.9	10.5 ± 0.3	7.1 ± 0.1	9.1 ± 0.1

The corresponding free-surface micrographs of the coatings depicted in Fig. 6 denoted significant differences between the coatings surfaces, also associated with the stockpowder used and the spraying conditions. Table 3 collects the characteristic parameters of each coating including thickness, porosity, 2D roughness and 3D surface values. These structural properties could have a marked influence on the intrinsic photocatalytic properties of the coatings that could be enhanced or diminished in function of their variation. To better clarify the extent of their possible influence, the decolorization efficiencies for 100 mL of the 0.43 mM AO7 solution at pH 7.0 after 180 min of SPEC treatment at j_{anod} = 1.0 mA cm^{-2} were represented against the measured values of each parameter, as shown in Fig. 7.

The coating thickness was not one of the most determining parameters on the photoelectrochemical behavior. Fig. 7a depicts that the percentage of color removal after 180 min of SPEC treatment rose slightly with increasing the film thickness up to

231.5 μm, whereupon dropped remaining around an average value of 45% for the thicker coatings. This kind of response is barely discussed in the literature as a result of two main effects. The first one is ascribed to the light penetration into the film to photogenerate the e$_{cb}^-$/h$_{vb}^+$ pair by Reaction (1). The maximum penetration depth of the incident light into the TiO$_2$ coating is defined by the function 1/α according to Hitchman and Tian [21], where α is the absorption coefficient of TiO$_2$ at a defined wavelength allowing light penetation up to a maximum depletion layer width (W$_{max}$). Any species photogenerated within the W$_{max}$ region could be efficiently diffused up to the coating surface when it is located in the minority carrier diffusion length of TiO$_2$. Thus, the increasing thickness of the TiO$_2$ coating could enhance the photogeneration of oxidants up to a limit, increasing the photoelectrocatalytic efficiency of the photoanode. The second effect related to the thickness is the coating conductivity. The SPEC process is based on the use of the TiO$_2$ as photoanode that implies the requirement of certain electric conductivity [16–29]. It is noticeable that the material resistivity (ρ) rises at higher thickness, diminishing the efficient removal of photo-promoted electrons by the external electric circuit [2,5]. This can explain the observed decay of the percentage of color removal for thicknesses >231.5 μm in Fig. 7a.

The porosity variation did not denote any considerable influence on the photoelectrocatalytic response, as can be deduced from Fig. 7b. Theoretically, an increase in porosity percentage should reduce the decolorization efficiency because lower photocatalyst would be present in the W$_{max}$ region where the oxidant can be photogenerated [1,21], as stated above. Moreover, greater porosity could increase dramatically the material resistivity giving rise to
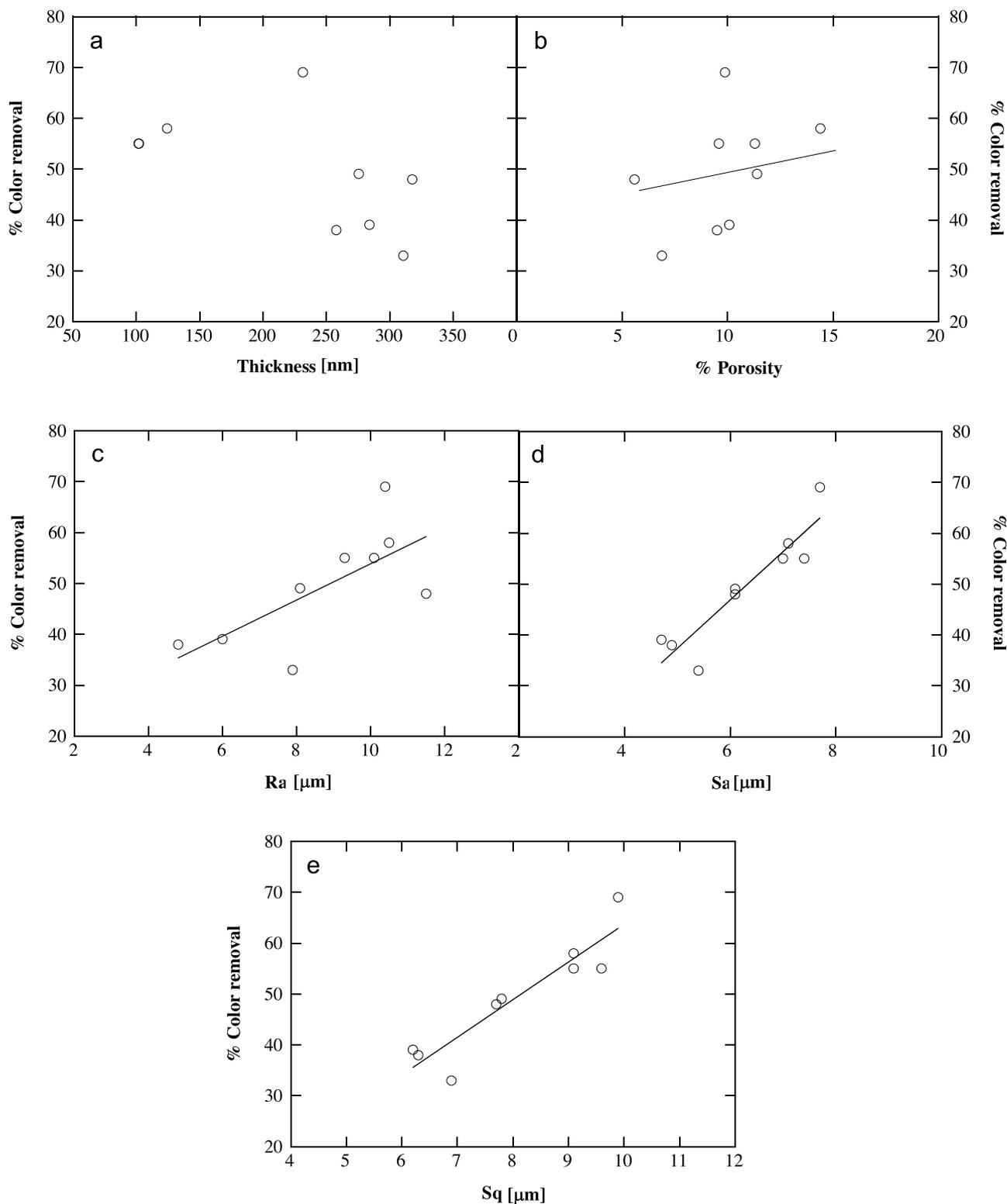
Fig. 7. Influence of the structural characteristics of the TiO$_2$ coating on the percentage of color removal at λ_{max} = 484 nm of 100 mL of a 0.43 mM Acid Orange 7 solution with 0.050 M of Na$_2$SO$_4$ at pH 7.0. and 35 °C by means of SPEC at j_{anod} = 1.0 mA cm^{-2} for 180 min. Coating parameters: (a) thickness, (b) porosity, (c) roughness, (d) superficial roughness average and (e) superficial roughness quadratic mean.

a lessening of the SPEC degradation [5]. However, these expected effects were not observed, probably due to the low porosity interval evaluated in the present work ranging from 5.6% to 14.4%.

The coating roughness was the main control parameter on the SPEC performance. Fig. 7c highlights that a higher decolorization was attained by the rougher surfaces. Nevertheless, this tendency

was more apparent when considering the superficial roughness average (Sa) and the superficial roughness quadratic mean (Sq), shown in Fig. 7d and e, respectively. These two 3D roughness parameters give information about specific surfaces of the developed coatings which seem to be fundamental for SPEC applications. This technology is strongly related to surface processes [1–4], hence

higher photocatalytic generation of the e_{cb}^-/h_{vb}^+ pair by Reaction (1) is expected by greater specific area of TiO_2 irradiated. The SPEC decolorization of the treated AO7 solution then demonstrates that the available surface to be directly irradiated plays a remarkable role on the process efficiency. Moreover, the degradation process can be mediated by surface adsorption processes of the pollutants molecules to react with the adsorbed oxidants (mainly $^\bullet OH$ and h_{vb}^+) that are more rapidly generated when a larger surface is exposed due to the higher number of catalytic sites [5,29].

Taking into account all the structural and phase distribution characteristics that are correlated with the SPEC efficiency for the decolorization of the AO7 solution, one can infer that the best synthesized coating acting as photoanode is the sample A3 since it contains the major proportion possible of crystalline phases (indistinctly rutile or anatase), the major roughness to dispose of a higher irradiation exposition area and an average thickness of about $230\,\mu m$ to possess an appropriate electrical conductivity.

4. Conclusions

It has been shown that atmospheric plasma spraying is a promising technology to synthesize highly stable supported TiO_2 photocatalysts with good intrinsic properties for their use in SPEC processes for pollution remediation. The influence of the spraying conditions on the final structural and phase distribution of the coatings has been assessed, correlating these characteristics with their performance as photoanodes to decolorize an AO7 solution by SPEC. It has been found that the crystalline phases of TiO_2 (anatase and rutile) are more photocatalytic than non-stoichiometric TiO_2 suboxides. The coatings with higher proportion of crystalline phases then present better photoelectrocatalytic performances. However, the generated TiO_2 sub-oxides enhance the coatings conductivity favoring their application as photoanodes, being the presence of these phases also relevant for SPEC application. The structural characterization of the coatings revealed a slight influence of the TiO_2 thickness with an optimum value of about $200–230\,\mu m$. The property with higher influence resulted to be the 3D superficial roughness because the photocatalytic processes take place on the coating surface. When a larger specific area is available to be irradiated, a major photogeneration of oxidants occurs, with a considerable enhancement of the SPEC degradation of AO7. The best SPEC photoactivity was obtained for the coating A3 due to its major content of crystalline phases (rutile and anatase), greater 3D superficial roughness and appropriate thickness.

Acknowledgements

References

[1] A. Fujishima, X. Zhang, D.A. Tryk, Surf. Sci. Rep. 63 (2008) 515–582.
[2] K. Nakata, A. Fujishima, J. Photochem. Photobiol. C 13 (2012) 169–189.
[3] D. Friedmann, C. Mendive, D. Bahnemann, Appl. Catal. B: Environ. 99 (2010) 398–406.
[4] U.G. Akpan, B.H. Hameed, J. Hazard. Mater. 170 (2009) 520–529.
[5] E. Brillas, C.A. Martínez-Huitle, Appl. Catal. B: Environ. 166–167 (2015) 603–643.
[6] B. Bayarri, E. Carbonell, J. Gimenez, S. Esplugas, H. Garcia, Chemosphere 72 (2008) 67–74.
[7] B. Smolkova, N. El Yamani, A.R. Collins, A.C. Gutleb, M. Dubinska, Food Chem. Toxicol. 77 (2015) 64–73.
[8] R. Handy, M. Whitt, M. Rodriguez, M.J. Jackson, in: W. Ahmed, M. Jackson (Eds.), Emerging Nanotechnologies for Manufacturing, Elsevier, Oxford (UK), 2015, pp. 255–269.
[9] L. Dou, L. Gao, X. Yang, X. Song, J. Hazard. Mater. 203-204 (2012) 363–369.
[10] H. Choi, S.R. Al-Abed, D.D. Dionysiou, E. Stathatos, P. Lianos, in: I.C. Escobar, A.I. Schäfer (Eds.), Sustainable Science and Engineering, 2, Elsevier, Oxford (UK), 2010, pp. 229–254.
[11] S. Parra, S. Malato, C. Pulgarin, Appl. Catal. B: Environ. 36 (2002) 131–144.
[12] C. Guillard, J. Disdier, C. Monnet, J. Dussaud, S. Malato, J. Blanco, M.I. Maldonado, J.M. Herrmann, Appl. Catal. B: Environ. 46 (2003) 319–332.
[13] J. Marúgan, J. Aguado, W. Gernjak, S. Malato, Catal. Today 129 (2007) 59–68.
[14] B.R. Garza-Campos, J.L. Guzmán-Mar, L.H. Reyes, E. Brillas, A. Hernández-Ramírez, E.J. Ruiz-Ruiz, Chemosphere 97 (2014) 26–33.
[15] M. Jiménez-Tototzintle, I. Oller, A. Hernández-Ramírez, S. Malato, M.I. Maldonado, Chem. Eng. J. 273 (2015) 205–213.
[16] Y. Bennani, P. Appel, L.C. Rietveld, J. Photoch. Photobiol. A 305 (2015) 83–92.
[17] J. Marugán, P. Christensen, T. Egerton, H. Purnama, Appl. Catal. B: Environ. 89 (2009) 273–283.
[18] H. Zhang, Y. Wang, P. Liu, Y. Han, X. Yao, J. Zou, H. Cheng, H. Zhao, ACS Appl. Mater. Interfaces 3 (2011) 2472–2478.
[19] R. Daghrir, P. Drogui, M.A. El Khakani, Electrochim. Acta 87 (2013) 18–31.
[20] P.S. Shinde, P.S. Patil, P.N. Bhosale, A. Brüger, G. Nauer, M. Neumann-Spallart, C.H. Bhosale, Appl. Catal. B: Environ. 89 (2009) 288–294.
[21] M.L. Hitchman, F. Tian, J. Electroanal. Chem. 538 (2002) 165–172.
[22] Q. Zhang, J. Zhu, Y. Wang, J. Feng, W. Yan, H. Xu, Appl. Surf. Sci. 308 (2014) 161–169.
[23] J.C. Cardoso, T.M. Lizier, M.V.B. Zanoni, Appl. Catal. B: Environ. 99 (2010) 96–102.
[24] Z. Zhang, D. Pan, J. Feng, L. Guo, L. Peng, C. Xi, J. Li, Z. Li, M. Wu, Z. Ren, Mater. Lett. 66 (2012) 54–56.
[25] S.K. Mohapatra, M. Misra, V.K. Mahajan, K.S. Raja, J. Catal. 246 (2007) 362–369.
[26] X. Cheng, G. Pan, X. Yu, Chem. Eng. J. 279 (2015) 264–272.
[27] X. Hua, Y. Zhang, N. Ma, X. Li, H. Wang, J. Hazard. Mater. 172 (2009) 256–261.
[28] Y. Liu, K. Mu, G. Yang, H. Peng, F. Shen, L. Wang, S. Deng, X. Zhang, Y. Zhang, New J. Chem. 39 (2015) 3923–3928.
[29] S. Garcia-Segura, S. Dosta, J.M. Guilemany, E. Brillas, Appl. Catal. B: Environ. 132–133 (2013) 142–150.
[30] C. He, X.Z. Li, N. Graham, Y. Wang, Appl. Catal. A: Gen. 305 (2006) 54–63.
[31] M. Gardon, S. Dosta, J.M. Guilemany, M. Kourasi, B. Mellor, R. Wills, J. Power Sources 238 (2013) 430–434.
[32] M. Gardon, O. Monereo, S. Dosta, G. Vescio, A. Cirera, J.M. Guilemany, Surf. Coat. Technol. 235 (2013) 848–852.
[33] M. Gardon, C. Fernández-Rodríguez, M.R. Espino Estévez, S. Dosta, I.G. Cano, J.M. Guilemany, J. Therm. Spray Technol. 23 (2015) 1135–1141.
[34] X. Florenza, A.M.S. Solano, F. Centellas, C.A. Martínez-Huitle, E. Brillas, S. Garcia-Segura, Electrochim. Acta 142 (2014) 276–288.

This fourth paper shows the results obtained by titanium suboxide coatings onto four lightweight standard electrode materials: thin steel film, thin aluminium film, carbon-polymer composite and nickel foam. Titanium dioxide feedstock powder was characterised and sprayed by means of APS technology. Substrate surfaces were adequately prepared in order to enhance the deposition of the molten particles and spraying parameters were also chosen as not to damage the substrates. The manufactured coatings were electrochemically assessed using cyclic voltammetry. Layers present optimal characteristics: on one side they provide electrical conductivity and on the other side they protect the substrates from the electrolyte solutions. A proof-of-concept 2V single-cell lead-acid battery was constructed using aluminium as the substrate and well-bonded homogeneous TiO_{2-x} as layers. The battery returned an energy density of 9 Ah/Kg of 45 Ah/L when operated using a current of 100 mA. This work highlights the versatility of APS technology, the possibility of spraying onto 3D substrates with high specific area and to scale-up these functional products.
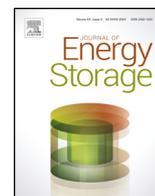
Enhancing the performance of common electrode materials by means of atmospheric plasma spray coatings

CrossMark

M. Robotti[a,*], S. Dosta[a], M. Gardon[a], I.G. Cano[a], J.M. Guilemany[a], M. Kourasi[b], B. Mellor[b], R. Wills[b]

[a] Thermal Spray Centre, CPT, University of Barcelona. Martí i Franquès 1, 08028 Barcelona, Spain
[b] Research Institute for Industry, Faculty of Engineering & the Environment, University of Southampton, SO17 1BJ Southampton, UK

A B S T R A C T

Atmospheric plasma spraying is used here to obtain titanium sub-oxide coatings on the following electrode substrates: a 316 stainless steel sheet, an aluminium alloy 2024 sheet, a carbon–polymer composite and nickel foam. It is necessary to increase the roughness of the substrate to aid the adhesion of the coating to the smooth electrodes; this is especially critical for the fragile carbon–polymer composite. High-energy conditions increase the strain caused by the mismatch between coefficients of thermal expansion when coating the thin steel and aluminium sheets, and degraded the carbon–polymer composite and nickel foam. Therefore, it is necessary to adjust the spraying parameters to lower-energy conditions in order to achieve well-bonded and homogeneous coatings on all four substrates and avoid the presence of cracks in their cross-section area. The suitability of the coated materials as battery electrodes was studied.

1. Introduction

To gain independency from the resource intermittency characteristic of renewable technologies, energy distribution or daily fluctuations in consumption, it is necessary to develop improved, large-scale electrochemical energy storage devices [1]. Bipolar batteries and redox flow batteries are being increasingly used in electrochemical energy storage and conversion systems. However, their efficiency and cycle life are strongly dependant on the chemical stability and bulk resistivity of the electrodes and bipolar plates, as well as the contact resistance between the two. Cost-effective and rapid manufacturing processes capable of coating these materials with electrically conductive materials that are resistant to corrosion are expected to improve their overall performance. Atmospheric plasma spraying (APS), a process that propels molten particles toward a substrate by means of a plasma jet, could achieve this [2]. APS can be used to build up well-bonded homogeneous metallic, ceramic or polymeric coatings on a wide variety of substrates; the technique can also be used to produce functional materials [3].

Despite the scarcity of published papers related to the application of thermal spray processes for the development of

battery components [4], patents exist related to many different electrode materials. In the early 1990s, Williams et al. [5] patented a stacked-cell-array bipolar battery with a thermally sprayed resistant lithium alloy and FeS_2 ceramic layer which sealed the cell and acted as a container for it. A similar design was proposed by Barlow et al. [6]. However, in this case, the cell was not hermetically sealed. Migration of the electrolyte around the bipolar wall and the further formation of ionically conducting paths were prevented by means of a non-wettable material strategically placed around the cells at the periphery of the bipolar walls. A method for producing an electrochemical capacitor was developed by Bai et al. [7] using bipolar plates made of cobalt, iron or nickel alloys which acted as both the cathode and the substrate upon which the anodes were formed. In one embodiment, this cathode/substrate layer was formed of a bismuth/antimony alloy and deposited by thermal spraying with a thickness of between 0.1 and 100 mm. A similar patent was filed by Muffoletto et al. [8] but a more detailed description of the APS conditions was given. Ye et al. [9] mentioned that the patent designed by Muffoletto et al. could have significant drawbacks, as the thermal instability of certain electrochemically active materials must be taken into account. Particularly, iron disulphide decomposes to FeS at about 550 °C; which is much colder than the flame temperatures of APS. The undesired decomposition of the active raw material was also tackled by Dai et al. [10]. In their work, the feedstock consisted of a mixture of a source of a thermally protective salt, LiCl or LiBr, and

Nomenclature

APS   Atmospheric plasma spray
CTE   Coefficient of thermal expansion
HEC   High-energy conditions
LEM   Low-energy conditions
LS   Laser scattering
NAM   Negative active material
PAM   Positive active material
SCE   Saturated calomel electrode
SEM   Scanning electron microscopy
SOFCs   Solid oxide fuel cells
XRD   X-ray diffraction
YSZ   Yttria-stabilised zirconia

nanostructured or microstructured active materials, such as sulfides. This mixture was sprayed onto 304 stainless steel and graphite. It was believed that the thermally protective salt prevented the decomposition of the active material by providing cooling via the heat of fusion. The energy associated with the fusion of the salt acts to cool the active material particles and thus prevent their thermal dissociation. Sulphur is a good choice for preventing powder degradation due to it being a poor heat conductor and therefore slowing the heating of the pyrite particles, as other authors previously reported. However, Dai et al. claim that the thermally protective salt has a number of advantages over sulphur the combination of the salt with the active material avoids leaching by flammable carbon disulphide; the amount of salt may be adjusted to control the final porosity of the coating; and the salt can function as an electrolyte, which is useful from the standpoint of electrochemical performance. Nonetheless, in a subsequence patent, the same authors also added sulphur to the elemental feedstock for the same purpose [11]. More recently, Batson [12] designed a bipolar battery electrode structure and sealed bipolar battery assembly. In this case, the electrode substrates and bipolar walls were configured as circular areas. A thermoplastic layer of material was applied by thermal spraying so as to electrically insulate the outer surface of the battery. However, in this case the active components of the device were not obtained as coatings by any process related to thermal spray technologies.

Thermal spray processes have also been widely used as a technique for developing electrode materials in solid oxide fuel cells (SOFCs) and many related scientific contributions have been published [13]. In SOFCs, electrochemical conversion produces electricity directly by oxidizing a fuel, while a solid oxide or

ceramic is used as the electrolytes. Despite the materials involved not performing in the same environment as the electrodes in standard bipolar or mobile batteries, it is worth reviewing some of the experimental procedures reported recently. Nie et al. [14] produced strontium-doped $LaMnO_3$ (LSM) perovskites as cathodes for SOFCs. A certain decrease in the electrical conductivity was observed due to the porous structure of the coating produced by APS, when compared to the bulk LSM sample. However, at 800 °C it met the conductivity requirements for the cathode of a high-temperature SOFC. Moreover, the porosity favoured air/O_2 transportation to reaction sites and thus reduced the degree of cathodic polarization. It was finally concluded that APS appears to be a plausible technique to produce porous LSM cathodes which perform well. Anode layers for SOFCs built up by APS using different feedstocks were studied by Hathiramani et al. [15]. To achieve high electrochemical activity, NiO- or Y_2O_3-stabilized zirconia was milled to a particle size of below 1 μm in diameter and then agglomerated to a size of less than 80 μm in diameter. This method provided powders with very good properties but which flowed less readily. So, the feedstock was mixed with commercially available materials. No differences were observed between the submicron-sized powders and —NiO and YSZ, which had larger grain sizes; however, better thermal cycle resistance was observed when the anodes were produced by injecting NiO and YSZ powder into the plasma plume. Kwon et al. [16] also worked along these lines. Spray-dried nano-sized and micron-sized NiO and YSZ powders sprayed at different Ar/H_2 ratios were compared. The mechanical properties and electrical conductivity of the coatings were strongly dependant on the nature of the powder feedstock. The coatings built up from spray-dried powders contained a nano-sized phase distribution and more three-phase boundaries, which led to higher electrical conductivity due to the more uniform distribution of the phases throughout the coatings when compared to the micron-sized feedstock. An increase of hydrogen in the plasma jet must also be taken into account as it has the capacity to lower the electrical conductivity of the anode. More recently, Guilemany et al. [17] used APS to produce all the components of a SOFC anode (YSZ–NiO), cathode (LSM) and electrolyte (YSZ). The three layers were properly assembled and adherent due to a gradual transition in the materials being produced, achieved by adjusting the feedstock flow rates during spraying.

It should be noted that these examples of the use of thermal spray technologies in energy storage devices are limited to the application of non-conductive seals or for the application of active materials in a morphologically attractive form. Titanium dioxides of reduced stoichiometry (TiO_{2-x}) are well known due to their characteristics and properties. The electrical conductivity in combination with the chemical resistance of this material is of interest for many applications in electrochemistry [18]. In this work, different substrates commonly used as electrodes in batteries, namely steel, aluminium, a carbon–polymer composite and nickel foam, were coated with titanium dioxides with reduced stoichiometry using APS.

2. Materials and methods

Feedstock powder comprising rutile TiO_2 doped with Magnéli phase Ti_8O_{15} and Ti_9O_{17} (Sulzer Metco, Germany) was sprayed using an APS A-3000 system with an F4 plasma torch (Sulzer Metco). The particle size distribution was measured using laser scattering (LS Beckman Coulter). Substrate materials were (i) sheet steel (0.5 mm thick); (ii) sheet aluminium (1 mm thick); (iii) a carbon–polymer composite (thickness: 4 mm); and (iv) nickel foam (thickness: 1 mm; diameter of Ni network: 80 μm). Substrates were cleaned using ultrasonic equipment (Ultrasons-HD, J.P. Selecta) and acetone (Panreac) before the spraying process,
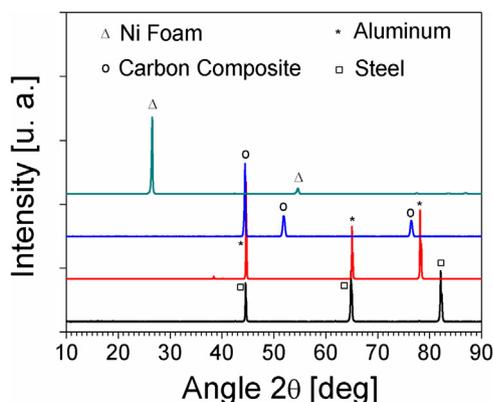
Fig. 1. X-ray diffraction spectrum of: (a) steel, (b) aluminium, (c) carbon–polymer composite and (d) nickel foam.

and their roughness was measured using a profilometer (SJ-210, Mitutoyo). The cross-section area of the coatings was studied using scanning electron microscopy (SEM; ProX Phenom). The coated samples were sectioned and mounted in a conductive phenolic resin (Konductomet, Buehler) followed by metallographic preparation. The electrolytes for electrochemical characterization of the electrodes were produced from deionized water obtained using a Purite water purifier. KOH and H_2SO_4 were used as received from Sigma–Aldrich. Electrochemical measurements were taken in a standard two-compartment glass electrochemical cell using an Autolab potentiostat/galvanostat operating with GPES acquisition software. Potentials were measured against a saturated calomel reference electrode (SCE) and a platinum counter electrode was used. Measurements were taken at 20 °C and the electrolytes were de-oxygenated using a vigorous stream of N_2 gas. Battery measurements were obtained using an MTI BST8-WA battery analyser operating with the MTI TC5.3 operating software.

3. Results and discussion

3.1. Coating development

A previous publication, presents the use of APS as a novel method of manufacturing TiO_{2-x}-coated electrode surfaces [19]. The coated samples exhibited encouraging mechanical properties; for example, microhardness and adhesion to steel substrates. In both acid and alkali environments, an increased potential range of operation compared to uncoated stainless steel electrodes was found. In addition, coated samples showed higher electrical conductivity in a simulated lead flow battery than the most commonly used standard commercial carbon–polymer electrodes. APS involves high temperatures [2]; therefore, the interaction of each different substrate material with the molten particles and the plasma jet may bring about very different results. This is accentuated by the strain resulting from the mismatch of coefficients of thermal expansion (CTEs) between the coating and substrate during the spraying. However, the operating conditions may be adjusted to produce satisfactory performance of the coating obtained. Besides this and as reported before [20], the composition of the plasma causes a varying degree of oxidation of the TiO_2 coating; specifically, the formation of different amounts of oxygen vacancies in the crystal lattice, which leads to a range of electric resistivity. Thus, neither the Ar/H_2 ratios nor the plasma intensity was altered in this study and the composition of the coating remained constant based on rutile TiO_2 and Magnéli phase

Table 1
Thickness and density of the spray-coated electrodes.

Substrate	Thickness (mm)	Density (g/cm^3)
316 stainless steel sheet	0.5	7.84
2024 aluminium alloy sheet	1.0	2.70
Carbon–polymer composite	4.0	1.85
Nickel foam	1.0	0.45

Ti_8O_{15}. Fig. 1 shows the XRD results for each substrate. The coatings previously prepared by APS used a relatively heavy-duty steel substrate, with a thickness of 6 mm [19]. Although this was sufficient to prove the concept of electrode manufacture, it is not practical to use such substantial substrates for many battery applications. The results presented in this paper focus on optimising the coating process to enable truly lightweight, corrosion resistant electrode materials to be produced. Thus, four further substrates were studied and are detailed in Table 1. Steel and aluminium were chosen specifically due to their instability in typical battery environments. For these materials, it is essential that the spray coating process does not perforate the substrate or deform it from its original shape. Furthermore, for the nickel foam, a coating covering all the surfaces throughout the porous structure is required.

3.1.1. Steel substrates

In this study, the starting powder was based on rutile TiO_2 and Magnéli phase Ti_8O_{15} and Ti_9O_{17}. The particles had an irregular morphology and their size distribution range was between 15 and 45 μm. The substrates were subjected to ultrasonic cleaning with acetone for 10 min in order to remove dirt and impurities present on the surface. Then, the metallic pieces were sprayed using the operating conditions described previously [19] and can which be understood in this study as high-energy conditions (HEC). Initially, however, the coatings obtained were not satisfactorily bonded, which we attributed to the smooth surfaces of the electrode materials. Molten particles did not anchor at the point of impact, which resulted in poor adhesion during re-solidification of the particle. Therefore, the metallic substrates were homogeneously grit blasted by a stream of 5 bar compressed air containing alumina particles with an approximate particle diameter of 700 μm. In this way, the surface roughness (R_a) was increased from 0.47 μm to 6.87 μm. Subsequently, the samples were cleaned and sprayed following the same procedure as above. Coatings were successfully built up and their cross-section area was studied by SEM (Fig. 2a).
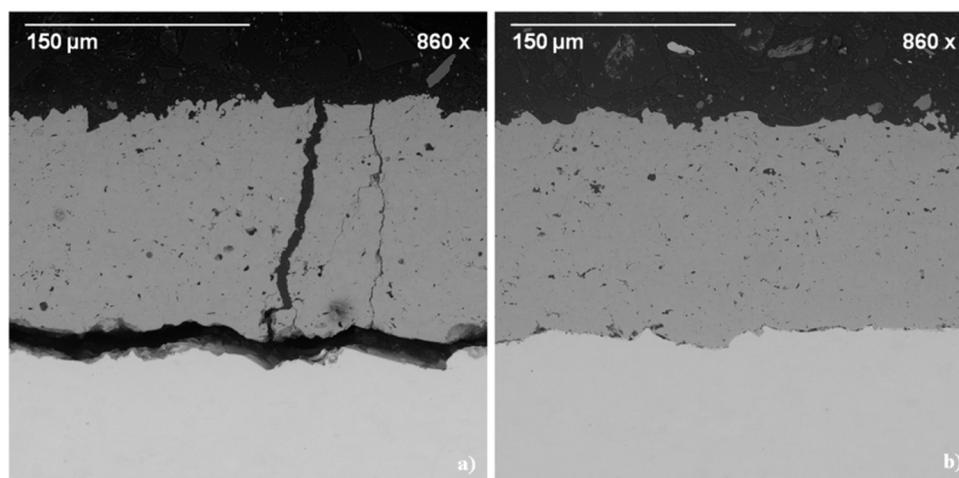
Fig. 2. SEM micrograph: (a) APS TiO_{2-x} coating on steel film obtained by HEC and (b) APS TiO_{2-x} coating on steel film obtained by LEC.
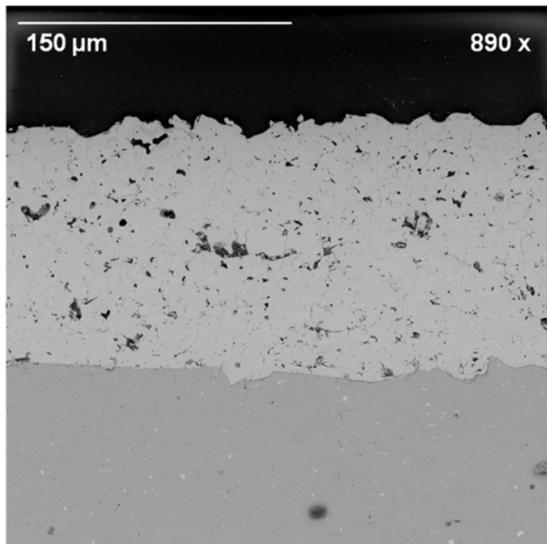
Fig. 3. SEM micrograph: APS TiO$_{2-x}$ coating on aluminium film obtained by LEC.

However, the coatings exhibited an almost complete lack of cohesion to the steel surface. Moreover, a considerable number of cracks were also observed normal to the surface. The mismatch between the CTEs of the metal oxide coating and the metallic substrate may result in considerable accumulation of residual stress, which results in either cracks or delamination of the coating. Two actions were carried out to avoid this. First, nitrogen was used to cool the metallic substrates. Then, the stand-off distance was increased from 40 to 60 and finally 80% of the initial
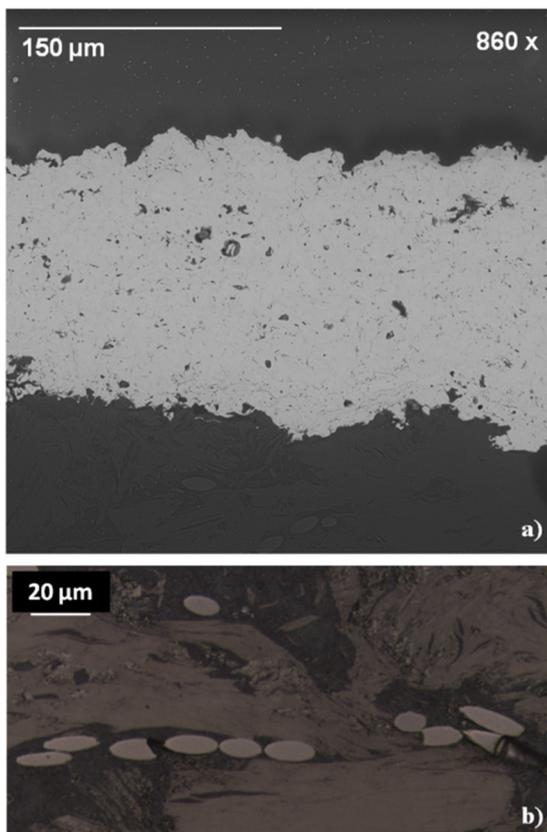
Fig. 4. (a) (Above) APS TiO$_{2-x}$ coating on carbon–polymer composite obtained by LEC (SEM micrograph). (b) (Below) Carbon–polymer composite structure (OM micrograph).

starting value (D0) (values D1, D2, D3 respectively). Significant differences were obtained as the spraying distance was increased. Samples sprayed at distances D2 and D3 were satisfactorily bonded, without cracks appearing or delamination between layers. A slight proportional decrease in thickness was also observed from D0 to D3. Both these findings could be the result of the temperature of the particles, which reduces over longer times of flight and distances. Therefore, particles at a lower temperature impacting on the steel, together with N$_2$ cooling, contributed to minimising the CTE mismatch, thus leading to less residual stress and cracking. The decrease in coating thickness observed could be attributed to the lower deposition efficiency when spraying the metal oxide particles at lower temperatures. These spraying conditions can be considered as low-energy conditions (LEC). Fig. 2b shows a properly bonded APS TiO$_{2-x}$ coating obtained using LEC.

3.1.2. Aluminium substrates

Following the optimization of the spray coating process using stainless steel substrates, aluminium was used to demonstrate that the APS TiO$_{2-x}$ coating provides a functional layer that is resistant to corrosion and suitable for lightweight electrodes. These substrates were also grit blasted to achieve an R_a value of 6.23 μm; again, the samples were adequately cleaned before the coating process. Similar CTE mismatch concerns indicated that spraying should be carried out under LEC rather than HEC [21]. On characterizing the cross-section area of the coatings, we observed that the samples did not exhibit cracks and were well adhered to the metal substrate (Fig. 3).

3.1.3. Carbon–polymer composite substrates

Electrodes based on carbon–polymer composites are attractive due to their moderate corrosion resistance and low weight. The corrosion of carbon at more positive potentials, for example in metal air batteries and fuel cells, is a well-known phenomenon, however, and a protective layer such as an APS coating would have significant benefits in such applications. The material is composed of a blend of different polymers with conductive carbon black. Bulk electrodes can be obtained by isostatic pressing. Therefore, developing enough roughness on the smooth composite material was critical bearing in mind its fragile inner granular structure (Fig. 4). Grit blasting fractured the substrate at high (standard) pressures. Thus, the pressure was decreased to 2 bar to prevent the substrate from fracturing. The impacting alumina particles did not plastically deform the composite, but very quickly removed the polymer and carbon material. Finally, an R_a value of 5.69 μm was obtained and no damage to the overall substrate structure was found. Due to the novelty of this composite for thermal spray technologies, both HEC and LEC were tested. Firstly, energetic conditions were used and the metal oxide coating was successfully built up. However, stress accumulated at the point of contact between the composite and the metallic support while thermal spraying, and led to localized fissures in the substrate and eventually the sample fragmented. Thus, LEC were selected and APS metal oxide layers were properly bonded with no fractures where the composite piece was fixed. The coating adhered well to the composite with no cracks parallel or transverse to the surface.

3.1.4. Ni foam

Ni foams have also attracted considerable attention because of their relatively high specific surface areas compared to planar electrode materials. Despite the internal complexity of the foam, APS technology may be used to coat non-planar pieces 3D-geometries such as foam. The substrate surface was not altered due to the impossibility of increasing the roughness of this material by means of grit. Consequently, samples were sprayed directly after ultrasonic cleaning with acetone. HEC damaged the filaments of
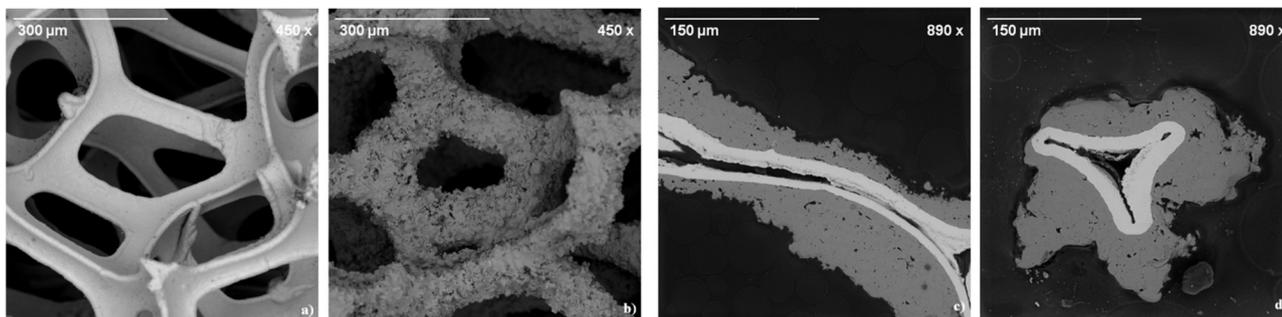
Fig. 5. (a) Ni foam, (b) Ni foam coated by APS TiO_{2-x}, (c) longitudinal cross-section area of a coated filament and (d) transversal cross-section area of a coated filament.

the foams dramatically and the structure was practically useless for the final application. In contrast, under LEC the Ni foam was homogeneously coated. Fig. 5a and b show uncoated and coated foam respectively. In addition, the cross section of the APS TiO_{2-x} coatings did not show any cracks and the coatings were well bonded to the nickel surface. However, the filaments were only coated on one side. Therefore, we coated both sides of the Ni foam to obtain a complete layer of TiO_{2-x} surrounding the material (Fig. 5a and d).

3.2. Electrochemical analysis

Cyclic voltammetry was used to assess the potential range over which the substrates and spray coated electrodes were electrochemically stable. This voltammetry was performed in sulphuric acid and potassium hydroxide electrolytes to simulate conditions within typical battery environments (e.g. lead-acid and NiMH). The potentials were cycled between oxygen evolution and hydrogen evolution regions. Each of the coated substrates displayed similar electrochemical responses. The voltammograms obtained for stainless steel and coated stainless steel are presented in Fig. 6, which presents the 4th consecutive voltammogram. In acidic media (Fig. 6a) the uncoated, stainless steel substrate showed significant oxidation currents commencing at circa 1.0 V vs. SCE,

corresponding to corrosion of the stainless steel (probably due to the Fe^{2+}/Fe^{3+} redox couple). At more positive potentials, bulk oxygen evolution was seen at 1.5 V vs. SCE. Meanwhile, hydrogen evolution was observed at potentials more negative than −0.7 V vs. SCE. The coated stainless steel showed a voltammetric response typical for Magnéli phase materials. Towards positive potentials, oxygen evolution commences at circa 2.0 V vs. SCE; toward negative potentials, hydrogen evolution commences at circa −1.0 V vs. SCE. Between −1.0 and −0.2 V vs. SCE some reversible redox activity of the titanium sub-oxides was observed; this is in agreement with previous studies [22]. Repeated voltammograms on the same electrode showed no shift in the electrochemical response. Moreover, it is important to note that no electrochemical features associated with the underlying stainless steel were observed, which suggests that the coating forms a satisfactory electrochemically isolating barrier between the electrolyte and substrate. The voltammograms suggest that the electrodes would be suitable for use in this acid electrolyte between voltages of −1 and +2 V vs. SCE. Fig. 6b presents the cyclic voltammograms obtained in the KOH electrolyte. In this media, the stainless steel substrate showed a small redox reaction 0.3 V vs. SCE, which was probably caused by one of the alloying elements present. At more positive potentials, commencing at 0.4 V vs. SCE, there was a sharp oxidation wave associated with corrosion and oxygen evolution.
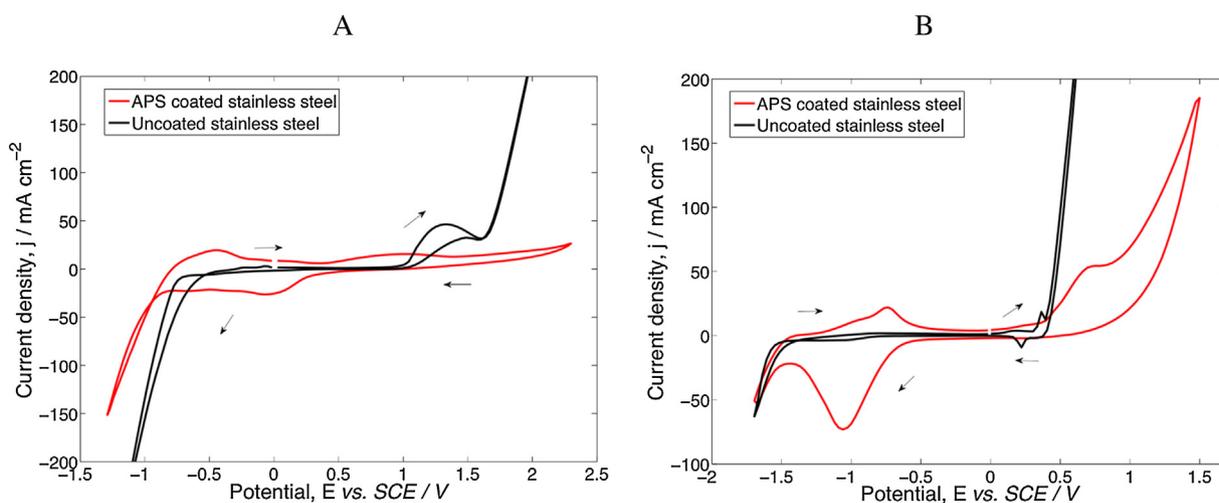
Fig. 6. Cyclic voltammograms obtained at (a) APS coated stainless steel [red line] and stainless steel substrate [black line] from an acid electrolyte comprising 1.0 mol dm^{-3} H_2SO_4 and (b) APS coated stainless steel [red line] and stainless steel substrate [black line] from an acid electrolyte comprising 4.0 mol dm^{-3} KOH at 295 K. Potentials recorded using a sweep rate of 50 mV s^{-1} vs. an SCE reference. Working electrode area = 1.13 cm^2. (For interpretation of the references to colour in this figure legend, the reader is referred to the web version of this article.)
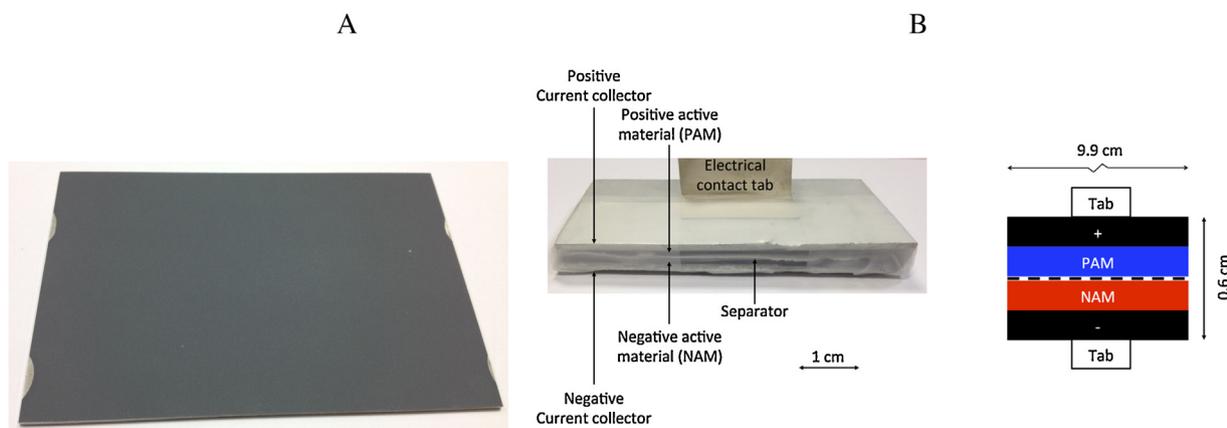
Fig. 7. (a) Aluminium spray coated substrates to produce the battery electrodes, (b) overall cell with dimensions of 10 cm × 5.6 cm × 0.6 cm.

The coated stainless steel, however, displayed the expected response for titanium sub-oxides in an alkaline electrolyte [22] and demonstrated that the coating substantially protects the underlying aluminium from corrosion.

3.3. Proof of concept lead-acid battery

A parallel-plate single-cell lead-acid battery was constructed to demonstrate the suitability of the spray-coated electrodes in a functional device. Positive (PAM) and negative (NAM) active material was removed from the lead grids of a commercial 2 V Cyclon D-cell via mechanical scraping. The powdered PAM and NAM was then layered manually onto the aluminium spray-coated substrates (Fig. 7a) to produce the battery electrodes. Electrical contact with the active material was simply made through contact, which is not ideal and introduced significant voltage losses, particularly at high charge/discharge rates. Nevertheless, the cell provided a good test for proof-of-concept operation of the novel electrodes. The positive and negative electrode each had dimensions of 9.9 cm × 5 cm and incorporated 20 g of active material. AmerSil FF60 was used as the inter-electrode separator. 1.29 s.g. sulphuric acid was used as the electrolyte. The cell was cased in a polypropylene wrap. The overall cell had dimensions of 10 cm × 5.6 cm × 0.6 cm, giving an overall volume of 33.6 cm^3 (Fig. 7b). The mass of the cell was 166 g, giving a density of 4.9 g cm^{-3}. The cell was subjected to a number of constant-current charge/discharge cycles using cell cut-off voltages of 2.6 V during charge periods and 1.2 V during discharge periods. The current was varied between 100 and 1000 mA. Fig. 8 presents a typical charge/discharge cycle at 100 mA constant current throughout. At this
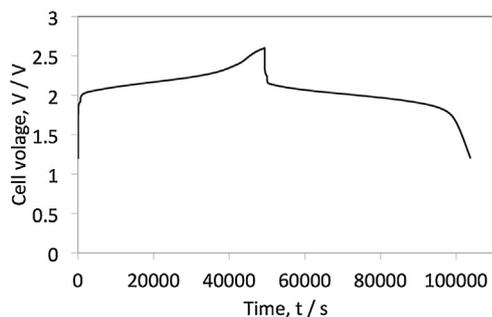
Table 2
Capacity as a function of discharge for the prototype battery using spray-coated aluminium electrodes.

Current (mA)	Capacity (mA/h)
100	1500
250	1100
500	630
750	350
1000	180

current density, the charge efficiency was >98% and the cell delivered a capacity of 1500 mAh. At higher currents, the charge efficiency remained high; however, the capacity decreased markedly. Table 2 shows that the capacity had dropped to 180 mAh when the cell was operated at 1000 mA. This reduction in the capacity is predominantly due to the high contact resistance and IR drop between the paste and the electrode surface associated with the use of second-hand PAM and NAM. This could be overcome by using paste formulated and applied specifically to these electrodes. Despite the limited current, the cell still returned an energy density of 9 Ah kg^{-1} or 45 Ah L^{-1} at 100 mA current draw.

4. Conclusions

Four different lightweight and corrosion resistance materials were manufactured from sheet steel, sheet aluminium, a carbon–polymer composite and nickel foam, APS. The initially smooth surfaces had to be mechanically modified in order to increase their roughness to aid adhesion of the molten spray particles. Spraying conditions were selected so as not to damage the substrates and to minimise the strain caused by the mismatch of CTEs between the coating and substrate. The coated substrates were electrochemically assessed using cyclic voltammetry to confirm that the coating provided an electrochemically isolating but electrically conductive layer, which protected the underlying substrate from contact with the electrolytes. A proof-of-concept 2 V single-cell lead-acid battery was constructed using aluminium as the substrate and LEC spraying conditions, which gave well-bonded homogeneous TiO$_{2-x}$ layers. The battery returned an energy density of 9 Ah kg^{-1} or 45 Ah L^{-1} when operated using a current of 100 mA. Further work will be undertaken to improve the electrical contact between the PAM/NAM and electrodes to enable high-current operation. This work highlights the versatility of APS, the use of thin substrates, the low-cost of the feedstock and the possibility of spraying onto 3D substrates with a high specific surface. Moreover, this spraying technology is suitable to scale-up these products due

Fig. 8. Typical charge/discharge cycle from the lead acid test battery. Charge and discharge performed at a constant current of 100 mA. Cell voltage cut-offs were set at 2.6 V during charge and 1.2 V on discharge.

to the short deposition times, electrochemical results and finally because of the proof-of-concept results in a real acid battery.

Acknowledgments

References

[1] M. Semadeni, Storage of energy, overview, in: C.J. Cleveland (Ed.), Encyclopedia of Energy, Elsevier, New York, 2004, pp. 719–738.
[2] L. Pawlowski, Science and Engineering of Thermal Spray Coatings, John Wiley & Sons, Chichester, U.K, 1995.
[3] M. Gardon, J.M. Guilemany. J. Mater. Sci. (2012) 10.1007/s10854-012-0974-4.
[4] D.E. Reiser, et al., J. New Mater. Electrochem. Syst. 2 (1999) 279–283.
[5] M.T. Williams, J.D. Briscoe, S.M. Oweis. United States Patent 5.254.415 (1993).
[6] G. Barlow, S.J. Specht. United States Patent 5.411.818 (1995).
[7] L. Bai, J.G. Kincs, M. Chason. United States Patent 5.568.353 (1996).
[8] B.C. Muffoletto, W.M. Paulot, J.E. Spaulding. United States Patent 5.716.422 (1998).
[9] H. Ye, C. Strock, T. Xiao, P.R. Strutt, D.E. Resiner. International Patent WO 99/64641 (1999).
[10] J. Dai, R.A. Guidotti, T.D. Xiao, D.E. Reisner. United States Patent 6.794.086 B2 (2004).
[11] R.A. Guidotti, H. Ye, T.D. Xiao, D.E. Reisner, D.H. Doughty. United States Patent 6.926.997 B2 (2005).
[12] D. Batson. United States Patent US2008/0090146 A1 (2008).
[13] D. Soysal, J. Arnold, P. Szabo, R. Henne, S.A. Ansar, J. Therm. Spray Technol. 22 (5) (2013) 588–598.
[14] H. Nie, W. Huang, T. Wen, H. Tu, Z. Zhan, J. Mater. Sci. Lett. 21 (2002) 1951–1953.
[15] D. Hathiramani, R. Vaben, D. Stöver, R.J. Damani, J. Therm. Spray Technol. 15 (4) (2006) 593–597.
[16] O. Kwon, S. Kumar, S. Park, C. Lee, J. Power Sources 171 (2007) 441–447.
[17] J.M. Guilemany, M. Torrell, I.G. Cano, J. Fernández, International Thermal Spray Conference Proceedings, Houston, USA, 2012.
[18] S. Andersson, B. Collen, U. Kuylenstierna, A. Magnéli, Acta Chem. Scand. 11 (1957) 5.
[19] M. Gardon, S. Dosta, J.M. Guilemany, M. Kourasi, B. Mellor, R. Wills, J. Power Sources 238 (2013) 430–434.
[20] M. Gardon, J.M. Guilemany, International Thermal Spray Conference Proceedings, Houston, USA, 2012.
[21] http://www.matweb.com/ (accessed 07/04/2013).
[22] R.G.A. Wills, F.C. Walsh, Electrochim. Acta. 55 (2010) 6342.

Tests on titanium dioxide coatings continued with the fourth topic of this PhD thesis: MOX gas sensors.

Nowadays contamination in urban atmospheres is increasing and more pollutants control in the environment is needed. Metal oxide (MOX) gas sensors coatings can help detecting quantities of hazardous particles in gas phase. The development of a TiO_{2-x} active layer by Atmospheric Plasma Spray (APS) in a gas sensor consisting of thin ceramic substrate (Fig. 32) was the target of this research. It was fundamental not to damage the fragile substrate and cover only circuits spots; for this purpose an aluminium mask was used during the spraying experiments.
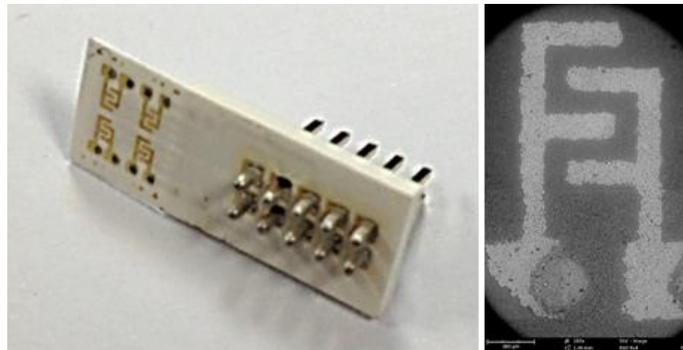
Fig. 32 Thin ceramic substrate with printed circuits

Thermal Spray (TS) techniques and in particular APS represent rapid manufacturing systems for depositing the active MOX layer. Morphology, particle size distribution and phase composition of the initial feedstock have been studied by Scanning Electron Microscope, Laser Scattering and X-Ray Diffraction (Fig. 33).
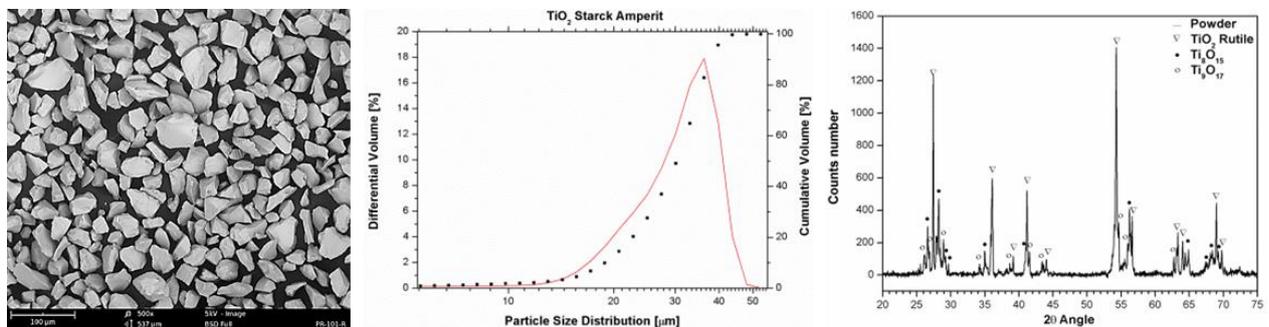
Fig. 33 SEM top surface micrograph, LS curve and XRD pattern of TiO_{2-x} powder

APS spraying conditions have been adjusted in order not to damage fragile substrate, printed circuits, to have good deposition and specific characteristics for the final application. As mentioned, the hydrogen present in the plasma jet reduces the MOX powder, favours the development of oxygen vacancies and this way increases the conductivity of the final coatings. The characterization of deposited TiO_{2-x} coatings is the consequent step, as shown in the following Fig. 34.
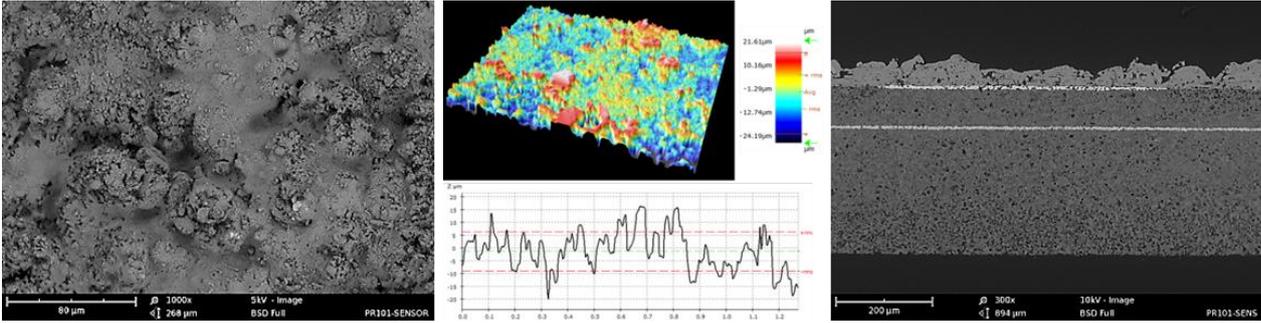
Fig. 34 SEM top surface micrograph, optical confocal analysis and SEM cross section micrograph of the manufactured TiO_{2-x} coatings

2D roughness parameters (Ra, Rq) and 3D superficial parameters (Sa, Sq) have been measured by confocal optical microscope and are reported in Tab.8 below. They are relevant data because are related to the specific area of the materials; the high is this parameter, the high is the surface where gas molecules can attach and react.

Tab.8 2D and 3D roughness parameters of TiO_{2-x} gas sensors

Ra [μm]	Rq [μm]	Sa [μm]	Sq [μm]
4.1 ± 0.5	4.9 ± 0.6	5.3 ± 0.9	7.3 ± 2.1

Coatings top surface and cross sections have been analysed by Scanning Electron Microscope. The first micrograph gives an idea about how rough is the surface, while the second one shows the thickness of the coating and its adhesion onto the substrate. In this specific case, high surface roughness, good adhesion onto printed circuits and low thickness are needed for the final application. Once all these scopes were obtained during this experimental work, the sensing properties must be checked. In 9*Fig. 35 a scheme of the gas chamber is shown, together with the design of experiments established for these TiO_{2-x} functional coatings.

CO	NO2	NH3	Ethanol
(100 ppm)	(10 ppm)	(100 ppm)	(100 ppm)
10	1	10	10
25	2.5	25	25
50	5	50	50
75	7.5	75	75
100	10	100	100
50	5	50	50
50	5	50	50

IDE	PCB
H+	SMA7
H-	2
1+	SMA4
1-	SMA3
2+	SMA2
2-	SMA1
3+	SMA8
3-	5
4+	6
4-	7
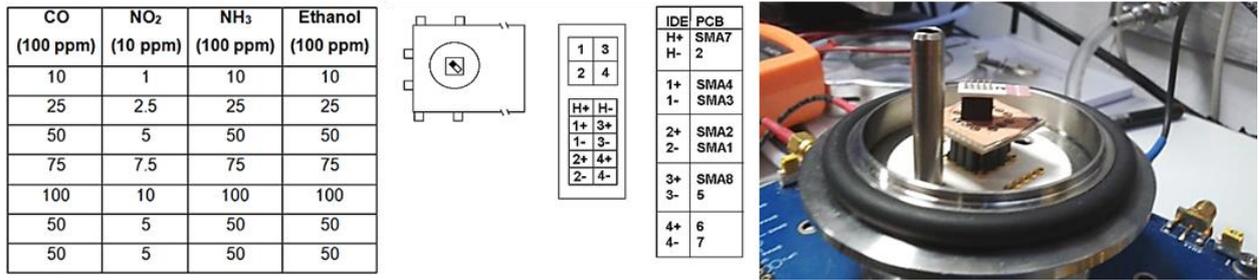
Fig. 35 Design of experiment and gas sensing equipment scheme

Experiments with CO, NO$_2$, NH$_3$, ethanol and humidity can be evaluated. The principle of operation of MOX devices is the change of the electrical resistance depending on the surrounding gas due to the chemical reactions that are developed onto the metal oxide surface. The performance depends on three key-steps: i) receptor function, which determines the adsorption of the gas on the metal oxide surface, ii) transducer function, which is in command to transform the chemical interaction towards an output signal and iii) approachability, that eases the access of the gas into the inner grains of the solid.
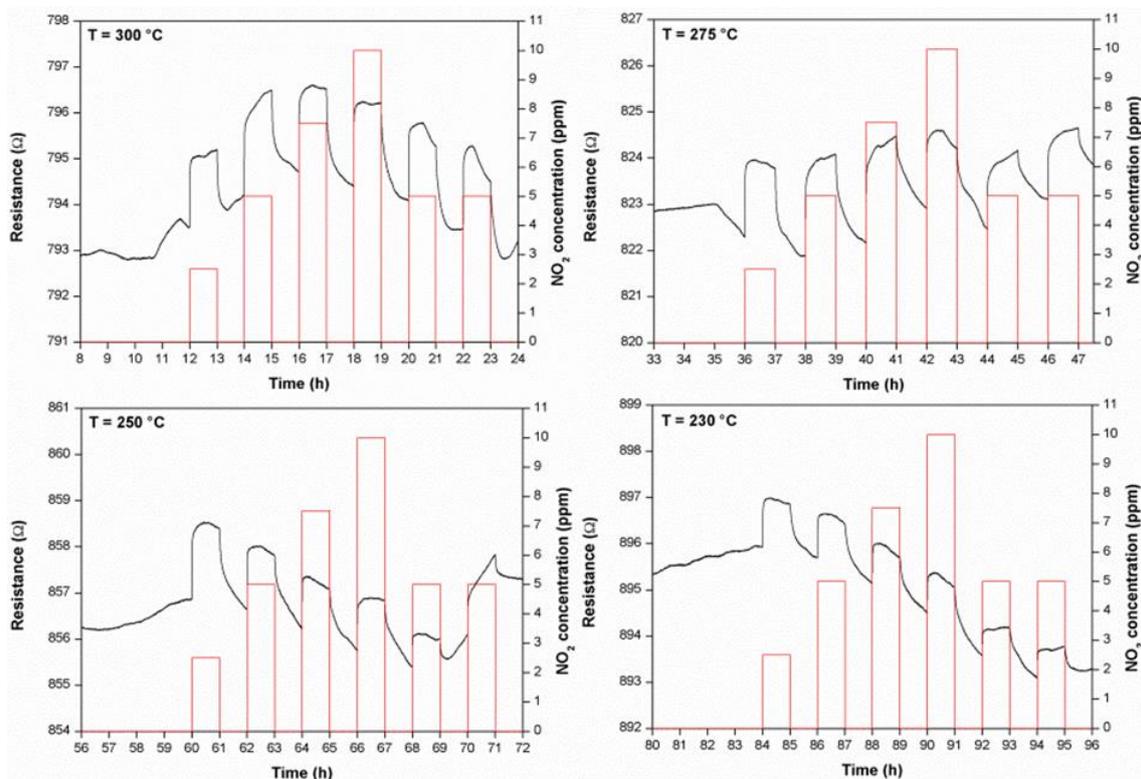
Fig. 36 NO$_2$ gas sensing response of the coatings at different temperatures

Performances of the devices have been tested using NO$_2$ gas at different temperatures and concentrations. These new types of sensors are able to detect NO$_2$ hazardous gas and show

sensing response at different working temperatures. The experimental set-up is going further with CO, NH$_3$ and ethanol in gas phase tests. These results represent an innovative trend for new advanced ceramic gas sensors which can be used at high temperatures and can detect various gases concentrations.

7 Conclusions

With the present PhD thesis, composite powder have been produced and corresponding coatings have been deposited by Low Pressure Cold Gas Spray and multifunctional coatings based on TiO_2 and TiO_{2-x} have been obtained by means of Atmospheric Plasma Spray. The performances of these advanced materials have been proved in different fields of application, such as photocatalysis, photoelectrocatalysis, electrodes for batteries and gas sensors. From this research, the following statements can be concluded:

7.1 Ceramic-polymeric composite LP-CGS coatings

1. New trends led to choose novel composite powder feedstock for LP-CGS process. Nanometric $C-TiO_2$ powder was successfully mechanically blended with a polymeric material by means of LEBM, AM and CM. Milling mechanisms involved in the different processes, such as particle size reduction, polymeric embrittlement, superficial deformation, crystalline phase maintenance and mechanical anchoring were explained.

2. Powder flowability was increased adding the ductile agent. These types of $C-TiO_2$/polymeric composite powders represent suitable feedstocks and were deposited by LP-CGS technology, which represents a novel, fast and cost-effective technology.

3. LP-CGS polymeric/$C-TiO_2$ photocatalysts degraded from 250 up to 750 ppb of NOx in less than 20 minutes. The photocatalytic properties toward NOx degradation are extremely successful with both UV light (>90%) and VIS irradiation (>60%). It was discovered that milling conditions do not affect the photocatalytic response of the LP-CGS coatings. Furthermore, mechanical properties, thickness, porosity and superficial roughness of the coatings were characterised.

4. Anatase phase presence on the top surface of manufactured coatings was confirmed. Photoactivity of LP-CGS composite coatings was compared with other catalysts, dip-coating (DC) layers and commercial paints. As-prepared LP-CGS products possess enhanced photocatalytic performances compared to the other materials.

7.2 Titanium dioxide and titanium sub-oxide APS coatings

5. APS is a promising technology to synthesize highly stable supported TiO_2 photocatalysts with good intrinsic properties for their use in SPEC processes for pollution remediation. The advanced photocatalytic coatings were tested under UV light and applied voltage to degrade azo dyes contaminants, such as AO7 and thus purify water.

6. The percentages of crystalline phases and non-stoichiometric ones were correlated to the photoelectrocatalytic performances of the coatings. It has been found that crystalline phases of TiO_2 (anatase and rutile) are more photoelectrocatalytic than non-stoichiometric TiO_2 sub-oxides. The property with higher influence resulted to be the 3D superficial roughness. When a larger specific area is available to be irradiated, a major photogeneration of oxidant species occurs, with a considerable enhancement of the SPEC degradation of AO7.

7. Versatile APS technology was used to deposit nanostructured, cost-effective, crushed and fused TiO_{2-x} powder onto four different lightweight and corrosion resistance materials, such as steel sheet, aluminium sheet, carbon-polymer composite and nickel foam. Spraying parameters were accurately selected not to damage the substrates and to obtain the lower quantity of residual stresses caused by the mismatch of CTEs among coating and substrate and to have the higher specific surface area.

8. The coated substrates were electrochemically assessed using cyclic voltammetry to confirm that the coating provided an electrochemically isolating but electrically conductive layer, which protected the underlying substrate from contact with the electrolytes. A proof-of-concept 2V single cell lead-acid battery was constructed using aluminium as the substrate and low energetic spraying conditions which gave well-bonded homogeneous TiO_{2-x} layers. The battery returned an energy density of 9 $A \cdot h \cdot kg^{-1}$ or 45 $A \cdot h \cdot L^{-1}$ when operated using a current of 100 mA.

9. Among many MOX powders, TiO_{2-x} feedstock was selected to be deposited and form the active layer of the gas sensor. Thin ceramic substrates with printed circuits were

effectively coated by means of APS TiO_{2-x}. Optimal stand-off distances and number of spraying cycles were properly selected not to damage fragile substrate, printed circuits, to have good deposition, thickness and surface roughness for the final application.

10. APS TiO_{2-x} coatings boost the receptor function due to the amount of oxygen vacancies present at the top surface and this fact led to a positive and reproducible response in front of NO_2 gas. The working temperature was changed during the experiments and the response was positive in all cases.

8 Future trends

At the end of this PhD thesis many conclusions were achieved. Different lines of research were defined and led to develop and manufacture materials for specific applications. On the other side, research does not stop; it is always going forward with the purpose to improve the materials which already exist and to explain the reasons why phenomena occur. The investigation is included inside the progress of the society. Starting from these considerations, next steps for the different application fields treated in this work, were identified and reported in the following list:

1. Study of the rheology of polymers. Viscosity, temperature and shear rate are interesting parameters related to the LP-CGS system and in particular to the heat transferred to the polymeric particles during the process. This knowledge could improve the know-how of the thermal spraying of polymeric materials. Moreover, other ductile agents, such as polyurethane, silicone and polyethylene can be utilised in the milling equipments. Different Tg would be involved in the mixing process and consequently deformations phenomena.

2. Investigate the role of the substrate on the deposition of the composite powder. Not only the heat and the deformation of the particles are important, but also the type of substrate onto which they impact. In many cases substrate heating or cooling is necessary and in this particular case of polymers the heating process should be improved and deeply investigated.

3. The excellent photocatalytic results encourage to apply the advanced coatings in a real test. In many cities photocatalytic areas, in particular quarters, streets and buildings are already tested. New cements, coatings, paints and other types of material are applied in these so-called *photocatalytic islands* and pollution values are constantly checked. The possibility to apply LP-CGS coatings inside these areas would have high experimental interest.

4. Compare LP-CGS coatings with photocatalytic cements. During this work, dip-coating procedure and commercial paints were compared to LP-CGS manufactured

coatings. The interest to include also cements in this comparison is high. Phenomena such superficial erosion and photocatalytic effect could be investigated. Moreover, the understanding of bonding mechanisms and consequently deposition of composite coatings onto cements would be highly interesting.

5. Change the catalyst material. Other metal oxide semiconductors, such as SnO_2, ZnO and Cr_2O_3 can be tested, together with the possibility to introduce elements in their structures (doping). Different metal elements can improve the energy band gap and subsequently the active range of the material for the photocatalytic and sensing applications.

6. Analyse the SPEC properties of other metal oxide coatings. Different semiconductors can be tested in this type of catalysis, such as ZnO, TiO_2 or mixture of them. The conductivity of these MOX based coatings can be measured, correlated to their band gap energies and consequently to their active response in the different application fields. Moreover the possibility to change the azo dye is relevant to study the degradation activity of these advanced materials toward other contaminants in water phase.

7. Study the degradation of other gases, in different concentrations and mixtures of them. The design of experiment decided for the TiO_{2-x} coatings can be improved and studied in a deeper way adding mixtures of gases. This new test can represent more precisely the environmental conditions.

9 Bibliographic references

[1] T. Hongxiang, Overview of the Development of the fluoropolymer Industry, Applied Sciences, 2 (2012) 496-512.

[2] C. Suryanarayana, Mechanical alloying and milling. Progress in Materials Science, 46 (2001) 1-184.

[3] P. J. Hubert, K. Kathiresan, K. Wakabayashi, Filler exfoliation and dispersion in polypropylene/as-received graphite nanocomposites via cryogenic milling, Polymer and science, (2011) 2275.

[4] D. B. Witkin; E. J. Lavernia, Synthesis and mechanical behaviour of nanostructured materials via Cryomilling, Progress in Materials Science, (2006) 1-60.

[5] J. M. Guilemany, N. Cinca, L. Casas, E. Molins, Ordering and disordering processes in MA and MM intermetallic iron aluminade powders, Journal of Materials Science, 44 (2009) 2152-2161.

[6] N. Cinca, E. Hurtado, I. G. Cano, J. M. Guilemany, Mechanical milling of a nanostructured ductile iron powder under dry, wet and cryogenic atmospheres, Revista de Metalurgia, 47 (2011) 197-204.

[7] G. Zhang, A.K. Scharb, S. Tria, O. Elkedim, Tensile and tribological behaviors of PEEK/nano-SiO_2 composites compounded using a ball milling technique, Composites Science and Technology, 68 (2008) 3073-3080.

[8] M. Senna, V. Šepelák, J. Shi, B. Bauer, A. Feldhoff, V. Laporte, K. D. Becker, Introduction of oxygen vacancies and fluorine into TiO_2 nanoparticles by co-milling with PTFE, Journal of Solid State Chemistry, 187 (2012) 51-57.

[9] D. Olmos, C. Domínguez, P.D. Castrillo, J. Gonzalez-Benito, Crystallization and final morphology of HDPE: Effect of the high energy ball milling and the presence of TiO_2 nanoparticles, Polymer, 50 (2009) 1732-1742.

[10] J. González-Benito, G. González-Gaitano, Interfacial Conformations and Molecular Structure of PMMA in PMMA/Silica Nanocomposites. Effect of High-Energy Ball Milling, Macromolecule, 41 (2008) 4777-4785.

[11] D. Olmos, E. Rodríguez-Gutiérrez, J. González-Benito, Polymer Structure and Morphology of Low Density Polyethylene Filled With Silica Nanoparticles, Wiley Online Library (2012).

[12] W. Mekprasart, W. Jarenboon, W. Pecharapa, TiO_2/CuPc hybrid nanocomposites prepared by low-energy ball milling for dye-sensitized solar cell application, Materials Science and Engineering B, 172 (2010) 231-236.

[13] R. Amade, P. Heitjans, S. Indris, M. Finger, A. Haeger, D. Hesse, Defect formation during high-energy ball milling in TiO_2 and its relation to the photocatalytic activity, Journal of Photobiology A: Chemestry, 207 (2009) 231-235.

[14] Y.G. Zhu, Z.Q. Li, D. Zhang, T. Tanimoto, PET/SiO_2 Nanocomposites Prepared by Cryomilling, Journal of Polymer Science: Part B: Polymer Physics, 44 (2006) 1161-1167.

[15] M. Fabián, G. Tyuliev, A. Feldhoff, N. Kostova, P. Kollár, S. Suzuki, F. Saito, V. Šepelák, One-step synthesis of nanocrystalline ZnO via Cryomilling, Powder Technology, 235 (2013) 395-399.

[16] S. Amirkhanlou, M. Ketabchi, N. Parvin, Nanocrystalline/nanoparticle ZnO synthesized by high energy ball milling process, Materials Letters, 86 (2012) 122-124.

[17] R. K. Sendi, S. Mahmud, Quantum size effect on ZnO nanoparticle-based discs synthesized by mechanical milling, Applied Surface, 258 (2012) 8026-8031.

[18] D. Ma, Y. A. Akpalu, Y. Li, R. W. Siegel, L. S. Schadler, Effect of Titania Nanoparticles on the Morphology of Low Density Polyethylene, Journal of polymer science: Part B: Polymer Physics, 43 (2005) 488-497.

[19] R. Quesada-Cabrera, A. Mills, C. O'Rourke, Action spectra of P25 TiO_2 and a visible light absorbing, carbon-modified titania in the photocatalytic degradation of stearic acid, Applied Catalysis B: Environmental, 150-151 (2014), 338-344.

[20] M. Robotti, M. Gardon, S. Dosta, A. Concustell, I. G. Cano, J. M. Guilemany, Self-cleaning, photocatalytic and superhydrophobic coatings obtained by Cold Gas Spray, Intellectual Property Protection IPP (2014).

[21] V. K. Champagne, The cold spray materials deposition process: fundamentals and applications (2007) CRC Press.

[22] A. N. Papyrin, European Summer University, ENISE, St.-Etienne, France, 2006.

[23] C.-J. Li, W. Li, H. Liao, Examination of the critical velocity for deposition of particles in cold spraying, Journal of Thermal Spray Technology, 15 (2006) 212-222.

[24] Y. Li, W. Li, Y. Wang, H. Fukanuma, Effect of spray angle on deposition characteristics in cold spraying, Proceedings of the Thermal Spray 2003: advancing the science and applying the technology Ohio, USA: ASM International (OH).

[25] M. Yamada, H. Isago, H. Nakano, M. Fukumoto, Cold Spraying of TiO_2 Photocatalyst Coating With Nitrogen Process Gas, Journal of Thermal Spray Technology, 19 (2010) 1218-1223.

[26] G. Bae, Y. Xiong, S. Kumar, K. Kang, C. Lee, General aspects of interface bonding in kinetic sprayed coatings, Acta Materialia, 56 (2008) 4858-4868.

[27] A. S. Alhulaifi, G. A. Buck, W. J. Arbegast, Numerical and Experimental Investigation of Cold Spray Gas Dynamic Effects for Polymer Coating, Journal of Thermal Spray Technology, 21 (2012) 852-862.

[28] A. Moridi, S. M. Hassani-Gangaraj, M. Guagliano, M. Dao, Cold spray coating: review of material systems and future perspectives, Surface Engineering, 36 (2014) 369-395.

[29] M. Gardon, C. Fernández-Rodríguez, D. Garzón Sousa, J. M. Doña-Rodríguez, S. Dosta, I. G. Cano, J. M. Guilemany, Photocatalytic Activity of Nanostructured Anatase Coatings Obtained by Cold Gas Spray, Journal of Thermal Spray Technology, 23 (2014) 1135-1141.

[30] M. Yamada, H. Isago, K. Shima, H. Nakano, M. Fukumoto, Deposition of TiO_2 Ceramic Particles on Cold Spray Process, International Thermal Spray Conference ITSC 2010, Proceedings.

[31] H. Guosheng, G. Daming, L. Xiangbo, X. Lukuo, W. Hongren, Numerical simulation on syphonage effect of laval nozzle for low pressure cold spray system, Journal of Materials Processing Technology, 214 (2014) 2497-2504.

[32] A. Astarita, M. Durante, A. Langella, M. Montuori, A. Squillace, Mechanical characterization of low-pressure cold-sprayed metal coatings on aluminium, Surface and Interface Analysis, 45 (2013) 1530-1535.

[33] Y. Xu, I. M. Hutchings, Cold spray deposition of thermoplastic powder, Surface & Coatings Technology, 201 (2006) 3044-3050.

[34] X.-J. Ning, Q.-S. Wang, Z. Ma, H.-J. Kim, Numerical study of in-flight particle parameters in low-pressure cold spray process, Journal of Thermal Spray Technology, 19 (2010) 1211-1217.

[35] D. M. Chun, S. H. Ahn, Deposition mechanism of dry sprayed ceramic particles at room temperature using a nano-particle deposition system, Acta Materialia, (2011) 2693-2703.

[36] 7 million premature deaths annually linked to air pollution, WHO report, March 2014.

[37] P. Qiu, H. Tian, C. Zhu, K. Liu, J. Gao, J. Zhou, An elaborate high resolution emission inventory of primary air pollutants for the Central Plain Urban Agglomeration of China, Atmospheric Environment, 86 (2014) 93-101.

[38] B. Zhao, S. X. Wang, H. Liu, J. Y. Xu, K. Fu, Z. Klimont, J. M. Hao, K.B. He, J. Cofala, M. Amann, NOx emissions in China: Historical trends and future perspectives, Atmospheric Chemistry and Physics, 13 (2013) 9869-9897.

[39] K. Nakata, A. Fujishima, TiO_2 photocatalysis: Design and applications, Journal of Photochemistry and Photobiology C, 13 (2012) 169-189.

[40] A. L. Linsebigler, G. Lu, J. T. Yates, Photocatalysis on TiO_2 Surfaces: Principles, Mechanisms, and Selected Results. Chemical Reviews, 95 (1995) 735-758.

[41] L.G. Devi, R. Kavitha, A review on non metal ion doped titania for the photocatalytic degradation of organic pollutants under UV/solar light: Role of photogenerated charge carrier dynamics in enhancing the activity, Applied Catalysis B: Environmental, 140-141 (2013) 559-587.

[42] M. V. Dozzi, E. Selli, Reviews, Journal of Photochemistry and Photobiology C: Photochemistry, 14 (2013) 13-28.

[43] H. Wang, P. Lewis James, Effects of dopant states on photoactivity in carbon-doped TiO_2, Journal of Physics: Condensed Matter, 17 (2005) 209-213.

[44] S. U. M. Khan, M. Al-Shahry, W. B. Jr. Ingler, Efficient photochemical water splitting by a chemically modified n-TiO_2, Science, (2002) 2243-2244.

[45] E. Borborini, A. M. Conti, I. Kholmanov, P. Piseri, A. Podestà, P. Milani, C. Cepek, O. Sakho, R. Macovez, M. Sancrotti, Nanostructured TiO_2 films with 2 eV optical gap, Advanced Materials, 17 (2005) 1842-1846.

[46] C. Xu, Y. A. Shaban, W. B. Jr. Ingler, S. U. M. Khan, Nanotube enhanced photoresponse of carbon modified (CM)-n-TiO$_2$ for efficient water splitting, Solar Energy Materials and Solar Cells, 91 (2007) 938-943.

[47] X. Wang, S. Meng, X. Zhang, H. Wang, W. Zhong, Q. Du, Multi-type carbon doping of TiO$_2$ photocatalyst, Chemical Physics Letters, 444 (2007) 292-296.

[48] Y. Li, D. S. Hwang, N. H. Lee, S. L. Kim, Synthesis and characterization of carbon-doped titania as an artificial solar light sensitive photocatalyst, Chemical Physics Letters, 404 (2005) 25-29.

[49] J. Orth-Gerber, H. Kisch, Titanium dioxide photocatalyst containing carbon and method for its production, U. S. Pat. Appl. Publ. US 2005226761, 19 (2005).

[50] R. Cucitore, S. Cangiano, L. Cassar, High durability photocatalytic paving for reducing urban polluting agents, WO/2006/000565 (2006).

[51] Y. Murata, H. Tawara, H. Obata, K. Murata, NOx-cleaning paving block, EP0786283 (2003).

[52] C. Águia, J. Ângelo, L. M. Madeira, A. Mendes, Influence of photocatalytic paint components on the photoactivity of P25 towards NO abatement, Catalysis Today, 151 (2010) 77-83.

[53] C. Águia, J. Ângelo, L. M. Madeira, A. Mendes, Influence of Paint components on photoactivity of P25 titania toward NO abatement, Polymer Degradation and Stability, 96 (2011) 898-906.

[54] R. Quesada-Cabrera, A. Mills, C. O'Rourke, Action spectra of P25 TiO$_2$ and a visible light absorbing, carbon-modified titania in the photocatalytic degradation of stearic acid, Applied Catalysis B: Environmental, 150-151 (2014) 338-344.

[55] J. B. Powers. Method for flame spraying polyethylene, US2718473 A (1955).

[56] E. Leivo, T. Wilenius, T. Kinos, P. Vuoristo, T. Mäntylä, Properties of thermally sprayed fluoropolymer PVDF, ECTFE, PFA and FEP coatings, Progress in Organic Coatings, 49 (2004) 69-73.

[57] C. Mateus, S. Costil, R. Bolot, C. Coddet, Ceramic/fluoropolymer composite coatings by thermal spraying – a modification of surface properties, Surface & Coatings Technology, 191 (2005) 108-118.

[58] L. Pawlowski, Science and Engineering of Thermal Spray Coatings, John Wiley & Sons, Chichester, U.K. (1995).

[59] G. Bertrand, N. Berger-Keller, C. Meunier, C. Coddet, Evaluation of metastable phase and microhardness on plasma sprayed titania coatings, Surface & Coatings Technology, 200 (2006) 5013-5019.

[60] A. Fujishima, K. Honda, Electrochemical photolysis of water at a semiconductor electrode, Nature, 238 (1972) 37-38.

[61] A. Fujishima, X. Zhang, D.A. Tryk, TiO_2 photocatalysis and related surface phenomena, Surface Science Reports, 63 (2008) 515–582.

[62] K. Nakata, A. Fujishima, TiO_2 photocatalysis: design and applications, Journal of Photochemistry and Photobiology C: Photochemistry Reviews, 13 (2012) 169–189.

[63] D. Friedmann, C. Mendive, D. Bahnemann, TiO_2 for water treatment: parameters affecting the kinetics and mechanisms of photocatalysis, Applied Catalysis B: Environmental, 99 (2010) 398–406.

[64] U.G. Akpan, B.H. Hameed, Parameters affecting the photocatalytic degradation of dyes using TiO_2-based photocatalysts: A review, Journal of Hazardous Materials, 170 (2009) 520–529.

[65] E. Brillas, C. A. Martínez-Huitle, Decontamination of wastewaters containing synthetic organic dyes by electrochemical methods. An updated review, Applied Catalysis B: Environmental, 166–167 (2015) 603–643.

[66] B. Bayarri, E. Carbonell, J. Gimenez, S. Esplugas, H. Garcia, Higher intrinsic photocatalytic efficiency of 2,4,6-triphenylpyrylium-based photocatalysts compared to TiO_2 P-25 for the degradation of 2,4-dichlorophenol using solar simulated Light, Chemosphere, 72(2008) 67–74.

[67] B. Smolkova, N. El Yamani, A. R. Collins, A. C. Gutleb, M. Dubinska, Nanoparticles in food. Epigenetic changes induced by nanomaterials and possible impact on health, Food and Chemical Toxicology, 77 (2015) 64–73.

[68] R. Handy, M. Whitt, M. Rodriguez, M.J. Jackson, in: W. Ahmed, M. Jackson (Eds.), Emerging Nanotechnologies for Manufacturing, Elsevier, Oxford (UK) (2015) 255–269.

[69] L. Dou, L. Gao, X. Yang, X. Song, Hierarchical architectures TiO_2: Pollen-inducted synthesis, remarkable crystalline-phase stability, tunable size, and reused photo-catalysis, Journal of Hazardous Materials, 203-204 (2012) 363–369.

[70] H. Choi, S. R. Al-Abed, D. D. Dionysiou, E. Stathatos, P. Lianos, in: I. C. Escobar, A. I. Schäfer (Eds.), Sustainable Science and Engineering, 2, Elsevier, Oxford(UK), 2010, 229–254.

[71] S. Parra, S. Malato, C. Pulgarin, New integrated photocatalytic-biological flow system using supported TiO_2 and fixed bacteria for the mineralization of isoproturon, Applied Catalysis B: Environmental, 36 (2002) 131–144.

[72] C. Guillard, J. Disdier, C. Monnet, J. Dussaud, S. Malato, J. Blanco, M. I. Maldonado, J. M. Herrmann, Solar efficiency of a new deposited titania photocatalyst: chlorophenol, pesticide and dye removal applications, Applied Catalysis B: Environmental, 46 (2003) 319–332.

[73] J. Marúgan, J. Aguado, W. Gernjak, S. Malato, Solar photocatalytic degradation of dichloroacetic acid with silica-supported titania at pilot-plant scale, Catalysis Today, 129 (2007) 59–68.

[74] B. R. Garza-Campos, J. L. Guzmán-Mar, L. H. Reyes, E. Brillas, A. Hernández-Ramírez, E. J. Ruiz-Ruiz, Coupling of solar photoelectron-Fenton with a BDD anode and solar heterogeneous photocatalysis for the mineralization of the herbicide atrazine, Chemosphere, 97 (2014) 26–33.

[75] M. Jiménez-Tototzintle, I. Oller, A. Hernández-Ramírez, S. Malato, M. I. Maldonado, Remediation of agro-food industry effluents by biotreatment combined with supported TiO_2/H_2O_2 solar photocatalysis, Chemical Engineering Journal, 273 (2015) 205–213.

[76] Y. Bennani, P. Appel, L.C. Rietveld, Optimisation of parameters in a solar light-induced photoelectrocatalytic process with a TiO_2/Ti composite electrode prepared by paint-thermal decomposition, Journal Photochemistry and Photobiology A, 305 (2015) 83–92.

[77] J. Marugán, P. Christensen, T. Egerton, H. Purnama, Synthesis, characterization and activity of photocatalytic SOL-GEL TiO_2 powders and electrodes, Applied Catalysis B: Environmental, 89 (2009) 273–283.

[78] H. Zhang, Y. Wang, P. Liu, Y. Han, X. Yao, J. Zou, H. Cheng, H. Zhao, Anatase TiO_2 crystal facet growth: mechanistic role of hydrofluoric acid and photoelectrocatalytic activity, Applied Materials & Interfaces, 3 (2011) 2472–2478.

[79] R. Daghrir, P. Drogui, M. A. El Khakani, Photoelectrocatalytic oxidation of chlortetracycline using Ti/TiO_2 photo-anode with simultaneous H_2O_2 production, Electrochimica Acta, 87 (2013) 18–31.

[80] P.S. Shinde, P.S. Patil, P.N. Bhosale, A. Brüger, G. Nauer, M. Neumann-Spallart, C.H. Bhosale, UVA and solar light assisted photoelectrocatalytic degradation of AO7 dye in water using spray deposited TiO_2 thin films, Applied Catalysis B: Environmental, 89 (2009) 288–294.

[81] M.L. Hitchman, F. Tian, Studies of TiO_2 thin films prepared by chemical vapour deposition for photocatalytic and photoelectrocatalytic degradation of 4-chlorophenol, Journal of Electroanalytical Chemistry, 538 (2002) 165–172.

[82] Q. Zhang, J. Zhu, Y. Wang, J. Feng, W. Yan, H. Xu, Electrochemical assisted photocatalytic degradation of salicylic acid with highly ordered TiO_2 nanotubes electrodes, Applied Surface Science, 308 (2014) 161–169.

[83] J. C. Cardoso, T. M. Lizier, M. V. B. Zanoni, Highly ordered TiO_2 nanotube arrays and photoelectrocatalytic oxidation of aromatic amine, Applied Catalysis B: Environmental, 99 (2010) 96–102.

[84] Z. Zhang, D. Pan, J. Feng, L. Guo, L. Peng, C. Xi, J. Li, Z. Li, M. Wu, Z. Ren, Enhanced photoelectrocatalytic activity in TiO_2 nanotube arrays modified with TiO_2 nanoparticles, Materials Letters, 66 (2012) 54–56.

[85] S. K. Mohapatra, M. Misra, V. K. Mahajan, K. S. Raja, A novel method for the synthesis of titania nanotubes using sonoelectrochemical method and its application for photoelectrochemical splitting of water, Journal of Catalysis, 246 (2007) 362–369.

[86] X. Cheng, G. Pan, X. Yu, Construction of high-efficient photoelectrocatalytic system by coupling with TiO_2 nano-tubes photoanode and active carbon/polytetrafluoroethylene cathode and its enhanced photoelectrocatalytic degradation of 2,4-dichlorophene and mechanism, Chemical Engineering Journal, 279 (2015) 264–272.

[87] X. Hua, Y. Zhang, N. Ma, X. Li, H. Wang, A new coral structure TiO_2/Ti film electrode applied to photoelectrocatalytic degradation of Reactive Brilliant Red, Journal of Hazardous Materials, 172 (2009) 256–261.

[88] Y. Liu, K. Mu, G. Yang, H. Peng, F. Shen, L. Wang, S. Deng, X. Zhang, Y. Zhang, Fabrication of a coral/double-wall TiO_2 nanotube array film electrode with higher photoelectrocatalytic activity under sunlight, New Journal of Chemistry, 39 (2015) 3923–3928.

[89] S. Garcia-Segura, S. Dosta, J. M. Guilemany, E. Brillas, Solar photoelectrocatalytic degradation of Acid Orange 7 azo dye using a highly stable TiO_2 photoanode synthesized by atmospheric plasma spray, Applied Catalysis B: Environmental, 132–133 (2013) 142–150.

[90] C. He, X. Z. Li, N. Graham, Y. Wang, Preparation of TiO_2/ITO and TiO_2/Ti photoelectrodes by magnetron sputtering for photocatalytic application, Applied Catalysis A: General, 305 (2006) 54–63.

[91] X. Florenza, A. M. S. Solano, F. Centellas, C. A. Martínez-Huitle, E. Brillas, S. Garcia-Segura, Degradation of the azo dye Acid Red 1 by anodic oxidation and indirect electrochemical processes based on Fenton's reaction chemistry. Relationship between decolorization, mineralization and products, Electrochimica Acta, 142 (2014) 276–288.

[92] M. Semadeni, Storage of Energy overview, Encyclopedia of Energy (2004) 719-738.

[93] D. Soysal, J. Arnold, P. Szabo, R. Henne, S. A. Ansar, Thermal plasma spraying applied on Solid Oxide Fuel Cells, Journal of Thermal Spray Technology, 22 (2013) 588-598.

[94] O. Kwon, S. Kumar, S. Park, C. Lee, Comparison of solid oxide fuel cell anode coatings prepared from different feedstock powders by atmospheric plasma spray method, Journal of Power Sources, 171 (2007) 441-447.

[95] J. M. Guilemany, M. Torrell, I. G. Cano, J. Fernández. Interational Thermal Spray Conference proceedings (2012) Houston, USA.

[96] S. Andersson, B. Collén, U. Kuylenstierna, A. Magnéli, Phase analysis studies on the titanium-oxygen system, Acta Chemica Scandinavica, 11 (1957) 1641-1652.

[97] M. Gardon, S. Dosta, J. M. Guilemany, M. Kourasi, B. Mellor, R. Wills, Improved, high conductivity titanium sub-oxide coated electrodes obtained by Atmospheric Plasma Spray, Journal of Power Sources, 238 (2013) 430-434.

[98] M. Gardon, J. M. Guilemany. Interational Thermal Spray Conference proceedings (2012) Houston, USA.

[99] R. G. A. Wills, F. C. Walsh. The continuing development of Magnéli phase titanium sub-oxides and Ebonex® electrodes, Electrochimica Acta, 55 (2010) 6342-6351.

[100] M. Gardon, O. Monereo, S. Dosta, G. Vescio, A. Cirera, J. M. Guilemany, New procedures for building-up the active layer of gas sensors on flexible polymers, Surface & Coatings Technology, 235 (2013) 848–852.

[101] M. Gardon, J. M. Guilemany, A review on fabrication, sensing mechanisms and performance of metal oxide gas sensors, Journal of Materials Science: Materials in Electronics, 24 (2013) 1410-1421.

10 Resumen

El tema principal de esta tesis doctoral es la fabricación de recubrimientos multifuncionales de dióxido de titanio mediante técnica de proyección fría (CGS) y proyección por plasma atmosférico (APS). Las características de cada tecnología de proyección representan un factor clave para la comprensión del comportamiento del material depositado. Además, las condiciones del proceso afectan en gran parte la respuesta funcional y la actividad de las capas de óxido metálico en los diferentes sectores de aplicación. La interacción de la materia prima con el plasma del sistema APS y con el nitrógeno del equipo CGS fue investigada. Activación, enfriamiento y precalentamiento superficial de los sustratos fueron algunos de los pasos fundamentales que se siguieron para entender y verificar los mecanismos de unión de los polvos de partida. Cada producto en forma de recubrimiento funcional encontró su sector de aplicación: i) fotocatálisis en fase gaseosa, ii) fotoelectrocatálisis en fase liquida, iii) electrodos para baterías y iv) sensores de gas.

El primer objetivo de esta tesis doctoral consistió en el desarrollo de recubrimientos nano-estructurados de TiO_2 anatasa mediante técnica de proyección fría CGS. Gracias a esta tecnología de proyección, se evita la fusión del material de alimentación durante su deposición y esto es fundamental porque permite preservar la fase meta-estable de anatasa del dióxido de titanio a temperatura ambiente. La grande superficie específica de este material nanométrico es útil para su aplicación en el campo de la fotocatálisis heterogénea y la degradación de los contaminantes en fase gaseosa. Con el fin de evitar fenómenos la obturación del polvo nanométrico y la no adecuada deposición de partículas cerámicas, fueron preparadas unas mezclas mecánicas con materiales dúctiles que presentan una adecuada fluidez en los conductos de alimentación del sistema CGS. La unión del material compuesto inicial sobre el sustrato es principalmente mecánica, debido a la energía cinética transferida de parte del gas durante el proceso y la deformación plástica de la componente dúctil del material. La presencia de la fase anatasa en la superficie superior de los revestimientos finales determina el desarrollo del proceso fotocatalítico. Las muestras obtenidas degradaron los gases NOx en breve tiempo y con eficiencias de degradación elevadas tanto con luz UV como con luz visible (en colaboración con el grupo FEAM Fotocatálisis y Espectroscòpia Aplicada al Medioambiente, Universidad de Las Palmas de Gran Canaria).

El segundo propósito de esta investigación consistió en proyectar tres diferentes tipos de TiO_2 (100% anatasa, 100% rutilo y sub-óxidos) por tecnología APS sobre acero al carbono y aleación Inconel y evaluar las actividades fotocatalíticas en fase liquida. El ratio Ar/H_2 del plasma atmosférico fue propiamente modificado para obtener varias composiciones en los recubrimientos finales. El rendimiento de los recubrimientos aplicados como fotoánodos fue analizado con el proceso SPEC Solar Photoelectrocatalysis. El estudio llevó a la conclusión que los recubrimientos con mayor parte de fases cristalinas (anatasa y rutilo), mayor rugosidad 3D de superficie y adecuado espesor presentan mejor desempeño fotoelectrocatalítico. 0.43 mM de colorante AO7 en solución Na_2SO_4 0.05M a 35 °C fueron degradados por parte de los recubrimientos funcionales en 180 minutos (en colaboración con el grupo LEMMA Laboratori d'Electroquímica de Materials i del Medi Ambient, Universitat de Barcelona).

La tercera finalidad de este trabajo fue depositar óxidos metálicos a base de dióxido de titanio por APS para ser aplicado como electrodos en baterías reales. En primer lugar, se llevó al cabo una profunda investigación bibliográfica y se estudiaron los recubrimientos convencionales. Se observó que el hidrógeno contenido en el flujo de plasma de APS es capaz de reducir el óxido metálico TiO_2 de partida, crear vacantes de oxígeno y compuestos no estequiométricos como sub-óxidos de titanio (TiO_{2-x}) o fases de Magnéli (Ti_nO_{2n-1}) durante el tiempo de permanencia en vuelo de las partículas. Esta falta de oxígeno en la estructura cristalina del TiO_2 conduce a un nivel de donantes en la banda de conducción; por lo tanto, se obtuvo un material cerámico con una conductividad mejorada y además resistente a la corrosión por su propia naturaleza. Fueron fabricados recubrimientos bien adheridos sobre diversos materiales como acero inoxidable, láminas de aluminio, material compuesto de polímero reforzado con carbono y espuma de níquel, los cuales se utilizan comúnmente como electrodos estándar. Cuatro placas de TiO_{2-x} sobre sustratos de aluminio se aplicaron como electrodos en una batería de escala de laboratorio. Se realizaron las curvas de voltametría cíclica y los ciclos de carga/descarga de la batería de plomo y los resultados fueron excelentes (en colaboración con la Facultad de Ingeniería y Medio Ambiente, Universidad de Southampton).

El último objetivo de este doctorado consistió en el desarrollo de nuevos sensores de gas funcionales a través de la tecnología de APS. Con el objetivo de ofrecer una mayor innovación a los sensores de óxidos metálicos convencionales, se estableció hacer crecer la

capa sensorica sobre un sustrato cerámico delgado. Este hecho permite aumentar la temperatura de trabajo respecto a los sustratos convencionales de tipo polimérico o metálico. Las condiciones de proyección fueron adecuadamente seleccionadas para alcanzar una buena deposición y no dañar el sustrato. El proceso de APS también ofreció la ventaja de aumentar la cantidad de vacantes de oxígeno en el recubrimiento final respecto al polvo inicial con el fin de mejorar la conductividad y en consecuencia, su función sensorica. Las respuestas de los dispositivos funcionales frente a diversos gases fueron positivas. La detección fue analizada a diferentes temperaturas de trabajos y los rendimientos fueron satisfactorios (en colaboración con el grupo MIND Micronanotecnologies I Nanoscòpies per Dispositius electrònics i fotònics, Facultad de Física, Universitat de Barcelona).

11 Acknowledgements

I would like express my gratitude to Prof. Josep Maria Guilemany, especially for the confidence that he gave me. The experience in his Centre de Projecció Tèrmica CPT made me grown very much. I want to thank Dr. Sergi Dosta for his thermal spray knowledge and fundamental guidelines in the development of this PhD Thesis. Special thanks go to Dr. Irene Garcia Cano for her advices and support. Certainly, my acknowledgements also go to the other Professors and Doctors of the CPT research group: Prof. Carlos Müller, Prof. Maria Sarret, Dr. Amadeu Concustell, Dr. Horacio Canales, Dr. Joan Ramon Miguel and Dr. Núria Cinca. Thank you very much for sharing with me your huge know-how during these three years. I would like also to thank very much those people who were inside the team and already got their PhD title or changed their path: Dr. María Villa Vidaller, Dr. Marc Gardon Ramos, Dr. Simona Iliescu and Dr. Miguel Couto.

I am highly grateful to all CPTer@s colleagues who accompanied me during these years: Aina Cabrer, Alessio Silvello, Anna Martin, Fernando Santos da Silva, John Henao, Juliana Bedoya, Kirian Zomeño, Maryam Bazyaran, Pablo Ozaeta, Victor Crespo, Victor Gómez and Victoria Gómez Pérez. Thank you very much for your help and kindness toward me.

Furthermore I want to transit my gratitude to all members of other research groups who participated in this PhD thesis: Dr. Cristina Fernández Rodríguez, Dr. Elisenda Pulido Melián, Maria José Hernández Rodríguez and Davinia Garzón Sousa of CIDIA group (ULPGC); Dr. Enric Brillas and Dr. Sergi Garcia Segura of MENTE group (UB); Dr. Richard Wills and Maria Kourasi of University of Southampton and Dr. Albert Cirera and Oriol Monereo of MIND group (UB).

Finally, I express my gratitude to Prof. Assis Vicente Benedetti, Prof. José Maria Gomez de Salazar Caso de los Cobos and Dr. Miguel Ángel Rodríguez.